UNIVERSITA' DEGLI STUDI DI PADOVA
DIPARTIMENTO DI INGEGNERIA INDUSTRIALE
CORSO DI LAUREA MAGISTRALE IN INGEGNERIA DEI MATERIALI

Tesi di Laurea in
Ingegneria dei Materiali
(Laurea magistrale IN 0523)

Determination of nanoscale ferroelectric domain distribution in multilayer piezoelectric actuators

Relatore: Prof. Paolo Colombo
Correlatore: Prof. Marco Deluca

Laureando: FELICE BOMBIERI

ANNO ACCADEMICO 2016-2017

Abstract

The subject of this Master Thesis is the characterization of the ferroelectric domains in piezoelectric actuators that have been subjected to mechanical stress, poling or in presence of cracks. This investigation has been done with a Piezoresponse Force Microscope (PFM), for 3 samples (one poled, one unpoled, and one mechanically compressed), in 3 different positions with respect to the electrodes. The PFM images of the measurements have been elaborated with the Wolfram Mathematica program, and several 3D images of the piezoresponse vector have been obtained. From the piezoresponse vector representations, the direction of polarization of the domains has been discussed with reference to the sample history. The experimental work has been carried out in the Physics Department of the Mining University (Montanuniversität) of Leoben, under the supervision of the Materials Center Leoben.

Index

Introduction

In this elaborate is resumed the work done in six months in the Physics Department of the Montanuniversität Leoben (experimental part) and in the Materials Center Leoben (data treatment part). The measurements have been done on lead zirconate titanate (PZT) multilayers with the Piezoresponse Force Microscopy (PFM) technique to characterize the surface direction of polarization. This Master thesis is divided into 5 chapters:

-Chapter 1: in this chapter is placed all the theoretical background that concerns with the piezoelectric materials and in the specific case the PZT structure and properties.

-Chapter 2: in this chapter the PFM method is described, so the principles of operation and the theoretical basics are discussed.

-Chapter 3: in this chapter the experimental part is described, therefore the instrumentation, the calibration sequence and the samples are presented.

-Chapter 4: in this chapter the results of the measurements are presented, that is: the three dimensional Piezoresponse map and a consequent discussion.

All the work has been done with the supervision of the Scanning Probe Microscopy Group Leoben and the Materials Center Leoben.

Chapter 1
Theoretical Background

1.1 Basics of ferroelectric materials

1.1.1 Ferroelectric materials

Ferroelectric materials are spontaneously polarized materials above the Curie Temperature (T_C), in which the direction of polarization can be permanently changed by the application of a sufficiently high electric field. The origin of this behavior comes from the polarization at lattice level, and occurs in non-centrosymmetric crystal structures with unique polar axis, like perovskite. Perovskite ferroelectric ceramics are now widely used in the development of components of various electromechanical devices. These ceramic crystals are cubic at their paraelectric phase above T_C, and below that temperature they are tetragonal, rhombohedral or orthorhombic (at different temperatures) at their ferroelectric phase. In these ferroelectric crystals there are regions of uniform polarization (along the same directions) called ferroelectric domains. In an unpoled material the macroscopic polarization is nearly compensated by the resulting (randomly oriented) domains structure. These domains are formed during the paraelectric-ferroelectric phase transition to minimize the depolarization and strain energy. The electromechanical properties change when a ferroelectric ceramic is subjected to a large electric field or a high stress, and this happens in function of the domain orientation texture. If a compressive stress is applied, the domains change their orientation in direction perpendicular to the stress orientation (also called ferroelasticity); if an electric field is applied, the domains tend to orient themselves parallel to the electric field. The number of allowed polar directions of each domain is limited by the crystal symmetries and the underlying grain orientation, so the alignment of a polycrystalline ceramic cannot be as perfect as in a single crystal [1].

1.1.2 Piezoelectric materials

If a mechanical stress is applied to a piezoelectric material it creates a polarization that changes in sign with the sign of the mechanical strain (traction or compression). This is called *direct piezoelectric effect* and is a linear reversible interaction between the mechanical and the electrical states. A ferroelectric material is necessarily a piezoelectric material (the opposite statement is not always true). This behavior is caused by the ability of these crystalline materials to shift electric charges in response to applied mechanical stress. On the other hand, the mechanical response to electrical stimulation is called *converse piezoelectric effect.*

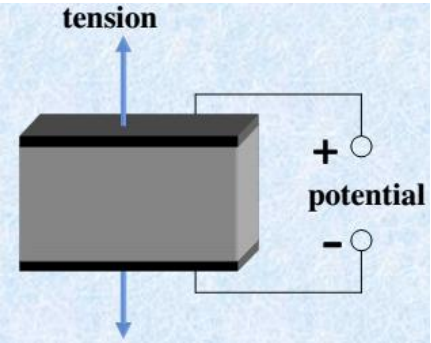

Figure 1.1 Mechanical response of a piezoelectric material with an applied voltage [2]

In an ideal piezoelectric crystal the polarization P_i is related with the mechanical stress matrix σ_{ij} as:

$$P_i = d_{ij}\sigma_{ij} \quad (1)$$

Where d_{ij} is the piezoelectric tensor. For a tetragonal material like $BaTiO_3$the piezoelectric tensor is (following the Einstein summation convention [3]:

$$d_{ij} = \begin{pmatrix} 0 & 0 & 0 & 0 & d_{15} & 0 \\ 0 & 0 & 0 & d_{15} & 0 & 0 \\ d_{31} & d_{32} & d_{33} & 0 & 0 & 0 \end{pmatrix} \quad (2)$$

Is important to know that the length variation is $\Delta L = \pm d_{33} V$, where V is the applied voltage on the tip.

These materials are used for numerous applications like high speed laser beam deflection, ultra-high density data storage or, in this case, for the production of Multilayer Piezoelectric Actuators (MPA) for the fuel injection valves in diesel common rail engines. The performance of these devices depends on the accuracy of the domains patterns, and this could be investigated with a Piezoresponse Force Microscope (PFM).

1.1.3 Perovskite structure

Perovskite-oxides have the structural formula ABO_3, in which A is the large cation (Ba^{2+} or Pb^{2+}) and B is a medium size cation (Ti^{4+} or Zr^{4+}). Ferroelectric perovskites are cubic at high temperatures, but below the T_C they become non cubic (tetragonal, rhombohedral, etc.) and polar. This behavior is due to the fact that in the cubic phase, the cations are located at the center of the oxygen cages, while in the polar phases they are shifted off the center in specific crystallographic directions, in a way that leads to the creation of dipoles oriented in parallel throughout the ferroelectric domain. With an electric field is possible to switch the direction of the displacement of the cations in reference to the oxygen in a way that upon removal of the electric field the dipole stays in the new orientation.

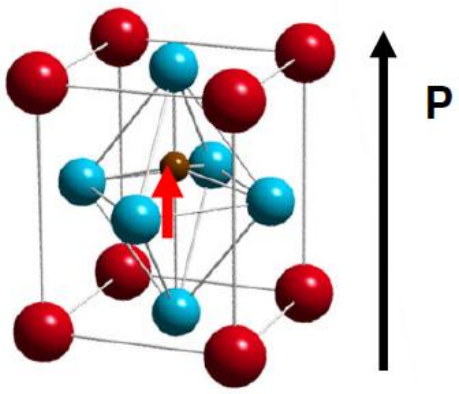

Figure 1.2 Graphic representation of the perovskite atomic structure [4].

1.1.4 Lead Zirconate Titanate PZT

Lead zirconate titanate, $Pb(Zr_xTi_{1-x})O_3$ with x=0.52-0.54, is the most widely used piezoelectric ceramic. PZT is a solid solution (alloy) of lead titanate and lead zirconate. From Figure 1.3 it is possible to see that PZT at the morphotropic boundary possesses a mixture of rhombohedral, tetragonal and monoclinic phases, which is at the basis of the highest piezoelectric d_{33} constant, *dielectric constant* and *electromechanical coupling factor* (the fraction of electrical energy it can convert into mechanical energy and vice versa) that is obtained in this compositional range. This is the composition most frequently used for piezoelectric sensors.

Sometimes the electrical properties of this material are modified with the substitution of a small fraction of the PZT cations by other cations. Doping by cations of lower valence than the substituted cations (acceptors), results in oxygen vacancies that can move in the oxygen sublattice and form reorientable dipoles with the dopant cations. This dipoles aligning in the direction of polarization in the domain, can create internal fields that stabilize the domain configuration, reducing the mobility of the domain walls. This are called *hard PZTs*. At the contrary if dopants with higher valence than the substituted cations (donors) are used, the material becomes elastically and mechanically softer. These materials are called therefore *soft PZTs* and are used for medical transducers and for sensitive pressure sensors.

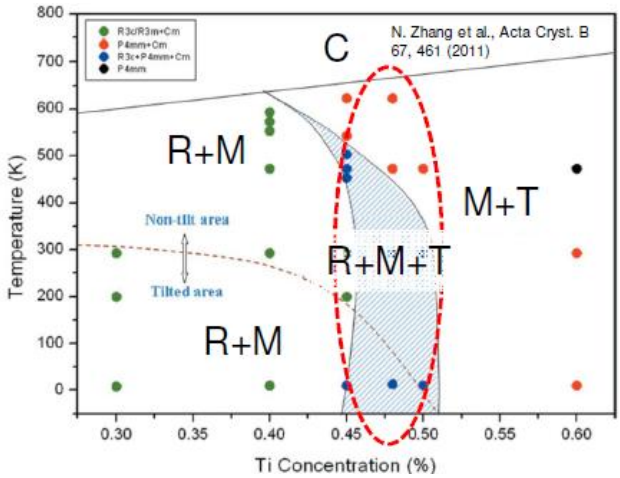

Figure 1.3 Phase Diagram of PZT ceramic. Is shown the morphotropic boundary and the phases at the different concentrations of Titanium [4]. R = rhombohedral, M = monoclinic, T = tetragonal phase.

1.2 Techniques different from PFM to characterize the microscopic texture of piezoceramics

These techniques are divided in macroscopic and microscopic techniques, and allow to determine the Domains Orientation Distribution like the PFM measurements. The texture of piezoceramics is represented as an Orientation Distribution Function (ODF), that is defined as a Multiple of a Random Distribution (MRD). MRD is the density of domains oriented in a certain direction (g) with respect to the density of domains in a randomly oriented material, with g given by Euler angles (ϕ,ϑ,ψ).

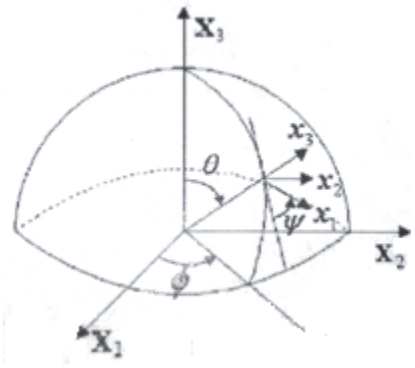

Figure 1.4 Representation of the Euler Angles on a hemisphere.[5]

1.2.1 Macroscopic methods

-*Etching*: Exploiting the differential etching speed of the different crystallographic directions it's possible to detecting the out-of-plane domain contrast. Is used only for qualitative comparisons.

-*Indentation:* The use of Vickers indentations and the measurement of the crack length (with respect to the sample or the poling axes) allows to evaluate the preferential domain orientation. Because the tensile stress at the crack tip induces the domain switching, so the domain tries to align themselves perpendicular to the crack, increasing the activation barrier of the crack propagation process. If the crack is parallel to poling it induces a non-180° domains switching; if the crack is perpendicular to poling it doesn't induce any switching. As a consequence, the crack parallel to poling are shorter than the perpendicular cracks. The unpoled material has an intermediate behavior between the 2 cases.
The *crack grow resistance* can be calculated by the following equation:

$$K_F = \chi \frac{P}{c^{3/2}} \qquad 3)$$

Where χ is a parameter related to the shape of the indentation crack, P is the indentation load (N), and c is the half of the length of the crack.

1.2.2 Microscopic methods

-*Diffraction Methods*: These methods can be divided in Laboratory X-Ray Diffraction (XRD), Synchrotron XRD and Neutron Diffraction. The first is readily achievable in many research institutions, but allows only surface-sensitive measurements. At the contrary, synchrotron XRD and neutron diffraction can penetrate in the materials further than laboratory XRD, but these sources can be obtained only in few facilities around the globe. These techniques display as a result the same diffraction pattern, or in the case of area detector, by the integration of the Debye-Scherrer rings is possible to obtain the traditional (2ϑ) diffraction pattern. The integrated intensity of a reflection peak is directly related to the number of crystallites in which the reflection is aligned with the direction of scattering. The ODF can be obtained by a simple measurement and is given in MRD, with respect to the non-oriented state.

-*Electron Back Scattered Diffraction*: This method is realized in a field-emission scanning electron microscope and is based on the diffraction of a collimated electron beam from lattice planes. The electron beam is impinged on the sample surface at an angle of 70° to improve signal intensity. The diffracted electrons are contained in an electron cone (with an opening 2ϑ, in which ϑ is the Bragg angle) that hit a phosphor screen and generate a pattern of intersecting lines. The position and orientation of these lines depend on the distance and the orientation of lattice plane, so it is possible to obtain an orientation map and an orientation histogram. EBSD is only sensitive to the geometrical constrains and thus is only capable of detecting non-180° domain boundaries. This method is not yet widespread because of the difficulty of sample preparation, in fact to obtain a good contrast in the intersecting lines an extremely well-polished surface is needed.

-*Raman Spectroscopy*: This method is based on the inelastic scattering of the light by matter. A monochromatic laser radiation is focused on the surface of the material by a microscope objective. The consequent scattered light is then collected by the same objective; the elastically scattered light is filtered out, and the Raman-scattered light is analyzed in a spectrograph equipped with a multichannel CCD

detector. The scattered radiation energy depends on the incident radiation energy and on the energy of the material's phonons. Phonons are influenced by chemical bonding character and bond length, phase symmetry/distribution and crystallographic direction. The Raman spectra are constituted by an ensemble of peaks, each with its own character, and the treatment of this spectra is performed with some spectroscopic functions or harmonic oscillators that are used to evaluate the ODF of the surface by monitoring the intensity of peaks in a polarized configuration. In such configuration, the polarized Raman spectral intensity is a function of the angle between the crystal main direction and the laser polarization. The angular dependence of the intensity upon sample rotation is thus a measure of the degree of orientation of the underlying domain distribution [4].

1.3 Introduction to piezoelectric actuators

These actuators belong to the class of the solid state actuators and have several properties in common with the other solid state actuators such as actuator based on magnetostriction or thermal expansion. In comparison to the conventional actuator, solid state actuators have a much lower displacement but a better displacement accuracy. The main advantage of the piezoelectric actuators is their high response speed. This unique performance together with the multilayer technology opens up new innovations leading to a breakthrough in piezoelectric actuator applications.

1.3.1 Piezoelectric multilayer actuators

These devices offer the advantage over their electromagnetic counterparts of smaller dimensions, less heat build-up and shorter attack time. However, a relatively high electric field (from 500 to 2000 V/mm) is required to realize the largest possible deformation of an actuator of a certain size. This means that these ceramics are poorly matched with conventional supply voltages (<200V), but the problem is solved by fabricating actuators from a number of very thin electrode layers. Due to the high sintering temperature of PZT ceramics, platinum electrodes were needed, but now is possible to use other type of electrodes applying a metal injection process for forming internal conductors and electrodes, or reducing the sintering temperature of PZT ceramics below 1130°C. The sintering temperature reduction can be done by optimizing the powder morphology, by the addiction of sintering aids, and with the application of a rate controlled sintering process. The largest application of these actuators is in the fuel injection valve driven by a piezoelectric multilayer actuator. It is possible to develop a multilayer actuator that fulfils the mechanical, electrical, reliability and cost requirements.

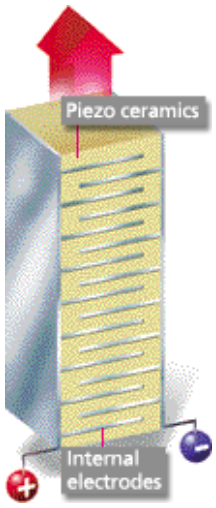

Figure 1.5 Piezoelectric Multilayer principals of operation [6].

In Figure 1.5 is shown the structure of the multilayer stack for Diesel injection. Due to the interconnection of the layer electrodes at the corner of the stack only very small non contacting areas are necessary, so the related inactive piezoelectric regions are also very small. This is important, on the one hand to increase the reliability of the device, avoiding the problems linked to large inactive regions of a normal multilayer capacitor; and on the other hand to still apply the inexpensive standard multilayer processing technology. The stacks with a size of 7x7x30mm^{3}are embedded in polymer and have about 360 single layers with 80 μm thickness. The actuator shows a large signal piezoelectric constant d_{33}=700pm/V , and a relative elongation of $1.4*10^3$ at a driving field strength of 2 kV/mm. It is possible to reduce the sintering temperature for a PZT with an high T_C(355°C) by pressure less sintering approach. In this way dense multilayer stacks are produced.
By the superposition of a static mechanical load, even under very hard driving conditions, a fatigue live time $>10^9$ cycles can be guaranteed, and with unipolar driving conditions no mechanical fatigue of the PZT ceramic occurs.
The modern common rail injection systems consist of a high pressure compressor, a control unit, and a fast fuel injection valve for each cylinder made by piezoelectric multilayer stacks. Due to the fast response of the injection valve some advantages have been achieved:

-noise reduction;

-reduction of NO_x emissions;

-more precise time control of the main injection, that results in a low smoke emission(reduction also of the NO_x and HC emission).

The measure of the domains of this devices is needed because the domain structure influences the piezoelectric performances, and the presence of stresses, temperature variations and cracks affect the domain structure. The last ones are detrimental for the performance and can be stopped by the domain switching (a sort of transformation toughening).

Figure 1.6 Modern multilayer actuators design [6].

1.4 Material aspects of PZT multilayer actuators

1.4.1 Design of multilayer actuators

From Figure 1.7 is possible to see a typical design of a *multilayer stack actuator*. The gray sheets are the inner electrodes made by Ag-Pd 70/30, the single layer thickness between 2 electrodes is 80 μm. The square inactive contact regions are small compared to the active cross section of the actuator, so the no-load deflection of the actuator is reduced (by only some percent) by the clamping of the inactive contact volume. The inner electrodes of one polarity are connected by sputtered electrodes or by burned-in silver paste strips, and the bond strength of these connections must be guaranteed.
Another structure very common is the *multilayer capacitor*, where two opposite areas are used for contacting. The advantage is the larger electrical contact area between external conductors and inner electrodes, the disadvantage is the reduced no-load deflection due to the increased clamping volume.

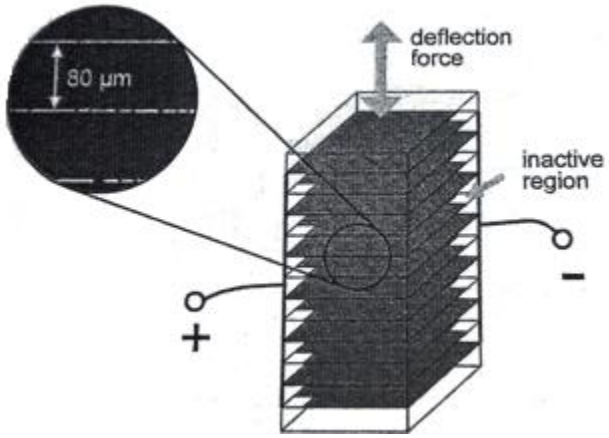

Figure 1.7 Multilayer stack actuator design in which the distance between the electrodes is shown.[7]

1.4.2 Stability of elongation and absolute length

The motor application must not only reach 10^9 operating fatigue cycles, but must also suffer thousand of temperature cycles between -40°C and 180°C, without changing its absolute length and elongation for a given load condition of the system. The thermal coefficient is related to domain configuration and the polarization, and can vary between $+7*10^{-6}$ and $-5*10^{-6}$. Is important to keep it constant during the lifetime in order to guarantee a correct system function.

1.5 Fracture mechanical properties in PZT ceramics

In PZT piezoceramics is important to understand the influence of the electric field on crack propagation in the failure mechanism, because these ceramics have low strength.

1.5.1 Fracture toughness without electric field

Fracture toughness measurements of unpoled PZT ceramics show a minimum at the MPB (Morphotropic Phase Boundary). In the tetragonal and rhombohedral phase, microcracking prevails and contributed more to toughening than domain switching process (at the MPB). On the other hand some investigations on Sr-doped PZT showed an increase in toughness upon the increase of the tetragonal distortion, whereas the rhombohedral phase revealed a constant fracture toughness identical to the value at the MPB. For Poled PZT ceramics there are 2 parameters that determine the toughening effect of the switching zone:

1) The energy needed for 90° switching (which distinguishes soft and hard ferroelectric ceramics);

2) The number of disposable domains for 90° switching, which is determine by the orientation of crack path and polarization.

From X-Ray diffraction the existence of 90° switching process trigging by the crack tip stress field have been demonstrated [8]. With the Vickers indentations reveals that samples poled parallel to the crack front have the highest toughness [8].

1.5.2 Fracture toughness under applied electric field

PZT ceramics poled perpendicularly to the crack plane clearly shows a decrease of the fracture toughness with increasing electric field. This is valid if the electric field is oriented in the poling direction. On the other hand, small electric fields applied opposite to the poling direction (negative electric fields), increase the measured fracture toughness [8]. Therefore, there is a toughening effect linked to the domain switching.

1.5.3 Toughening mechanisms and models

The crack opening displacement measurements show that the crack surfaces are pressed together, which can be interpreted as stress-induced ferroelastic 90°domain switching. The high tensile strength around the crack tip, oriented perpendicular to the crack, enforce the domain to switch ferroelastically by 90° to orient themselves as near as possible parallel to the tensile stress direction. The domain switching is accompanied by a positive inelastic strain perpendicular to the crack plane, which reduces the crack opening. This explains that piezoelectric materials with higher piezo and ferroelastic strain often have higher toughness. After unloading some surface depressions remains on the material, these are due to the stress induced 90° switching process from the out-of-plane oriented domains to in-plain oriented domains. There is also an inelastic domain switching zone, the existence of which is proved by the presence of surface depression close to the crack surface (behind the crack tip), but no elastic stresses are present directly at the crack surface.
For the description of the switching zone a switching criterion is necessary. The simplest criterion is to assume a critical energy which is the product of the spontaneous polarization P_S and the coercive field E_c. The energy necessary for domain switching is delivered by mechanical or electrical work. The switching criterion is [8]:

$$\sigma_{ij}\Delta\varepsilon_{ij}+E_i\Delta P_i \geq 2P_S E_C \qquad 4)$$

Where: σ_{ij} is the stress tensor (because the ferroelastic domain switching is a shear process), $\Delta\varepsilon_{ij}$ is the change in spontaneous strain (inelastic strain), ΔP_i is the change in spontaneous polarization. This criterion is strictly valid only for a single domain, single crystal. In presence of an electric field there is a change of mechanical stresses for the domain switching, so the inelastic strain changes in magnitude. For electric fields parallel to the crack, $\Delta\varepsilon_{ij}$ will increase, at the contrary for electric fields perpendicular to the crack, $\Delta\varepsilon_{ij}$ must decrease.
Before talking about the toughening effect is important to define the *stress intensity factor* K that is an index of the of stress intensity nearby the crack tip. K is function of the sample geometry, the size and location of the crack, and the magnitude and modal distribution of loads on the material. There are three type of load that are categorized as Mode I, Mode II and Mode III :

-Mode I: is an opening (tensile) mode where the crack surfaces move directly apart;

-Mode II: is a sliding (in-plane shear) mode where the crack surfaces move relative to one another in a direction perpendicular to the leading edge of the crack.

-Mode III: is a tearing (antiplane shear) mode where the crack surfaces move relative to one another and parallel to the leading edge of the crack.

Therefore, the stress intensity factor are designated for the three different modes KI, KII and KIII.
The toughening effect is proportional to h and $\Delta\varepsilon_{ij}$, but there are no commonly accepted models which predict the toughening of ferroelectric ceramics.

The toughening ΔK_B depends on the grain size, and the frontal zone of the crack leads an additional toughening ΔK_F that is influenced by the applied electric field E and by eventually existing crack bridging. During the crack extension the frontal zone moves until the maximum $\Delta K_{W,max}$ is reached.

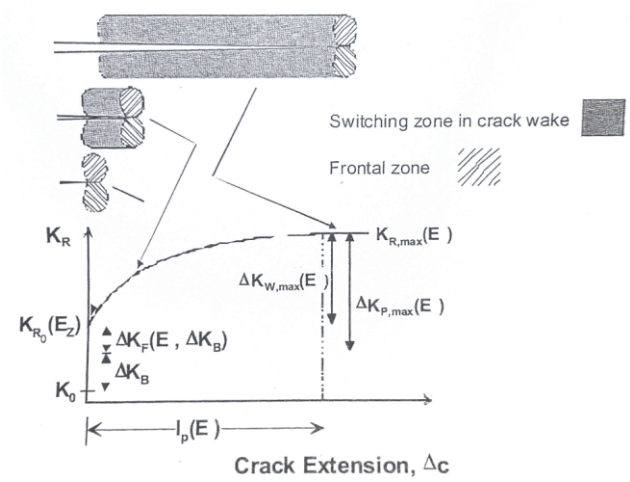

Figure 1.8 Switching zone model with corresponding R-curve [8].

1.5.4 Interface Fracture in Actuators

The lifetime of piezoelectric ceramic actuators depends on the fracture properties of the piezoceramic, and on the extension of the electrode/ceramic interface. As explained above, in this devices some inactive zones are present and during the poling of the actuator, tensile stresses acting on this regions could cause a severe failure phenomenon. In this case the cracks run along the electrode-ceramic interface. The toughness inside the PZT-ceramic layer as well as the toughness of a crack driven perpendicular to the electrodes is higher than the last case in which the crack was parallel to the electrode interface.

Chapter 2
Piezoresponse Force Microscopy

2.1 Introduction to Scanning Probe Microscopy

The SPM family is composed by numerous techniques that use a probe (a sharp tip) to scan the surface at high resolution. The most important techniques in this family are the Scanning Tunneling Microscope (STM), the Atomic Force Microscope (AFM) and the Piezoresponse Force Microscope (PFM) that is a type of AFM with a voltage applied to the tip.

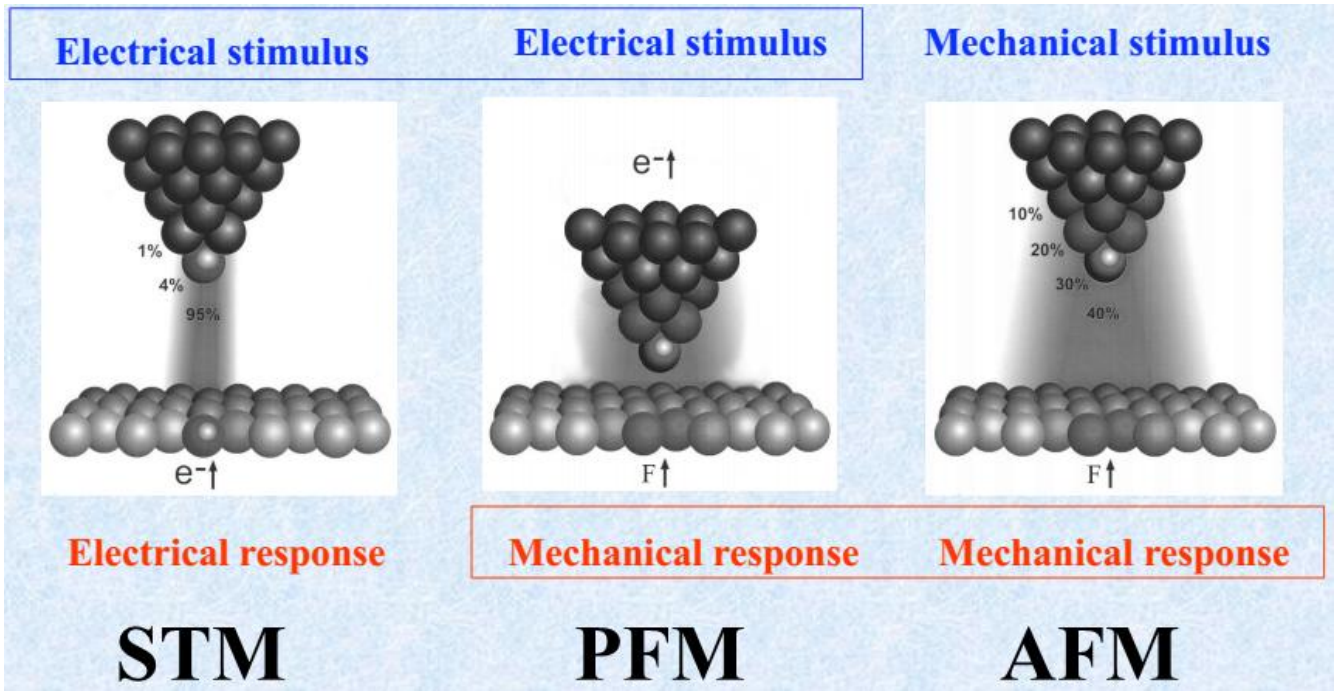

Figure 2.1 Principal of operation of the 3 most important technique of the SPM family [2].

In Figure 2.1 are shown the differences between the 3 methods. STM is based on the tunnel effect that take place from the tip to the surface. This mean that there is an electrical stimulus that produce an electrical response from the surface. The other two methods measure the mechanical response of the surface produced by a mechanical stimulus (AFM) or an electrical stimulus (PFM).

2.2 Piezoresponse Force Microscope

A PFM is a non-invasive imaging method with a good lateral resolution (about 10nm) in which a Scanning Force Microscope (SFM) is operated in contact mode with an applied voltage applied to the conductive tip.

2.2.1 Principle of operation

The tip follows the thickness changes due to the bias-induced piezoelectric surface deformation; this produces a deflection of the cantilever that is read out with a segmented photo-detector (by the deflection of a laser beam). So the measured signal is dominated by the piezoelectric deformation of the ferroelectric sample.

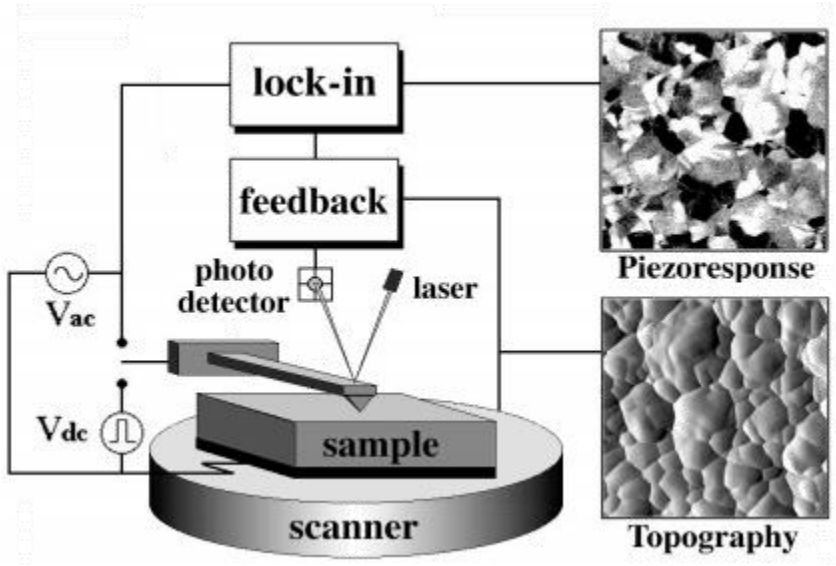

Figure 2.2 Standard configuration of PFM [9]

By the feedback, the topography graph of the sample surface is obtained and by the lock-in amplifier the piezoresponse of the sample surface is achieved. There are 3 possible movements of the cantilever due to forces acting on the tip: deflection, buckling and torsion:

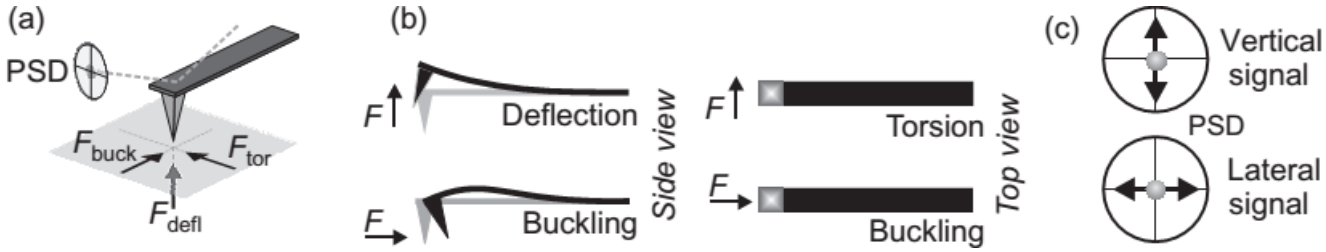

Figure 2.3 The 3 possible movements of the cantilever due to forces acting on the tip: deflection, buckling and torsion [9].

PFM is not restricted to specific crystallographic orientation because recording the torsion of the cantilever is possible to reveal the in-planes movements of the sample surface. The torsion of the cantilever is measured in the Lateral-PFM (LPFM) that is an imaging method to evaluate the in-plane component of polarization. This is the way to map the domains structures of crystal faces which do not exhibit an out-of-plane response (change in thickness of the sample). To obtain full information about the local deformation of the sample underneath the tip the out-of-plane and 2 in-plane PFM signals have to be recorded; this is done to separate deflection and buckling (read out as vertical signals). The separation

is possible because all the angular-dependent contributions are attributed to buckling. This means that for a complete characterization of the ferroelectric domains is necessary a three dimensional (3D) reconstruction of polarization using a combination of two Vertical-PFM and two Lateral-PFM (one at 0° (x-LPFM) and one after rotation at 90° y-LPFM).

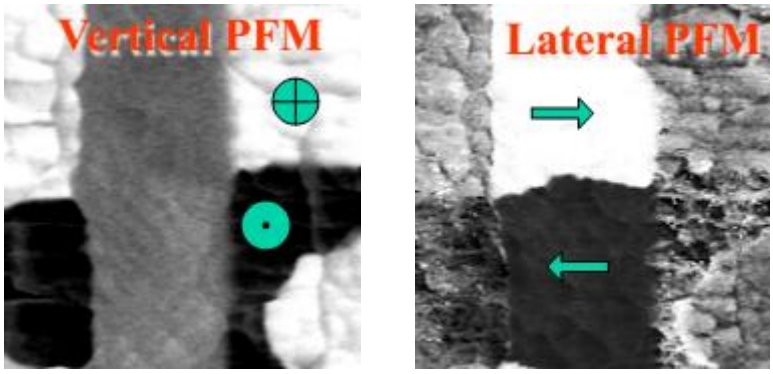

Figure 2.4 Images of a Vertical PFM and a Lateral PFM in which is shown that from the vertical one is possible to see only the vertical displacement, and from the Lateral one, only the lateral displacement [2].

2.2.2 Conductive Tip

The tip is attached on the top of a cantilever-type spring and connected to an alternated voltage (V_{ac}). It could be made by n-doped silicon, but an oxide film of a few nm thickness could grow on its surface. As a consequence, the electric field spread and decay with the oxide layer that reduces the lateral resolution. Therefore, is possible to use tips with conductive coatings such as Ti, TiN, PtIr, Au, CrAu with a radius as small as 20nm. However, this tips suffer from a fast degradation, since operation of the SFM in contact mode has an abrading effect on the coating. To solve this problem, also diamond coated tips exist that have been proven to be more resistant, at the expense of a relative large tip radius (60nm). In the last years another type of tip has been developed, a single multiwalled carbon nanotube has been attached to the pyramidal tip of a silicon cantilever. The carbon nanotube can completely bend because it has high elastic modulus, is conductive and has a radius of 20 nm. Otherwise there are also Electron Beam Deposited Tips, that are high density carbon tips (diamond-like carbon).

2.2.3 Cantilever

The stiffness of the cantilever is in first approximation no role for PFM operation. However, very soft cantilevers with a spring constant $k<1N/m$ generally yield inferior PFM images. This is probably due to an uncontrollable wobbling of these cantilevers. Consequently it's better to use rather stiff cantilevers ($k>1N/m$). Much more important than the stiffness of the cantilever is its *resonance frequency* f_{free} and in particular the *contact resonance frequency* f_{cont}. The assumed relationship between these two frequencies is $3\text{-}5f_{free}=f_{cont}$, and it depends on the sample stiffness. This is important for dynamic

processes in which faster scanning is required and thus a higher frequency f of the alternating voltage is applied to the tip. There are two possibilities for choosing f:

-as in standard PFM, f is set far from the resonance frequency f_{cont}, and it allows to scan faster with otherwise unchanged performance.

-is possible to take advantage from the resonance-enhancement and set $f \approx f_{cont}$. This operation mode is named *resonance PFM.*

However, high-frequency PFM has not attained much attention, because the standard PFM yields images with sufficient quality and a possible improvement of the quality using these methods has not been demonstrated so far.

2.2.4 Lock-In Amplifier

Is used to detect the oscillation of the cantilever during the PFM measurements. The LIA can calculate X-, Y-, R- or ϑ- output, and the signal range of the output range from -10.5V to +10.5V.
The sensitivity S of the LIA has to be maximized as long as one does not suffer from overload.
The time constant τ is related to the scanning parameters: scanning speed v, pixel number n, and image size s x s. The sampling frequency can be expressed by $f_s = vs/d$. The lock-in time constant must be set so that $\tau > (\pi f_s)^{-1}$ to allow an optimum data acquisition. But τ must be as small as possible to achieve maximum scanning performance, so a good compromise is $1/f_s > \tau > 1/3f_s$. The setting of τ is determined by the noise of the system and therefore by the magnitude of the PFM signal and the sensitivity S of LIA. The scanning speed should be chosen to be $\frac{\frac{1}{3}S}{n\tau} < v < \frac{S}{n\tau}$.

2.2.5 Standard parameter configuration of PFM

For standard PFM the voltage V_{AC} is set to values of f=10-100kHz and the amplitude V=1-10V. The frequency f has to be:

- High enough to not affect the recording of the topographical image performed simultaneously (the time constant of the feedback should be large with respect to $1/f$;

-Small with respect to the contact resonance frequency f_{cont} of the cantilever. This condition is fulfilled using stiff cantilevers.

It's also important to avoid any other resonance of the system because any measurement close to a resonance is very sensitive with respect to amplitude and phase information.
Due to the small tip radius, even moderate voltages lead to extremely high local electric fields which might modify the domain patter by poling. The amplitude V of the voltage has to be:

-for thick bulk samples V=10V;

-for thin films V<1V is most appropriate.

2.2.6 PFM measurements in Contact Mode

The PFM measurements in contact mode requires that the tip is permanently in direct contact with the surface. Two methods exist to operate the contact mode:

1) Constant Height method: This is the oldest one, because it doesn't need a feedback system. It consists on maintain constant the level of the cantilever, with respect to the first point of measurement, during all the scanning process.

2) Constant Force method: this mode is more complex than the last one, because it requires a feedback system to constantly adjust the piezoelectric actuator (in the z-direction) to maintain the applied force on the cantilever constant. The topographic image results from the recorded motion of the actuator in z-direction. The experiments of this work have been done with this method.

2.3 Principles of PFM

2.3.1 Deflection, Amplitude, Phase and Magnitude

The tip in contact with the surface detects the piezoelectric response as the first harmonic component $A_{1\omega}$ of the tip deflection, $A=A_0+A_{1\omega}\cos(\omega t+\varphi)$ induced by the periodic bias $V_{tip}=V_{dc}+V_{ac}\cos(\omega t+\varphi)$ applied on the tip. $A_{1\omega}$is the *deflection amplitude* and is given by the tip motion in units of length. Another important parameter is the phase φ that yields information on the polarization direction below the tip. If the application of positive tip bias results in the expansion of the sample the surface oscillations are in phase with the tip voltage $\varphi=0°$; therefore, this is a c^- ferroelectric domain. At the contrary the opposite c^+ ferroelectric domain present a phase $\varphi=180°$.Sometimes the phase is denoted by ϑ. The piezoresponse *amplitude* $A=A_{1\omega}/V_{ac}$ ([nm/V]) defines the local electromechanical activity of the surface. In the acquisition of PFM data there are some difficulties due to:

1) Non-negligible electrostatic interactions between the tip and the surface A_{el};

2) Nonlocal contribution due to capacitive cantilever-surface interaction A_{nl}.

The measured piezoresponse amplitude is: $A=A_{el}+A_{piezo}+A_{nl}$. Perhaps for quantitative PFM imaging is necessary to maximize the electromechanical contribution (A_{piezo}) to achieve predominantly the electromechanical contrast. However PFM images can be conveniently represented as $A_{1\omega}\cos\varphi/V_{ac}$, but the real collected signal is the output of the lock-in amplifier: $Pr=aA_{1\omega}\cos\varphi/V_{ac}$ (given in[V]), where a is a calibration constant determined by the lock-in settings and the sensitivity of the photodiode. The Pr

signal also known as Amplitude, is the X-output of the LIA (Lock-In Amplifier) and contains the complete information (the Y-output is free of any information) about the scanned surface. Amplitude graph can be displayed by the LIA in 2 graphs, one for the Magnitude (PR or R) and one for the Phase (φ or ϑ). The Magnitude R of the Amplitude is a quantitative measure for the local piezoelectric constant that is symmetric to the component d_{33} of the piezoelectric tensor. The phase ϑ carries the information of the domains orientation, which could be parallel or anti-parallel (0°/180°). The Amplitude images show only the domains boundaries, but the domain orientation is not visible from them.

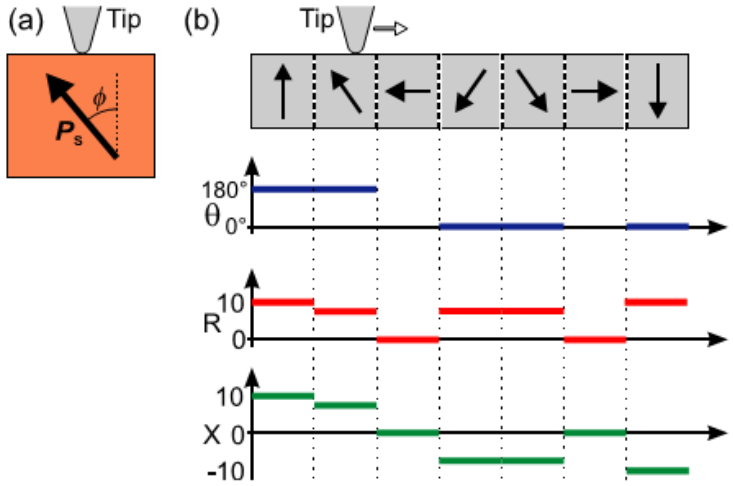

Figure 2.5 (a) A sample exhibiting a ferroelectric domain whose polarization vector is oriented at an angle φ with respect to the sample surface. (b) Phase ϑ, amplitude R and X-output obtained on a sample with the polarization vector pointing in different directions [10].

The relation between X-Y representation and R and ϑ is that X=Rsinϑ and Y=Rcosϑ; the LIA determines (X,Y) electronically and calculates (R,ϑ) in a subsequent step. So R and ϑ outputs signals implicate a nonnegligible update rate and thus have a significant data hole (Figure 2.6).

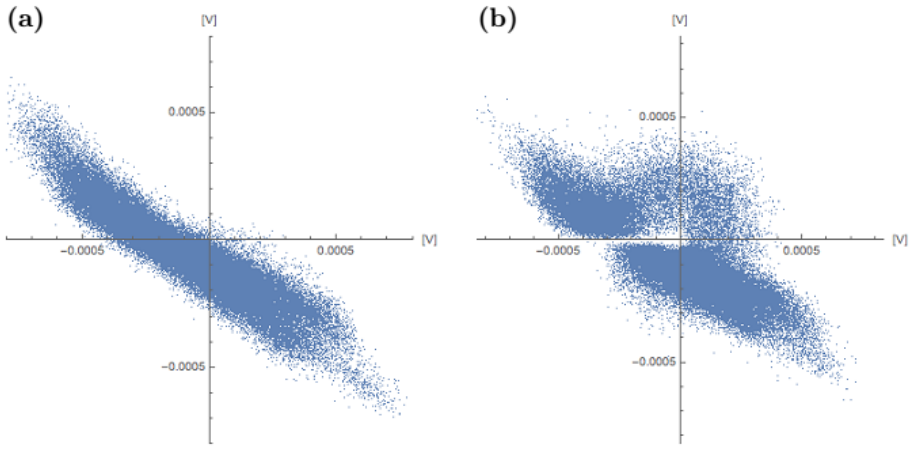

Figure 2.6 Data of an out-of-plane measurement. (a) X- and Y-output of the LIA; (b) R-and ϑ-output of the LIA presenting a significant data hole and divergent data distribution around the origin of the x-y graph [11].

2.4 PFM image formation

The vertical displacement of the tip w_3^t, results from a bending of the cantilever by the angle $\vartheta_d \sim w_3^t/L$, where L is the cantilever length. In normal contact mode imaging the AFM employs a feedback loop to keep the cantilever deflection at a set point value by adjusting the *height* of the cantilever base while scanning. This feedback signal provides a *topographic image* of the surface, which is relatively insensitive to the exact details of cantilever and tip motion.

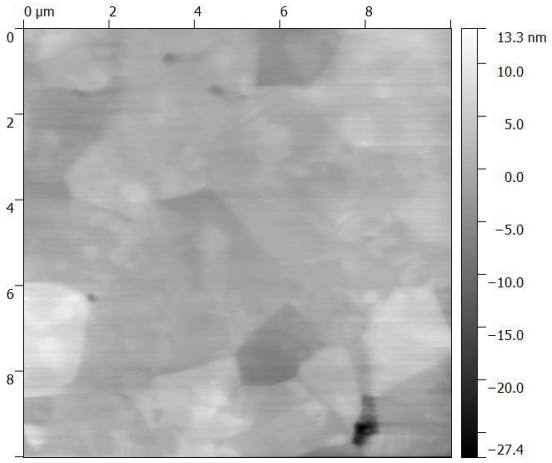

Figure 2.7 Example of topography image of the unpoled sample made with a HA-HR-DCP tip. It is possible to see the grains boundaries.

If there are only pure vertical motions of the tip, the measured signal can be directly related to the tip displacement (with a calibration procedure) because $A=w_3^t$. But there is another contribution in the deflection signal that takes place from the buckling oscillations of the cantilever. These oscillations are the primary source of nonlocal electrostatic signal contribution in PFM contrast, and can be reduced by increasing cantilever stiffness. The longitudinal motion of the tip end, w_1^t, results in the cantilever bending $\vartheta_d \sim w_1^t/H$, where H is the tip height. The piezomechanical response of a domain is called *PFM signal*, and the difference between PFM signal obtained from different domains (in a multi-domain sample) is denoted by *PFM contrast*. The maximum contrast achievable is between two 180° domains oriented normal to the sample surface (↓↑).

2.4.1Vertical Displacement

With an arbitrary crystallographic orientation the application of an AC-Voltage results in the surface displacement $\mathbf{w}=(w_1,w_2,w_3)$. The usual interpretation of the data is that the displacement of the tip apex in contact with the surface is equal to the surface displacement ($\mathbf{w}_t=\mathbf{w}$). This is valid for the normal component of the tip displacement ($w_3^t=w_3$), if the tip-surface spring constant is 2-3 orders of magnitude higher than the cantilever spring constant. Alternatively, is possible to amplify the effective PFM signal, one-setting the regime when the tip loses contact with the surface. This is useful for example when PFM imaging at cantilever resonance or using high modulation amplitudes. However the assumption $w_3^t=w_3$,

can be applied with a proper calibration approach of the tip-surface junction spring constant that must not vary.

2.4.2 In-plane components

The use of a four-quadrant photodetector allows to detect the lateral piezoresponse components in the direction normal to the cantilever axis. These components are evaluated as torque of the cantilever.
The cantilever orientation is **n**=(cosϑ_c,sinϑ_c,0), where ϑ_c is the angle between the long axis of the cantilever, and x-axis of the laboratory coordinate system. The Lateral-PFM signal is proportional to the projection of the surface displacement on the vector perpendicular to the cantilever axis:

$$PR_p=b(-w_1\sin\vartheta_c+w_2\cos\vartheta_c) \quad 5)$$

But if the surface has low symmetry this description become more complex because of the difficulty to find the relevant parameters. There are two problems in the determination of the LPFM:

-The response amplitude doesn´t scale linearly with the modulation like in VPFM but could eventually saturate, because the displacement of the tip apex can be significantly smaller than that of the surface (for example due to the onset of sliding fiction).

-The presence of a piezoresponse component along the cantilever axis (buckling) given by a longitudinal displacement that also results in the change of the deflection angle. This means that is an additive contribution to the VPFM signal:

$$PR_l=c(w_1\cos\vartheta_c+w_2\sin\vartheta_c) \quad 6)$$

that become:

$$PR_v=aw_3+c(w_1\cos\vartheta_c+w_2\sin\vartheta_c) \quad 7)$$

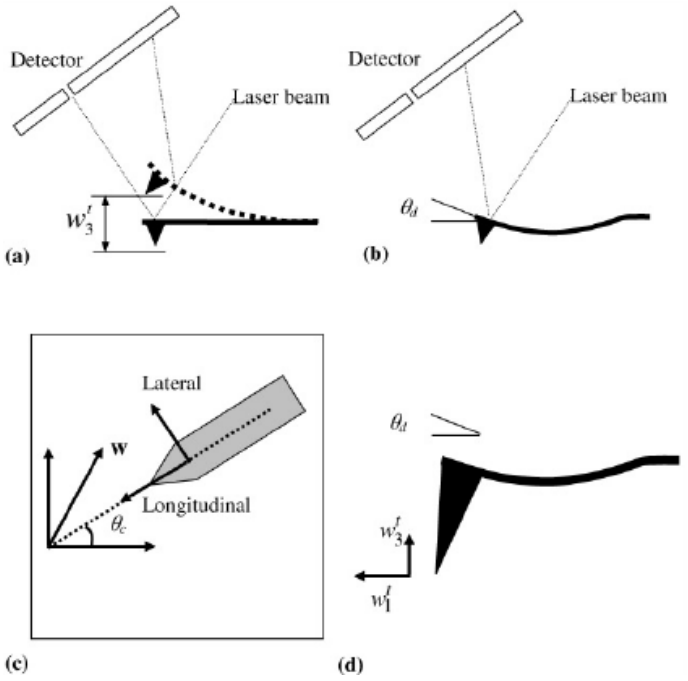

Figure 2.8 a) Vertical tip displacement in beam-deflection AFM is achieved through the detection of cantilever deflection angle. b) Distributed force results in cantilever buckling and change in the deflection angle, detected as apparent tip-height change. c) Contributions to cantilever deflection. In-plane cantilever orientation in the arbitrary laboratory coordinate system including lateral perpendicular to the cantilever axis. And longitudinal along the cantilever axis components. d) Longitudinal surface displacement along the long cantilever axis results in the change in deflection angle, providing contribution to the VPFM signal [9].

2.4.3 Three Dimensional Piezoresponse Vector

The determination of the contribution of buckling to the vertical signal can be done from comparison of VPFM images obtained for two different cantilever orientation (0° and 90°). The problem is that the proportionality coefficients are different for VPFM and LPFM and are unknown. This means that the single combination of one VPFM and one LPFM are not sufficient to determine the 3D Piezoresponse Vector of a surface. The complete 3D reconstruction of electromechanical response from VPFM and LPFM is possible only if:

-the buckling contribution in VPFM signal is small ($c \ll a$) ;

-the vertical and lateral sensitivities are carefully calibrated;

-the number of possible orientations of polarization vector is known and limited.

The problem of the 3D reconstruction is that the sample has to be symmetrically rotated with respect on the cantilever and is necessary to locate the same microscale region on the surface after sample rotation.

For this measurements 2 LPFM images of 2 orthogonal direction of the sample with respect to the cantilever are necessary: x-LPFM (ϑ_c=0) and y-LPFM (ϑ_c=π/2).
The x-LPFM signal is $xPR_l=bw_2$, the VPFM signal is $xPR_v=aw_3+cw_1$; the y-LPFM signal is $yPR_l=bw_1$ and the VPFM signal is $yPR_v = aw_3 + cw_2$. The proportional coefficient b is assumed to be the same for both x-LPFM and y-LPFM. Thus the relationship between the measured piezoresponse signal and the surface displacement vector is:

$$\begin{pmatrix} xPR_v \\ xPR_l \\ yPR_v \\ yPR_l \end{pmatrix} = \begin{pmatrix} c & 0 & a \\ 0 & b & 0 \\ 0 & c & a \\ c & 0 & 0 \end{pmatrix} \begin{pmatrix} w_1 \\ w_2 \\ w_3 \end{pmatrix} \quad 8)$$

Assuming that the VPFM does not contain a significant contribution from the longitudinal surface displacement (buckling) c=0 and the x-VPFM and y-VPFM image are identical so $xPR_v=yPR_v=vPR$:

$$\begin{pmatrix} xPR_l \\ yPR_l \\ vPR \end{pmatrix} = \begin{pmatrix} 0 & b & 0 \\ b & 0 & 0 \\ 0 & 0 & a \end{pmatrix} \begin{pmatrix} w_1 \\ w_2 \\ w_3 \end{pmatrix} \quad 9)$$

This equation contains 2 calibration constants: a and b. a can be determined by using an external reference (a piezoelectric sample with well-known piezoelectric constant) or alternatively by mounting the sample on a calibrated piezoelectric transducer that calibrates the tip oscillation amplitude. b isthe calibration constant for the LPFM and strongly depends on the properties of the tip-surface contact. It is possible to measure the LPFM signal on a sample with known properties and verify the linearity of response with driving amplitude. This approach is limited by the lack of exact solution for lateral deformation in PFM geometry and the high sensitivity to surface conditions. Alternatively, it is possible to perform a relative calibration of sensitivities of VPFM and LPFM signals. Comparing the absolute value of the electromechanical response (R=Magnitude) of different regions in VPFM and LPFM images, it is possible to determine the relative sensitivities between VPFM and LPFM.
However, for homogeneous ferroelectrics, using the condition $w_1^2+w_2^2+w_3^2$=const that provides an additional constraint, a combination of VPFM , x-LPFM and y-LPFM is sufficient to reconstruct completely the displacement vector without the evaluation of the a/b ratio. For inhomogeneous ferroelectrics, like two-phase or biological materials is necessary a calibration, so the ratio a/b must be known for rigorous 3D reconstruction of the response vector. Using this approximation, the results presented in this work are only qualitative evaluations, because PZT multilayers have not an homogeneous phase, but have a mixture of tetragonal and rhombohedral phases.

2.4.4 Relationship between the electromechanical response vector and the piezoelectric properties

With a proper calibration the piezoresponse data are converted into the full electromechanical response vector $w=(w_1,w_2,w_3)$. From this vector, the surface displacement amplitudes in the laboratory

coordinate system are $vPR=w_3/V_{ac}$, $xPR_l=w_2/V_{ac}$ and$yPR_l=w_3/V_{ac}$. The piezoelectric properties of materials are described by the piezoelectric constant tensor d_{ij} (i=1,…,3;j=1,…,6) that defines the relationship between the strain tensor and the electric field:

$$X_j=d_{ij}E_i \qquad 10)$$

The d_{ij} is given in the laboratory coordinate system in which axis 3 is normal to the sample surface and axis 2 is oriented along the long cantilever axis. The piezoelectric constant d_{33} determines the mechanical response in the z direction due to the electric field in the z-direction, and is typically identified by the VPFM signal. For the same tip-sample geometry x-LPFM is related to d_{32}(displacement in y direction due to a z-direction electric field) and y-LPFM is proportional to d_{31}(displacement in x direction due to a z-direction electric field).
The problem is that for vertically oriented c domains the x-LPFM and y-LPFM signals are equal to zero, but the relatives piezoelectric constants $d_{31}=d_{32}\neq 0$. To solve this problem it is important to know that the strain and displacement are not equivalent, and the strain tensor is related to the components of the displacement vector, $\mathbf{u}=(u_1,u_2,u_3)$ as:

$$X_{ij}=\begin{pmatrix} \frac{\partial u_1}{\partial x_1} & \frac{1}{2}\left(\frac{\partial u_1}{\partial x_2}+\frac{\partial u_2}{dx_1}\right) & \frac{1}{2}\left(\frac{\partial u_1}{\partial x_3}+\frac{\partial u_3}{dx_1}\right) \\ \frac{1}{2}\left(\frac{\partial u_1}{\partial x_2}+\frac{\partial u_2}{dx_1}\right) & \frac{\partial u_2}{\partial x_2} & \frac{1}{2}\left(\frac{\partial u_2}{\partial x_3}+\frac{\partial u_3}{dx_2}\right) \\ \frac{1}{2}\left(\frac{\partial u_1}{\partial x_3}+\frac{\partial u_3}{dx_1}\right) & \frac{1}{2}\left(\frac{\partial u_2}{\partial x_3}+\frac{\partial u_3}{dx_2}\right) & \frac{\partial u_3}{\partial x_3} \end{pmatrix} \qquad 11)$$

Therefore, relating the displacement to the electric field requires a partial differential equation system that has to be solved for proper boundary conditions. From equation 11) is possible to find the strain tensor X_{ij}, and use it in 10) to find the piezoelectric constant tensor. The difficulty in this procedure is that the tip acts as a movable top electrode that gives a highly non-uniform electric field. For the ideal case in which the electric field is uniform in z direction on a rectangular symmetric block, the displacement at the center is:

$$u=(d_{35}V,d_{34}V,d_{33}V) \qquad 12)$$

So the component of the piezoelectric constant tensor d_{33} is given by the VPFM signal: $d_{33}=vPR$, the component $d_{35}=xPR_l$ and the component $d_{34}=yPR_l$. d_{31} and d_{32} results in axially symmetric deformation of material that does not contribute to displacement at the center. For materials with low symmetry these solutions can be assumed to provide a good first approximation to describe PFM data.

2.4.5 Crystal orientation effects

It is conventional to represent the piezoelectric constant tensor with the coordinate system related to the orientation of crystallographic axis of the material d_{ij}^0. This allows to tabulate the material-specific values, and limit the number of non zero components. Assuming that $vPR=d_{33}$, the specific PFM signal

can be related to crystal orientation using a coordinate transformation that aligns the z-axis of the crystal coordinate with the z-axis of the laboratory coordinate system by using two rotation angles. This is not valid for LPFM signals, because in this case 3 rotation angles are needed, which can be described by the Euler angles (ϕ,ϑ,ψ). In this case the definition is used, in which the identity transformation corresponds to $\phi=\vartheta=\psi=0$. The relationship between the d_{ij} and the d_{ij}^0 is:

$$d_{ij}=A_{ik}d_{kl}^0N_{lj} \qquad 13)$$

where A_{ik} and N_{lj} are rotation matrices that can be found in the appendix a and b of [2].

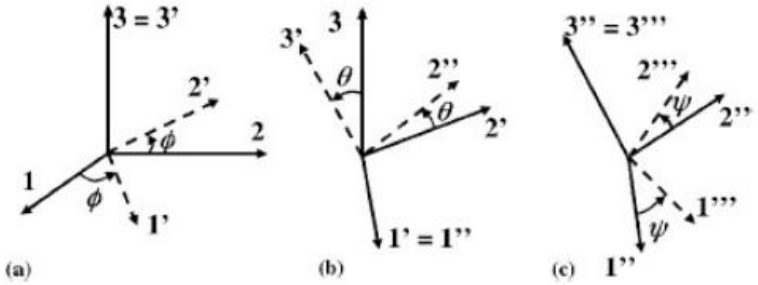

Figure 2.9 Transformations for transition from crystal to laboratory coordinate system [9].

For example, for tetragonal PZT is possible to find the response components:

$$\begin{aligned}
&\rightarrow d_{33}=-(d_{15}+d_{31})\sin^2\vartheta\cos\vartheta+d_{33}\cos^3\vartheta \\
&\rightarrow d_{34}=-\left(d_{31}-d_{33}+\left(d_{15}+d_{31}-d_{33}\right)\cos2\vartheta\right)\cos\psi\sin\vartheta \\
&\rightarrow d_{35}=-(d_{31}-d_{33}+(d_{15}+d_{31}-d_{33})\cos2\vartheta)\sin\psi\sin\vartheta
\end{aligned} \qquad 14)$$

Equation 13) allows to evaluate semi-quantitatively the elements of the d_{ij}^0 tensor from the vector PFM or the 3D-PFM measurements, if the crystallographic orientation of the sample is known exactly. But for the case where the sample has an arbitrary crystallographic orientation the individual components of the d_{ij}^0 cannot be determined. However for materials with known piezoelectric constants, d_{ij}^0, the local crystallographic orientation in each point (electromechanical orientation imaging) can be determined from vector 3D-PFM data.

2.4.6 Polarization orientation from PFM data

The *local polarization vector,* $\mathbf{P}=(P_1,P_2,P_3)$ in the general case is not tractable by PFM. Vector PFM measures the components of the local electromechanical response vector related to the elements of the piezoelectric tensor, d_{ij}. From this data the piezoelectric constant of the material d_{ij}, and the local orientation map can be obtained. However, the conventional approach for measurement of ferroelectric polarization requires charge measurement during polarization reversal, which is impossible in PFM

because of the extremely small amount of switching charge. So PFM gives information about the direction of polarization, not about the verse of polarization. Therefore, in general PFM is used to map local crystallographic orientation from which the local polarization orientation is deduced assuming that the relationship between polarization and crystal orientation is the same on the nanoscale as for the macroscopic crystal.

2.4.7 3D Vector Image

The representation of a 3D Vector field requires the VPFM and x, y-LPFM images like explained before. This images have to be normalized with respect to the maximum and minimum values of the signal amplitude, so that the intensity changes between -1 and 1, that is vpr,xlpr,ylpr∈(-1,1). This 3D vector data could be mapped on red, green, blue color scale that are represented as a vector (R,G,B) where R,G and B are mutually orthogonal and vary from 0 to 1. The magnitude of the z-component is represented by the lightness/darkness variation in direction in the x-plane. The y-plane is given by hue, and the magnitude of the vector is represented by the color saturation (black and white are colors). The (R,G,B) coordinate system is rotated and shifted so (R,G,B)=(0.5, 0.5, 0.5) corrisponds to zero in PFM coordinate system, (vpr,xlpr,ylpr)=(0,0,0). Analitically the transformation is expressed by:

$$\begin{pmatrix} R \\ G \\ B \end{pmatrix} = \frac{1}{2}\left(\frac{1}{\sqrt{3}} \left(R_x(\vartheta_r) * R_z(\phi_r) \right)^T + \begin{pmatrix} 1 \\ 1 \\ 1 \end{pmatrix} \right) \qquad 15)$$

Where $R_z(\vartheta_r)$ and $R_z(\phi_r)$ are rotation matrices:

$$R_z(\vartheta_r) = \begin{pmatrix} \cos\phi_r & \sin\phi_r & 0 \\ -\sin\phi_r & \cos\phi_r & 0 \\ 0 & 0 & 1 \end{pmatrix} \qquad 16)$$

$$R_x(\vartheta_r) = \begin{pmatrix} 1 & 0 & 0 \\ 0 & \cos\vartheta_r & \sin\vartheta_r \\ 0 & -\sin\vartheta_r & \cos\vartheta_r \end{pmatrix} \qquad 17)$$

And the Euler angles are: $\vartheta_r = \tan^{-1}\sqrt{2}$, $\phi_r = \frac{\pi}{4}$.

As assumption, light shading indicates the vector pointing out of the page and dark shading indicates a vector pointing into the page. Gray areas indicate regions where the magnitude of the response vector is relatively small, intense or saturated hues indicate a strong lateral response with small vertical component.

2.5 System-inherent background

The frequency dependence of the PFM contrast is explained by taking into account the background. This is caused by the SFM head that is a mechanically complex entity with a wealth of resonance that if exited can produce a complex frequency spectrum. The amplitude of system-inherent background is in the order of some pm V^{-1}, and PFM is sensitive to surface displacement of about 0.1 pm of amplitude. This means that for materials with d> 100pmV^{-1} like PZT the frequency dependent background is negligible, whereas in samples with d<10pmV^{-1} the background can predominate, leading to changes in the PFM contrast when changing the frequency. Obviously any quantitative analysis of PFM measurement fails when not taking into account the background, and also it can shift the domain walls. In fact, the phase signal does not show the required 180° phase difference between opposite domains like show in Figure 2.10

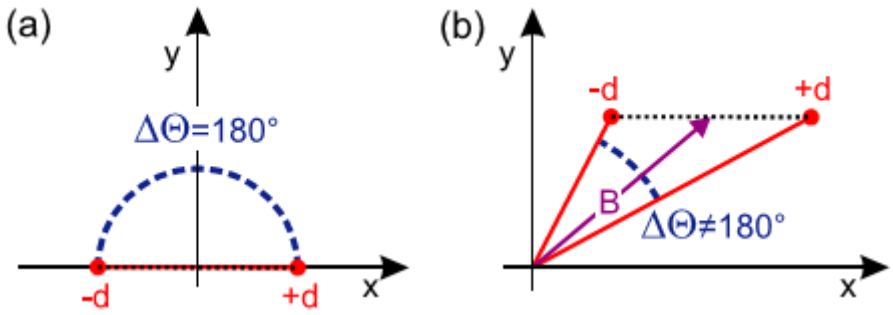

Figure 2.10 a) x/y-representation of the PFM signal obtained on a two-domain sample [↑↓] with piezoresponse *+d and -d*. The two axes correspond to the X- and Y-output channels of the lock-in amplifier. The angle $\Delta\vartheta$ denotes the phase difference of the PFM signals on the two domains. This is the situation with no background present. b) This is the real situation with the background B [10].

In Figure 2.10 b) the position of the origin (0,0) now is shifted by the B vector, as a consequence the magnitudes R of the PFM signals of the 2 domains are no longer equal, and their phase difference is $\Delta\vartheta\neq180°$. And since the background vary with the frequency, also the phase and the magnitude will depend on the frequency. A very simple way to circumvent the background problem consist in recording the X-output signal of the LIA for PFM imaging, that therefore contains the complete information of a PFM measurement.
For determining the system-inherent background a non-piezoelectric sample (glass slide) can be used to perform a PFM measurement. The result is the frequency-dependent background signal like shown in Figure 2.11.

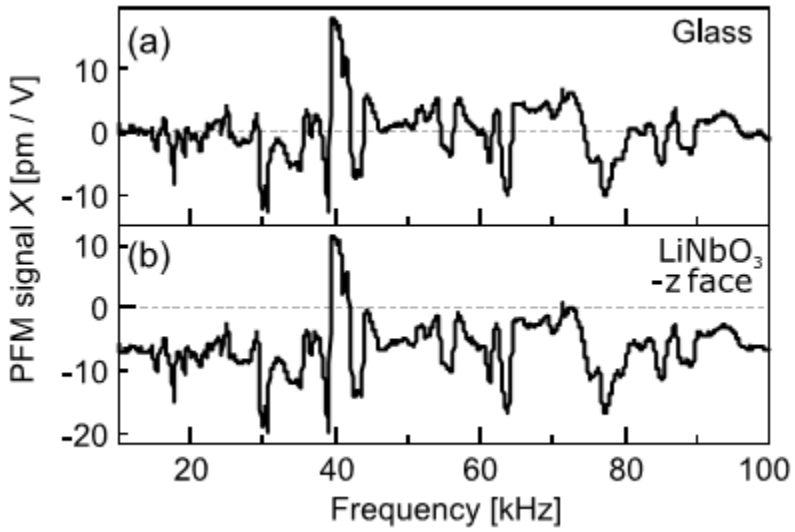

Figure 2.11 Determination of the system-inherent background: (a)on a glass slide and (b) on the−z face of LiNbO3, recorded consecutively with the same tip. Note that both curves display an identical frequency spectrum [10].

It is also possible to produce a sample in which 180°(↑↓) domains normal to the sample surface can automatically yield the background as the mean value of the ↑ and the ↓ PFM signals. When the background is determined, any sample with a known piezoelectric coefficient can be used for the PFM calibration, yielding the required conversion between the vibration amplitude of the sample surface and the PFM signal.

During the measurements, the system background has been evaluated with a glass microscope slide, and had been removed from the experimental data during the ODF calculation with the Mathematica Program [11].

Chapter 3
Experimental

3.1 Samples

The samples are piezoelectric actuators with internal Ag-Pd electrodes, and are used commercially as components of modern fuel injection systems. These multilayers have been supplied by the company EPCOS OHG (Deutschlandsberg, Austria), a member of the TDK Corporation.

3.1.1 Production and preparation of the samples

The samples have been produced by the following processing steps: (i) Tape-casting of ceramic slurry; (ii) dryng, electrode screen-printing and punching; (iii) thermo-compression; (iv) debonding (at 750° C) to remove the organic components, and (v) sintering in excess of PbO (to avoid losing Pb by volatilization). The received samples were prepared with mechanical polishing to obtain a mirror-like surface, as needed for PFM measurements.
The piezoceramic layers in between the electrodes have a composition near to the tetragonal side of the morphotropic phase boundary and are ~80μm of thickness. The actuators are constituted by 2 zones:

-Active zone where the electrodes are close together; this zone elongates during the actuator's operation.

-Passive zone that is located in the outer part of the electrode (towards the lateral surfaces) and is approximately 1 mm wide.

In the inactive zone, two near electrodes are connected to the outer contact on the same side, therefore they have the same polarization; on the other hand, in the active zone, two neighbouring electrodes are connected on opposite sides of the actuator, which gives them opposite polarity and thus enables elongation by converse piezoelectricity within the whole active zone.
The measurement surface has been polished with diamond paste down to 0.25 μm, and then with a basic OPU suspension (pH=9.8) based on colloidal silica for obtaining a smooth-stress free surface. Electrical cables were connected to the samples to make an "Earth connection", only on one side of the sample to avoid short-circuits. This drain connection has been done using a silver conductive solution as shown in Figure 3.1.
Three samples have been examined:

-*Mechanically Compressed multilayer*: that has been compressed with 150 MPa in direction perpendicular to the electrodes length.;

-*Electrically Poled multilayer*: that has been subjected to 210 V poling (~2.6 kV/mm electric field) on the electrodes, after being compressed by 15MPa, to prevent the formation of cracks within the ceramics layer. The poling creates an electric field perpendicular to the electrodes in the position in between the

electrodes, and a wave-like one on the top of the electrodes. The inactive zone (70/80 μm away from the electrode top) is not influenced by the electric field.

-*Unpoled multilayer*: without any treatment.

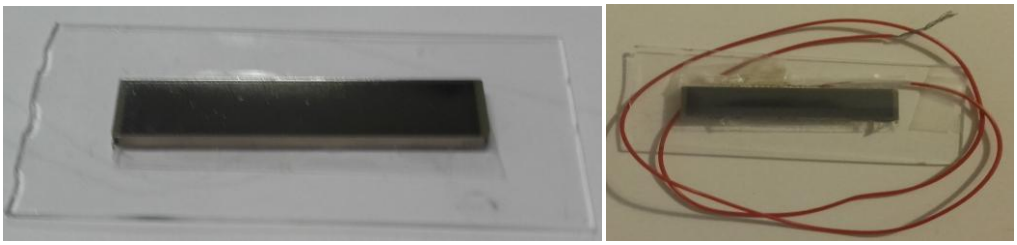

Figure 3.1 Unpoled sample before and after drain connection.

3.1.2 Introduction of cracks

The introduction of cracks has been done with the use of a Vickers indenter, with a 0.2Kg load. The Vickers indenter has a pyramidal shape with dimensions of the diagonals of 15X15μm. The cracks originate from the corners of the indentation, as visible in Figure 3.2 The top of the crack has been investigated to see the influence of the crack to the Piezoresponse vector orientation of ferroelectric domains.

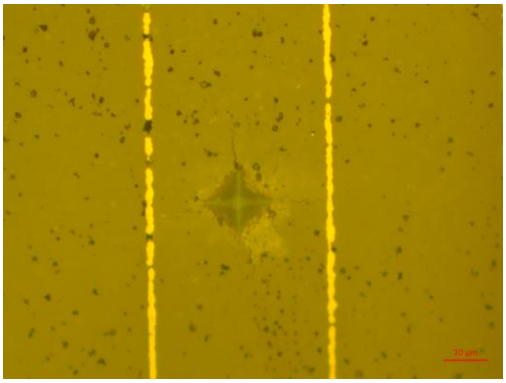

Figure 3.2 Optical microscope image of the indentation done on the poled sample.

3.2 PFM Instrumentations

In this paragraph the instruments and their principle of operation will be discussed.

3.2.1 AFM System

The measurements have been performed with an MFP-3D Stand Alone Atomic Force Microscopy system, manufactured by Asylum Research. This machine is composed by a scanning unit and a controller shown in Figure 3.3 and 3.4.

Figure 3.3 PFM Scanning Unit [12]

In order to obtain good measurements, is important to keep the PFM system away from noise-making instruments such as pump or AC units, and place it on a concrete slab ground floor. This is because of the high sensitivity of PFM to noise and vibrations. In fact, the scanning unit is placed on a pneumatic oscillation damping system, to avoid oscillations that could negatively affect the measurement. It is necessary also to maintain a quite constant temperature and humidity, because quick changes of temperature or humidity could cause noise and drift in the system.

Figure 3.4 PFM Controller [12].

A closed-loop scanner is built into the scanning unit and allows to select the desired scan area, that could be at maximum 80x80µm. Two schematic images of the internal part of PFM head are shown in Figure 3.5 and Figure 3.6. It's possible to see the laser beam focused on the cantilever and reflected with a PD Mirror to the Photodetector (segmented photodiode, PD). PFM also uses piezoelectric devices to move the sample along the x- and y- axis, to move the cantilever along the z-axis and to oscillate the cantilever in AC-mode.

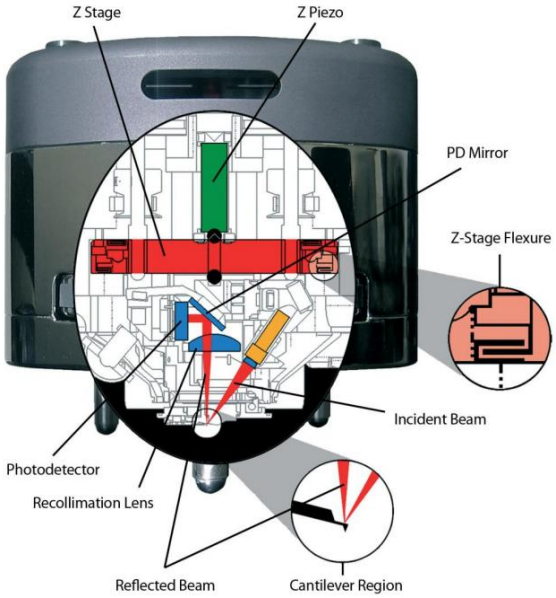

Figure 3.5 Front view of the PFM head [12].

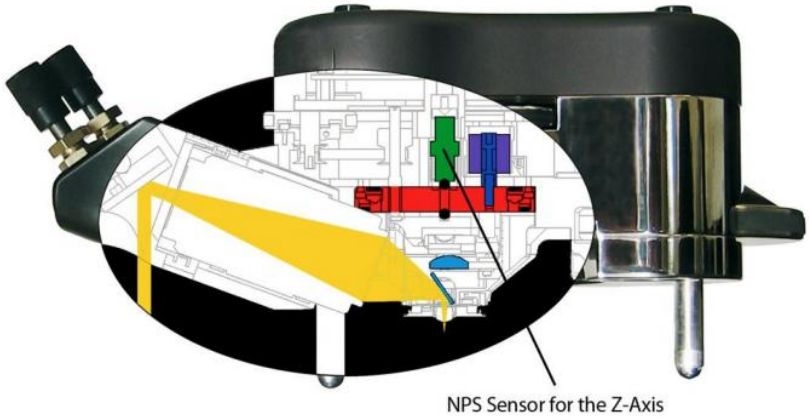

Figure 3.6 PFM head side view [12].

The photodetector is segmented into four quadrants, the voltage generated from each quadrant is proportional to the light hitting it. Figure 3.7 is a schematic representation of the 4 quadrants of the photodiode.

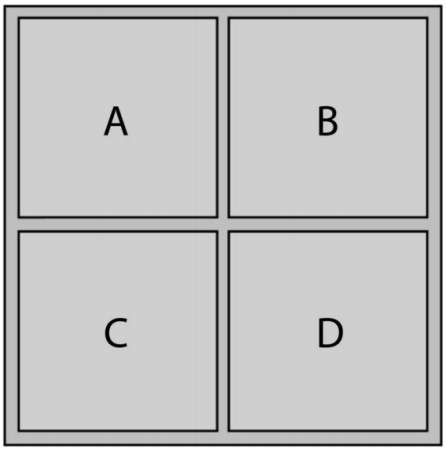

Figure 3.7 Schematic representation of the 4 quadrants of the photodiode [12].

The Deflection signal is calculated as the difference between the voltage generated in the top quadrants, and the voltage generated in the bottom quadrants:

$$\text{Deflection}=V_{top}-V_{bot}=(V_A+V_B)-(V_C+V_D) \quad (18$$

The lateral signal is calculated as the difference between the voltage generated in the left quadrants, and the voltage generated in the right quadrants:

$$\text{Lateral}=V_{left}-V_{right}=(V_A+V_C)-(V_B+V_D) \quad (19$$

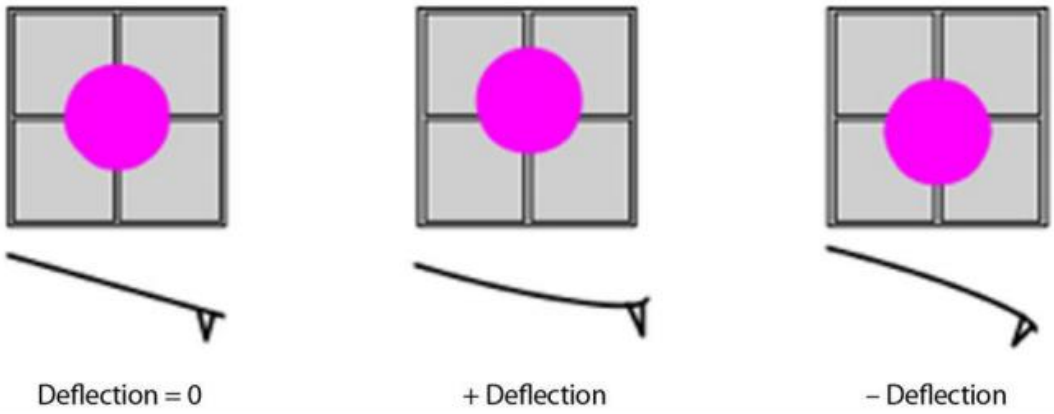

Figure 3.8 Representation of the deflection with respect to the laser spot position on the photodiode [12].

The signal generated by a certain amount of cantilever deflection is called Optical Laser Sensitivity OLS. This parameter is influenced by the shape and the length of the cantilever and the laser alignment, and changes from one experiment to the next. For convenience in PFM the invOLS (inverse OLS) is used for converting the volts to meters, but is not needed for the height data (topography) because the height feedback loop keeps the cantilever at a constant deflection; so is the calibrated motion of the Z-piezo that scales with the height data (Figure 3.9)

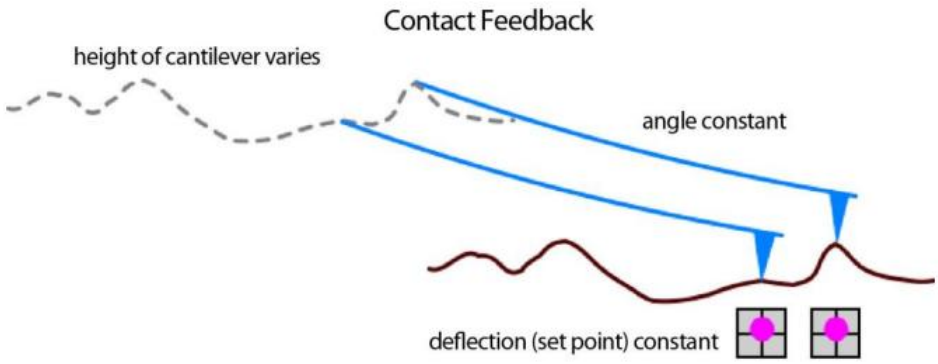

Figure 3.9 Height data are collected using the contact mode feedback that maintain the angle constant and thus, the deflection constant [12].

However, the head of the instrument contains the optical detection system and the Z-Piezo, which is used to monitor and control the deflection of the cantilever. The surface topography map is created by detecting (as said before) the Z position of the cantilever or in other words, the topographic map is generated by applying the Z piezo voltage required to maintain a constant deflection of the cantilever, and then measuring the Z piezo voltage.

3.2.2 Lock-In Amplifier (LIA)

To achieve the data from the oscillation of the cantilever, in PFM measurement, a LIA is necessary. The LIA used for the measurements is an external one made by Stanford Research, and is the model SR830. The output signal can be the X- and Y-signals, or it can calculate the R- and ϑ- signals. However, all the output signals are in the range from -10.5 to +10.5 V. From the LIA is possible to control several parameters like the time constant and the sensitivity that are very important to reach the best contrast of the image.

Figure 3.10 Photograph of the Stanford Research Lock In Amplifier [11].

3.2.3 Voltage Amplifier

The voltage amplifier is used to increase the applied voltage of the PFM tip. This is done to increase the mechanical response of the sample, because the MFP-3D Stand Alone Atomic Force Microscopy system of Asylum Research allows only an applied voltage from -10 to +10 V. The voltage amplifier used in the measurements(an F10A of FLC Electronics AB) is shown in Figure 3.11, and can amplify the voltage 10 times linearly up to a frequency of 1 MHz. The voltage applied in all performed measurements is 15 V.

Figure 3.11 Photograph of the Voltage Amplifier [11].

3.2.4 Wiring setup

The wiring setup and the crosspoint panel settings are shown in Figure 3.12 and in Figure 3.13. From the crosspoint panel is possible to change from lateral and vertical imaging.

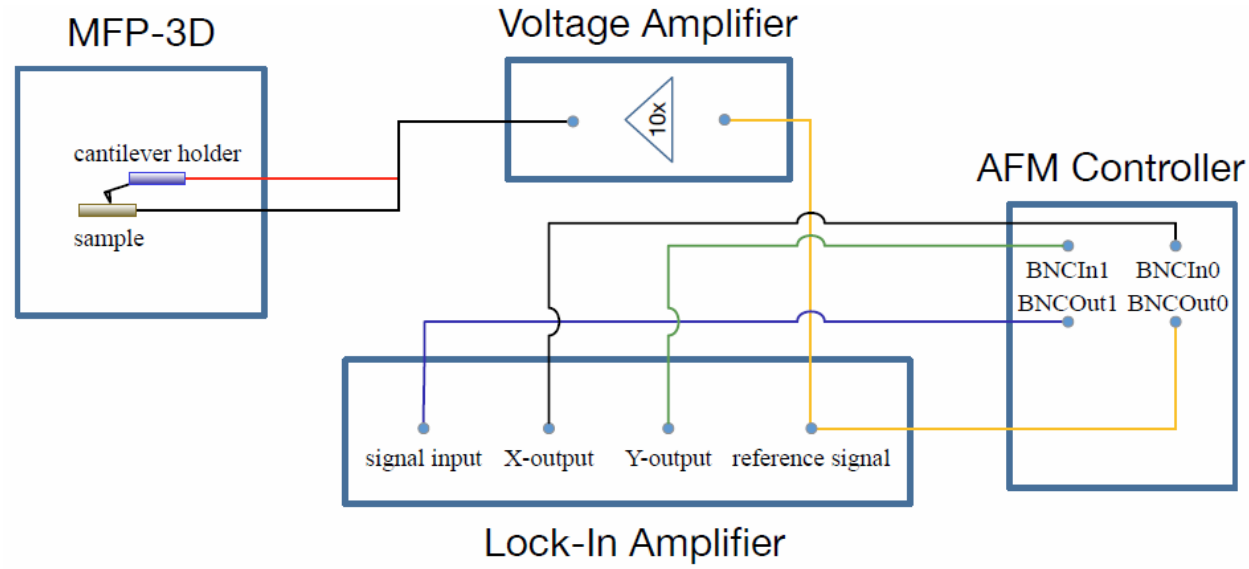

Figure 3.12 Wiring setup of the PFM complete System [11].

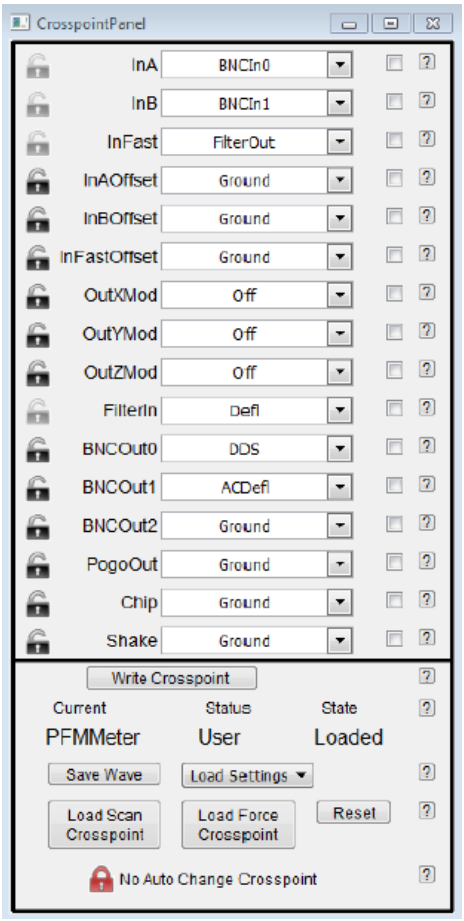

Figure 3.13 Screenshot of the cross-point panel and the settings [11].

3.3 Measurement Procedure and Parameters

All the measurements have been conducted with the PFM in contact mode, with the constant force method. The contact mode has been used because is the most used method to measure the topography of the hard surfaces like in this case of PZT multilayers.

3.3.1 Set up and calibration

After the cantilever loading, that has to be done manually, it is important to focus the laser beam on the cantilever like shown in Figure 3.15. This is done by using a photosensible card and watching the changing of the sum signal. When the laser is on the cantilever the sum signal changes, because it measures the total amount of light collected by the photodetector, and is a good measure of how well the light source is aligned on the cantilever.

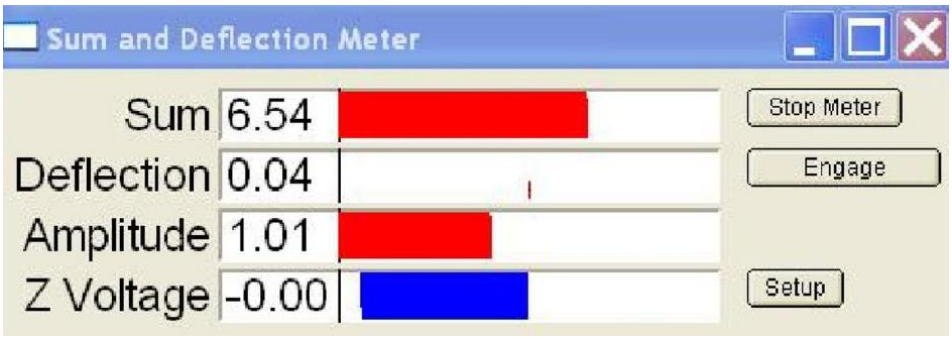

Figure 3.14 Screenshot of the Sum and Deflection meter. Usually the values of the sum of the measurements done in this thesis work were around 5 [12].

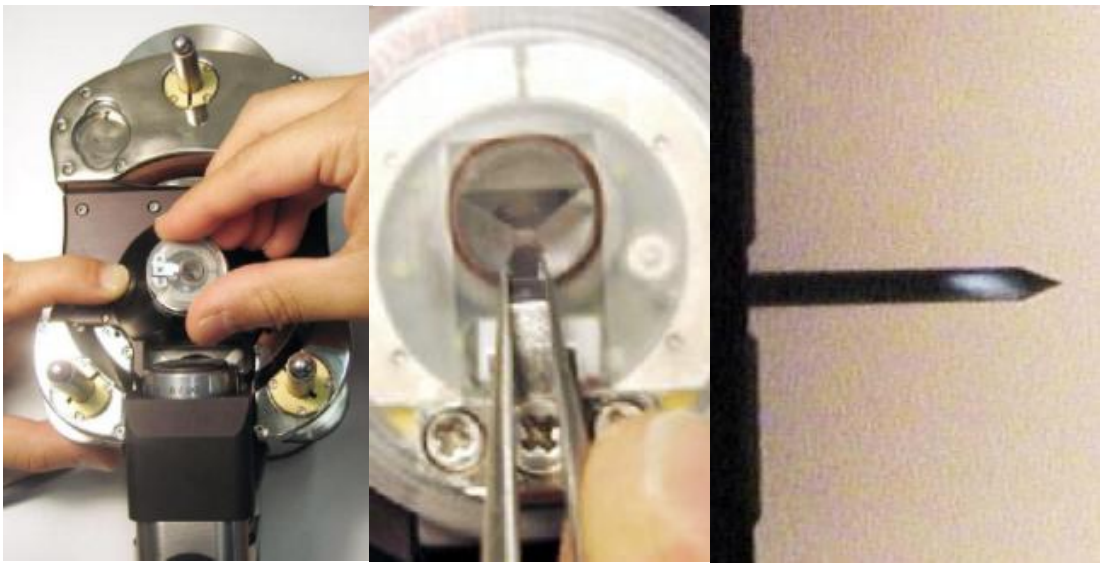

Figure 3.15 In the first image is shown the cantilever holder and in the second, the loading of the cantilever. The third image represent a microscope image of the cantilever with laser spot focused on it [12].

To focus the laser beam on the cantilever the knobs have been used, like shown in Figure 3.16: the 2LDX moves the laser along the direction parallel to the cantilever axes, the 4LDY moves the laser in the perpendicular direction with respect to the cantilever axes. The PD (photodiode) knob tilts the mirror that directs light reflected off the cantilever at the photodiode, and is used to bring the deflection value to 0.

Figure 3.16 In this figure are shown the knobs (2LDX and 4LDY) to focus the laser beam, and also the PD knob that is needed to bring the deflection at a 0 value [12].

The first step to calibrate the PFM is to find a value of the virtual deflection. The virtual deflection is an artifact of the system that consist in the fact that the AFM collect a little value of deflection also when there isn't contact. This value has to be evaluated and subtract from the total deflection value. This can be done (after bringing the deflection to 0) by obtaining the virtual deflection line, setting the trigger channel: "none" and clicking "single force". The fitting of the virtual deflection line gives back the value of the virtual deflection. This is done before engaging the surface.

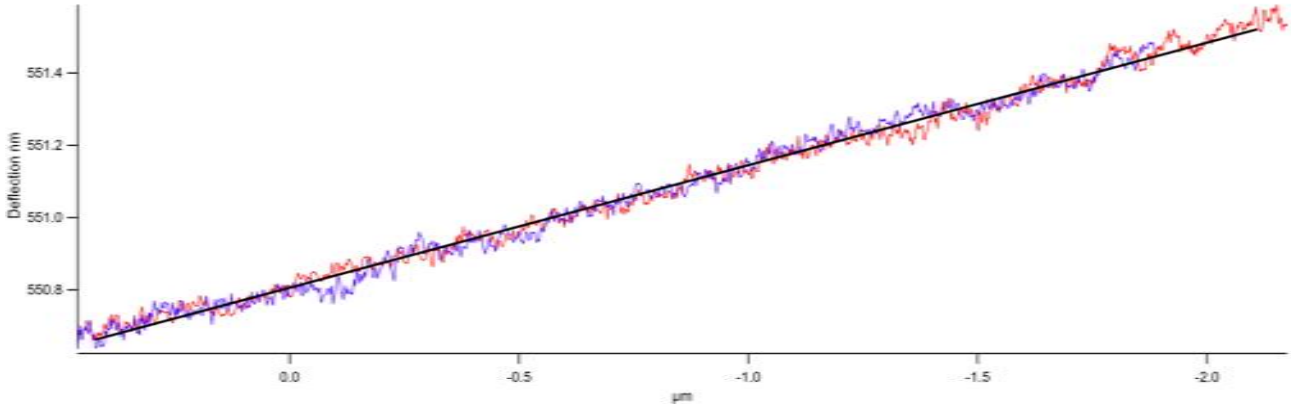

Figure 3.17 Virtual Deflection Line Graph.

The second step is to engage the surface. In order to have a good engage is necessary to fix the set point of the deflection, that depends on the type of cantilever that is used (the cantilever stiffness) and the hardness of the surface. The set point is the parameter that corresponds to the deflection of the cantilever during the scan. The higher is the set point and the higher is the force applied by the tip on the sample; and the higher is the difference between the free deflection with respect to the set point, the higher the tip will push on the surface. That is the reason why the virtual deflection is calibrated before the invOLS, and

the deflection is set to be as near as possible to zero. It is important to know that the deflection channel tells the error signal of the feedback, that means that in ideal condition of the feedback and of the calibration, the deflection signal would be 0. As mentioned, after the surface engage, is important to do the calibration of the invOLS, which is achieved by the fitting of the Deflection-Zsensor graph. This graph is obtained by setting:

-Start distance: 4µm;

-Force distance: 2µm;

-Trigger channel: “invOLS” and clicking:“single force”. The graph obtained is given in Figure 3.18:

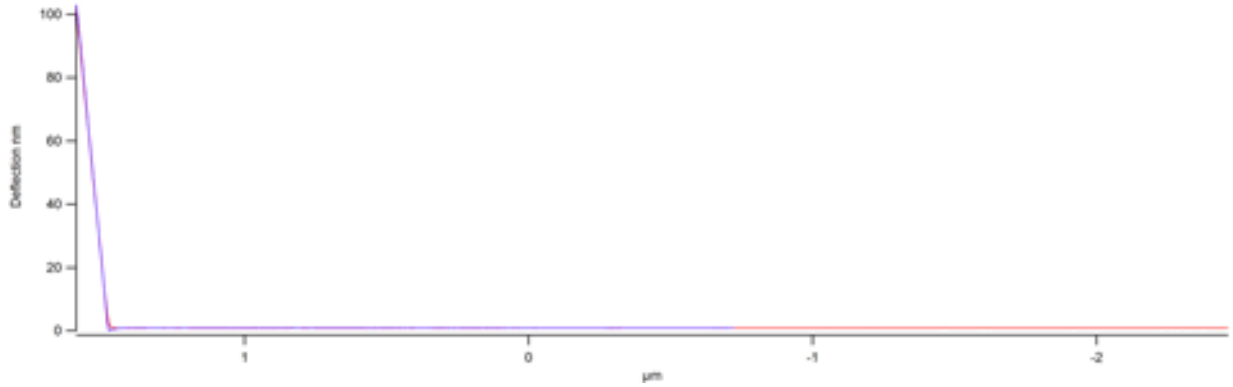

Figure 3.18 Deflection invOLS graph.

It is important to select the first part of the curve to have the best fitting of the collected data that gives the value of the Deflection InvOLS. When the invOLS is calculated, the third step is to evaluate the spring constant of the cantilever. Before doing this, it is generally a good idea to move the tip away from the surface. Then to set the spring constant of the cantilever it is necessary to start from thermal panel and do the thermal capture. In this way, fitting the peak, the resonance frequency, and the spring constant of the cantilever are obtained, and have to be similar to the value guaranteed by the cantilever producer. The spring constant is directly proportional to the cantilever stiffness.

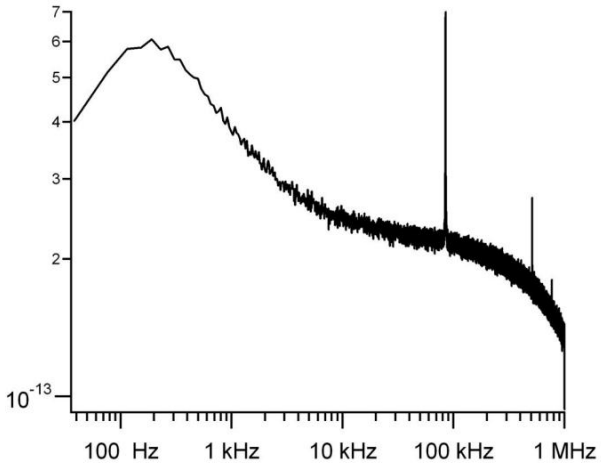

Figure 3.19 Thermal Power Spectral Density Graph where is placed the Resonance Frequency peak [12].

3.3.2 Measurement of the in-plane and out of plane responses

To correctly evaluate a 3D reconstruction of the piezoresponse vector, it is necessary to measure the Vertical and the two Lateral signals of the same area. For the out-of-plane response (Vertical), only one measurement is needed; on the contrary, for the in-plane response, 2 measurements are needed, one in the current position, and one rotated by 90°. This means that after the vertical measurement and the first lateral measurement, the sample has to be physically rotated by 90° and the same scan area has to be relocated to do the second lateral measurement. It is mandatory for the analysis that both measurements are exactly on the same places; otherwise artefacts can be created in the image due to the wrong superposition of the 3 images. This is a difficult task and usually requires extra measurements to relocate exactly the same area (10X10µm) again. The measurement procedure is this:

1) Select the place for the measurement (on the top of the electrode, in between two electrodes, in the inactive zone).

2) Scan an overview scan area of 30X30 µm and select an area of 20X20µm in which there are less metal inclusions (due to the electrode material) as possible and without cracks or defects. This can be done drawing a marker on the scanned area of 30X30 µm and selecting the command “edit zoom zoom”. This will set up the coordinates x-and y- of the cantilever position in order to scan the selected area.

3) Select the final 10X10µm area from the 20X20 µm one and measure the vertical and lateral signals of that area.

4) Rotate the sample by 90° clockwise. This is easier to do with reference to the electrodes that rotates from vertical to horizontal like shown in the scheme of Figure 3.20.

5) Relocate the cantilever on the same previus area of 30X30µm, and after that select again the area of 20X20 µm and then the area of 10X10µm.

6) Scan the refound area to obtain the 90° lateral signal. In this step is important to collect again the vertical signal, because is needed by the program to do the image correlation.

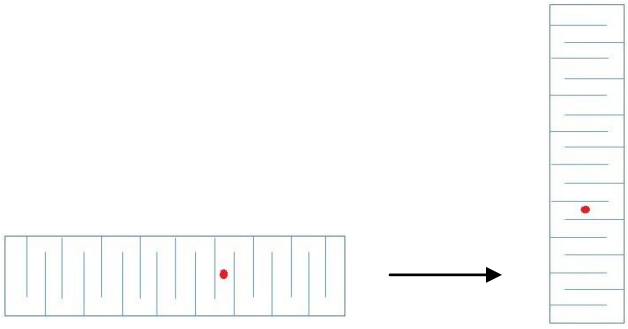

Figure 3.20 Measurement of the 2 Lateral signals in the 0° and 90° sample orientations. In all the 3D reconstructions is always assumed that 0° corresponds to the sample oriented horizontal with respect of the position under the head of the instrument. That means that is oriented parallel to the cantilever long axis, and in this case, the vertical signal image is oriented parallel to the sample's length.

After these six steps, the images found are input data for the program that do the evaluation. To decrease the procedure time is possible to do the first two steps with a resolution of 256X256 pixels and the frequency of 0,4 Hz, that corresponds to ~10 minutes for one scan. Furthermore, it is advisable to turn off the voltage amplifier during steps 1), 2) and 5), because a decrease of the response with the time of measure has been found, probably due to an accumulation of charge; moreover in this step, is not important to collect signals other than the topography.

3.3.3 Parameters

The parameters that can be changed in the measurements are:

-Sensitivity: is a scaling factor that has to be modified in order to have an output signal that does not exceed the range from -10.5V and +10.5V. All the values out of this range are lost.

-Frequency: is in principle the scan rate, and for the lateral signal measurements is better to use a scan rate lower than for the vertical one. For the poled and compressed samples, a scan rate equal for collecting the lateral and the vertical signals has been used. This because the longer the tip lasts on the sample and the more the sample takes the charge, with a consequent decreasing of the signal achieved.

-Scan Angle: is the angle in which the cantilever moves with the higher velocity. If it is parallel to the cantilever axis is 0°, if it is perpendicular 90° like shown in Figure 3.19. It has been noticed that the vertical gives a better signal with a scan angle of 90° and on the contrary the lateral with 0°, Therefore all the lateral signals have been done with a scan angle of 0° and all the vertical with 90°.

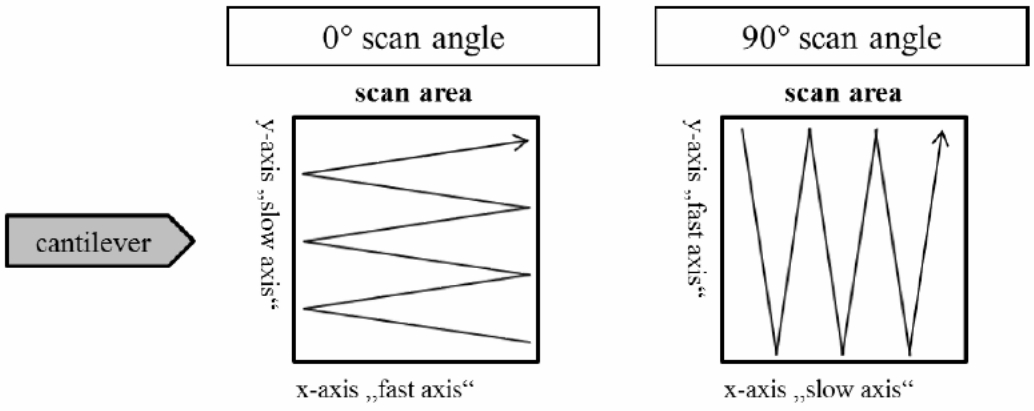

Figure 3.21 Schematic representation of the scan angle [11].

-Set point: the set point used for all the measurements has been 0.1V (for DCP11 tips). Furthermore, is possible to evaluate the force on the surface F_N with the follow equation:

$$F_N[nN]=setpoint[N]*DeflInvOLS\left[\frac{nm}{V}\right]*k[nN/nm] \quad 20)$$

Where DeflInvOLS is the inverse optical lever sensitivity of the deflection signal, seen before; and k is the spring constant. Therefore, a medium value of this force in this measurements is around 80 nN.

-X-; Y-; R; ϑ: Lock-in Amplifier has been set to give only X- and Y- signals, which contains all the data, like discussed in the paragraph 2.3.

-Number of pixels: at the beginning the number of pixels was 256X256, but to increase the image quality 512X512 has been used.

-Drive amplitude and drive frequency: all the measurements have been conducted with 15V drive amplitude and 10kHz drive frequency applied to the AFM probe.

The parameters used for the measurements done with the DCP11 tip was this:

Sample	Measurement	Sensitivity	Frequency	Scan Angle °
Unpoled	Vertical	$1mV$	$0{,}4Hz$	0°
	Lateral	$200\mu V$	$0{,}3Hz$	90°
Poled	Vertical	$1mV$	$0{,}4Hz$	0°
	Lateral	$100\mu V$	$0{,}4Hz$	90°
Compressed	Vertical	$1mV$	$0{,}4Hz$	0°
	Lateral	$100\mu V$	$0{,}4Hz$	90°

Figure 3.22 Parameters applied in the different measurements.

3.3.4 Data evaluation procedure

From every measurement, it´s possible to get 8 images that are:

-Two Height images, which are the topographies of the area, one in trace and one in retrace.

-Two Deflection images, one in trace and one in retrace.

-Two X- signal images, one in trace and one in retrace.

-Two Y-signal images, one in trace and one in retrace.

For the evaluation with the Mathematica program, only the X-,Y- (retrace) and the Height (retrace) images are used. Before to use that is important to process these data with the free-source program Gwyddion. For the topography it is important to do a step line correction and flatten the data with a mean plane subtraction. The X-and Y- data have not to be corrected and then all the files are transformed in .txt files that can be directly processed by Mathematica. All the txt files created have to be renamed with a file IDs that allows the program to recognize the files. There is also an additional parameter file, where

the parameters like DefInvOLS and the sensitivity of the measurement have to be placed every time, and also the files that concern the background correction, which are fixed for all the measurements. The program has been created by the Engineer Michael Lasnik following the theory described in the Chapter 2, from [9].
The Program is divided in 5 parts:

1) Importing of the files. All the txt files are converted in black and white images and the parameters are defined.

2) The Height data of the out-of-plane scans are used to do the image correlation and then the image cropping. A transformation matrix is created and all images are rotated according to this matrix, to have the same orientation of the 0° rotated sample. The problem is that the images do not represent exactly the same scan area, therefore are cropped to represent exactly the same area. The more precise is the second area founded, and the more are the pixel number of the final image. After cropping the PFM images are transformed in PFM data.

3) Correction of the measured data and calculation of the PFM signal in x-, y-, and z- direction. If there are R- and ϑ- signal, they are converted into X- and Y- signals, then a background correction is done. The background corrected data are then rotated so that the regression line through the data points is parallel to the X axis (Figure 2.6) This can reduce the background because the Y- signal is considered to contain only noise.

4) There are 2 different calculations:

- the first is a qualitative calculation that shows the polarization vectors distributed among the octants of a sphere considering only the sign of the PFM signals.

- the second one determines the two solid angles (ϑ and ϕ) considering the magnitude of the PFM signal.

For this calculation the PFM signals are separately normalized assuming that there are measurements errors, so every PFM signal is divided by a value that is determined by comparing one of the smallest (negative) with one of the largest (positive) measured values, and the final results are set to -1 and 1.
Both calculation yield a list of the 2 solid angles of each pixel of a measurement scan, respectively ϑ ranges from 0° to 180° and ϕ from 0° to 360° to cover the surface of a sphere.

5) The results are here presented as an illustration of the octants of a sphere calculation, or more as detailed illustrations in which every pixel is colored according to the polarization vector orientation. In the appendix there is the program used in this work.

Chapter 4
Results

In this chapter initially the problems that have been found during the measurements are shown, then the solutions involved, and in the end the results of the entire work.

4.1 Image Contrast

4.1.1 Drain contact and surface polishing

In PFM measurements, in order to get good images of the surface and, more importantly, good piezoresponse from the sample surface, a good electrical connection of the sample in order to drain away the charges is needed. This can be tricky in the case of piezoelectric multilayer samples. Initially the electrical contact was done on the short face of the samples, which however led no noisy X and Y responses and it wasn´t possible to distinguish any domain. The problem was attributed to a wrong polishing, arguing that with the OPU solution, did not gave a perfect surface, as it possible to see from the optical microscope images of Figure 4.1.

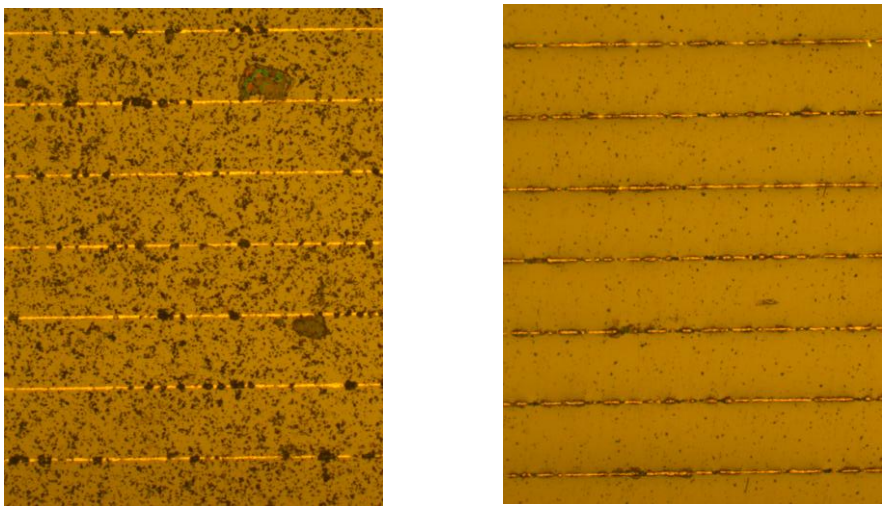

Figure 4.1 Unpolished and polished surface of the poled sample.

OPU polishing was redone, however contrast problems remained also on the re-polished samples. Afterwards a solution allowing taking better images was found, that is: measure without the drain contact. The structure of the multilayer stack needs a precise way to do the drain contact, because if all the electrodes of both sides of the actuator are connected together, probably a short-circuit is induced. The short-circuit is thought as the cause of the non responsivity achieved at the beginning of the measurements. The polishing was done only on the poled and mechanically compressed samples, and the unpoled sample (remained unpolished) gave the best contrast, as it is possible to see in Figure 4.2.

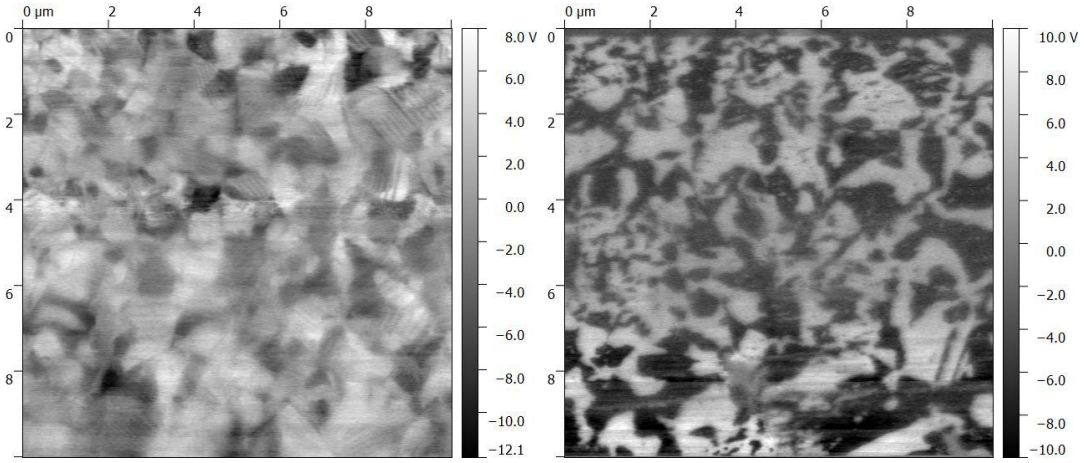

Figure 4.2 The 2 images are the X signal of the Vertical response from the surface of the unpoled sample (left image) and of the mechanically compressed sample (right image). These images have been done without the drain contact.

However, the OPU solution polishing was repeated again on the poled and mechanically compressed samples, to reach a better contrast, and then the samples gave good vertical images, but lateral images with poor contrast, like shown in Figure 4.3.

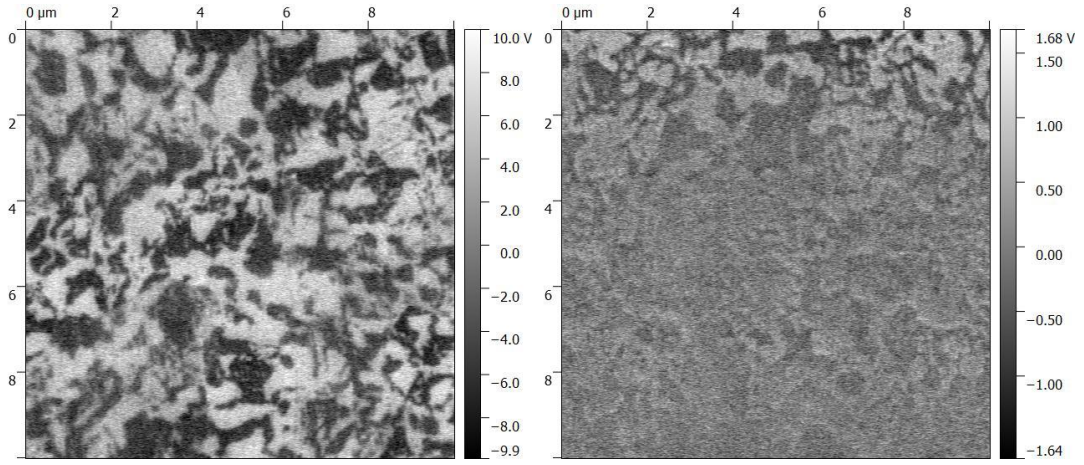

Figure 4.3 X-signal of the Vertical(left) and Lateral signals of the mechanically compressed multilayer.

This problem in the lateral signal was due to the wrong polishing direction of the mechanically compressed and the poled samples. These two samples had been polished in a direction parallel to the electrodes length, and this is the cause of the difference in thickness in between the electrodes, because the ceramic material is less hard than the electrodes, and is more subject to wear. After the polishing in a direction perpendicular with respect of the electrodes, the lateral signal was better, but in any case didn't reach the quality of the lateral signal of the unpoled sample.

4.1.2 Optimal resolution

At the beginning of the measurements, the images were done with a resolution of 256 X 256 pixels. This is a normal resolution that could be run with a quite high scan rate (0,4 Hz). In order to increase the contrast to see the "stripe-like" domains, it was decided to increase the number of pixels to 512 X 512, that means more time for a measurement and, in some cases, the use of a scan rate of 0.3Hz to reach a good quality of the contrast. The image quality increased greatly, as it is possible to see from Figure 4.4.

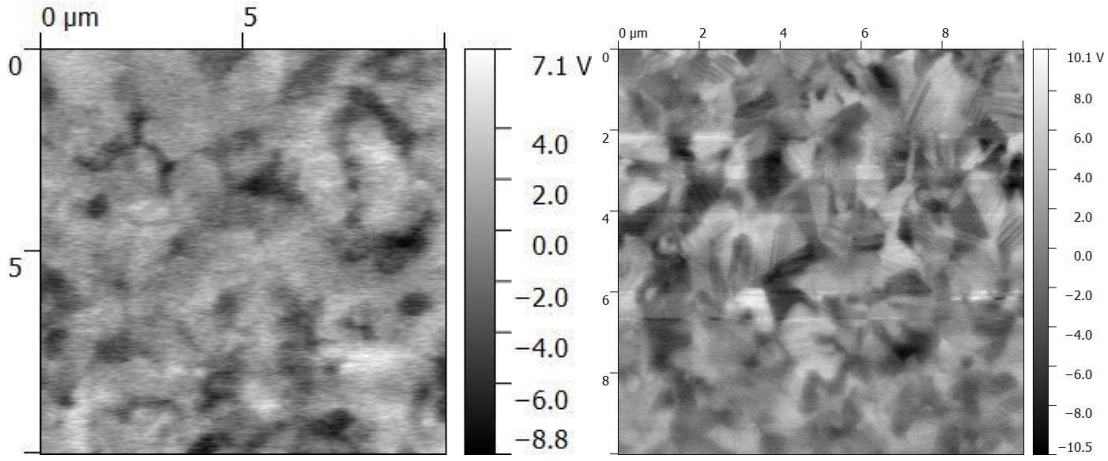

Figure 4.4 Two images of the X output signal of the lateral response of the unpoled sample.

4.1.3 Line defects and changing of the contrast during the measurements

In most images, there were some line defects due to the presence of little particles attached on the tip, which affect the image contrast as evident from Figure 4.6. The possible solutions of these problems can be:

-Change the type of polishing;

-Perform more scans on the same area to clean the surface with the passage of the tip. The problem of this solution is that the tip is subjected to wear.

-Change of the type of tip used.

Tip type	Cantilever Spring constant
HA-HR-DCP	Around 50nN/nm
DCP 11	Less than 10nN/nm

Figure 4.5 Tip used and relative Spring Constant of the cantilever.

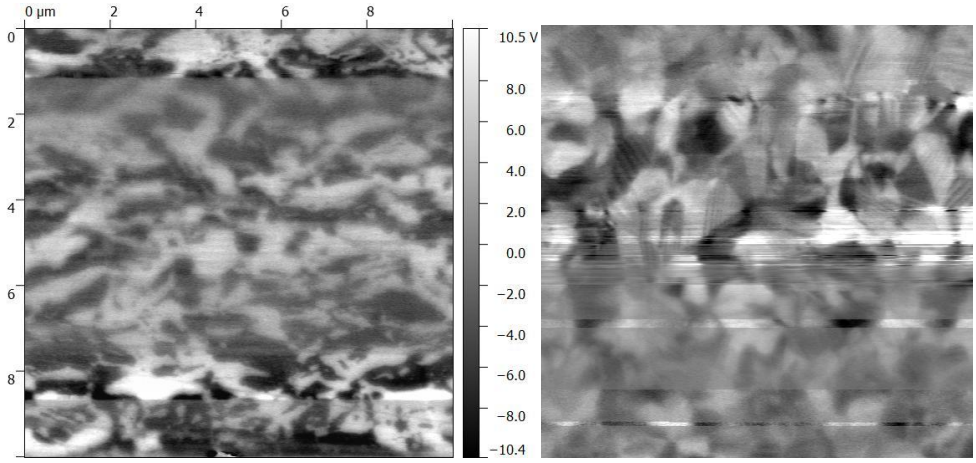

Figure 4.6 Presence of lines and contrast change defects in the mechanically compressed (left) and in the unpoled sample (right). These images have been obtained with HA-HR-DCP tips.

Changing the type of the tip used for the measurements has been the way to solve this problem. As a matter of fact, using DCP11 tips in place of the HA-HR_DCP tips used at the beginning, allows some benefits to the contrast quality during all the measurement. This is due to the different spring constant of the 2 types of tips, being that on the HA-HR-DCP ~50 nN/nm, and that on DCP11 less than 10nN/nm. This means that the DCP11 are less stiff than the HA-HR-DCP and thus are capable of better accommodating defects caused by attached particles. In Figure 4.7 two images are shown, one done with HA-HR_DCP (left) and one with DCP11 (right).

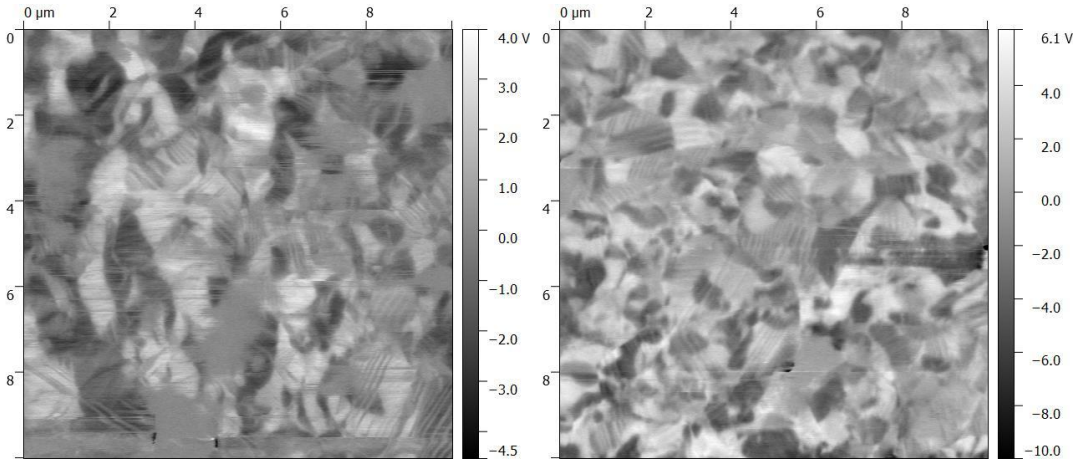

Figure 4.7 Increase of the contrast quality given by the changing of the tip type in the unpoled sample. Left: HA-HR-DCP tip. Right:DCP11 tip.

4.1.4 Corresponding points

In order to obtain a 3D image of the response vector, a Mathematica code has been used. The program has been developed by the Engineer Michael Lasnik of the Leoben University and correlates the 2

topography images (one orientated on 0° and one on 90°) to find the corresponding points to evaluate the 3D image of the piezoresponse vector. For some images used for the reconstruction of the 3D representation of the polarization vector, the program was not able to find the same points in the 2 different images. This was thought to be due to the presence of an initial line with wrong contrast produced by the too slow cantilever approach with the surface. This line produced a strong contrast changing during the correction of the topography images, like shown in Figure 4.8.

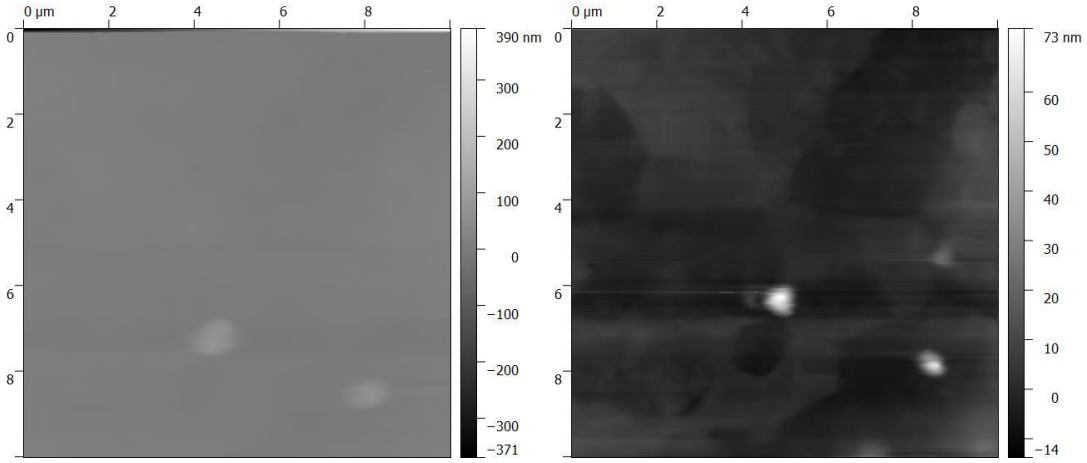

Figure 4.8 The presence of an initial line with wrong contrast can compromise the quality of all the image, like shown in the left image. The right image is of the same area without the wrong contrast line. These images have been obtained with HA-HR-DCP tip on the unpoled sample.

This was easily solved by increasing the integral gain in the crosspoint panel and engaging the surface before starting the scan. But also with this procedure, with good topography images, the program was not able to find the corresponding points in the images. This is because of the quite perfectly flat surface of the actuators, which lacks of appreciable reference points. However, with the help of Michael Lasnik, the Mathematica program was changed in order to have a manual selection of the corresponding points in the images; therefore is different from the one in [11] and then the program has been trascribed in the appendix of this thesis. Is important to know that, the better is the topography of the images and the better will be the corresponding points step, and the final 3D reconstruction of the Piezoreponse vector as well. The increasing of the quality of the topography images has been done also with the use of the new tips DCP11, like shown in Figure 4.9.

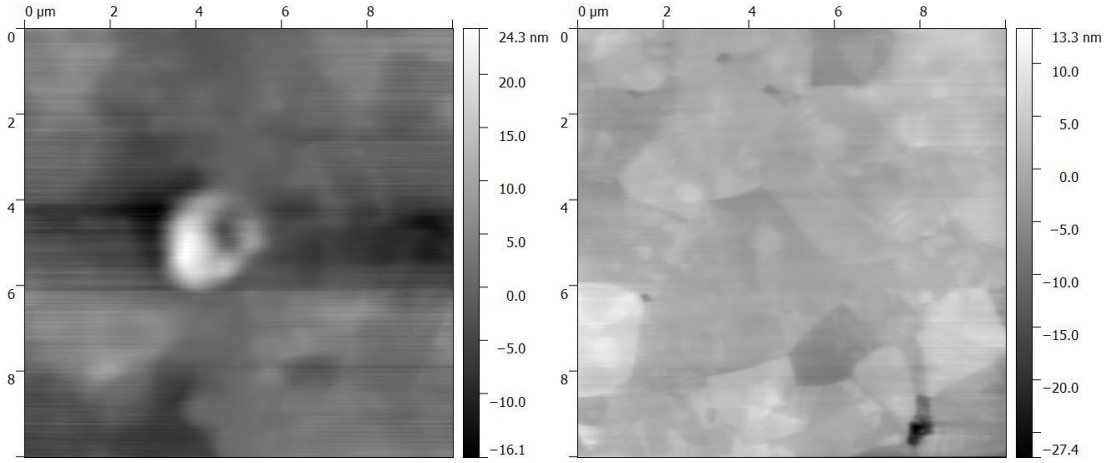

Figure 4.9 Change of the topography images quality, with the use of different tips, on the left HA-HR-DCP, on the right DCP11. In the right image is possible to distinguish the grain boundaries. These topography images have been done on the unpoled sample, on different areas.

4.1.5 Decreasing of the response intensity with consecutive measurements

Scanning consecutively the same area, results in the decreasing of the response intensity. This is translated in a decreasing contrast quality of the signal and is probably due to the charging of the surface that without any drain connection takes place. This is also due to the insulating behavior of the PZT material. This problem was partially solved using a "drain connection" on the lateral part of the samples. Taking into account the structure of this devices, connecting only a lateral part of the multilayer, only one half of the electrodes are connected. This way there is no short-circuit as seen before, and a flow of the current away from the sample surface is allowed. But the problem is solved only for the measurements located in between the electrodes, not for the ones located on the top of the electrodes, because of the distance from the electrodes during these measurements. In Figure 3.1 the samples before and after the connection are shown.

4.1.6 Absence of lateral signal

The lateral signal of the poled and mechanically compressed samples was absent. On the contrary the vertical signal was good. The problem was thought to be due to a wrong surface polishing, that gave some line shape irregularity in the topography and the difference of thickness between the electrode zone, and the zone in between the electrodes. This behavior is shown in Figure 4.10.

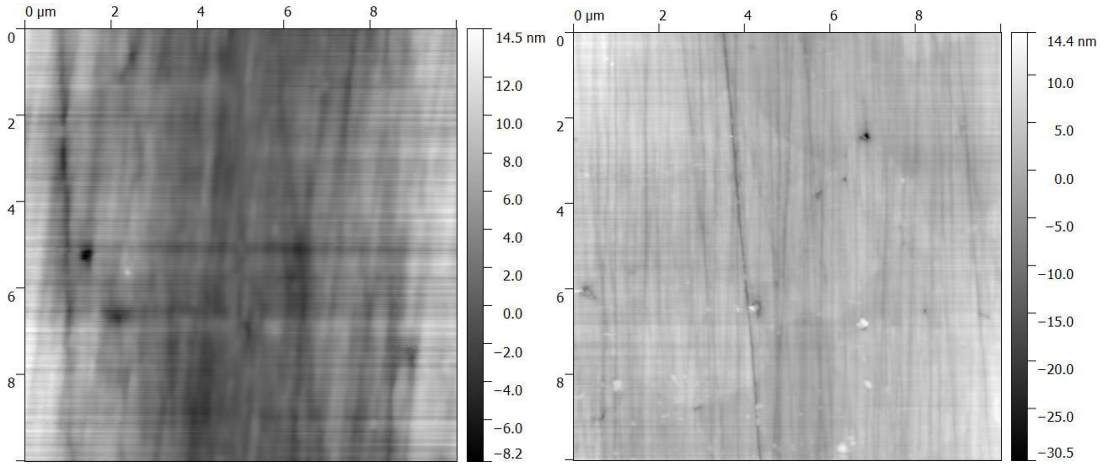

Figure 4.10 Line shape irregularities on the poled (left image) and on the mechanically compressed (right image) samples. These images have been obtained with DCP 11 tips.

The possible cause of the total absence of the lateral signal in those two samples, is the wrong polishing. The polishing has been done in the parallel direction with respect with the electrodes, whereas a correct polishing has to be done in direction perpendicular to the electrodes. Otherwise, the consequence is the wear of the ceramic part in between the electrodes. The unpoled had not this problem because was correctly polished. In Figure 4.11 is possible to see the difference between the correctly polished samples and the wrong polished ones. By the use of the drain connection and the last polishing (in direction perpendicular to the electrodes length), the lateral signal was acceptable, but the intensity of the signal was lower and noisier than the unpoled one. The motivation can be linked with the preparation of this samples, the compression(150MPa) and the electric poling (which aligns the domains) could have sensibly decreased the lateral signal intensity.

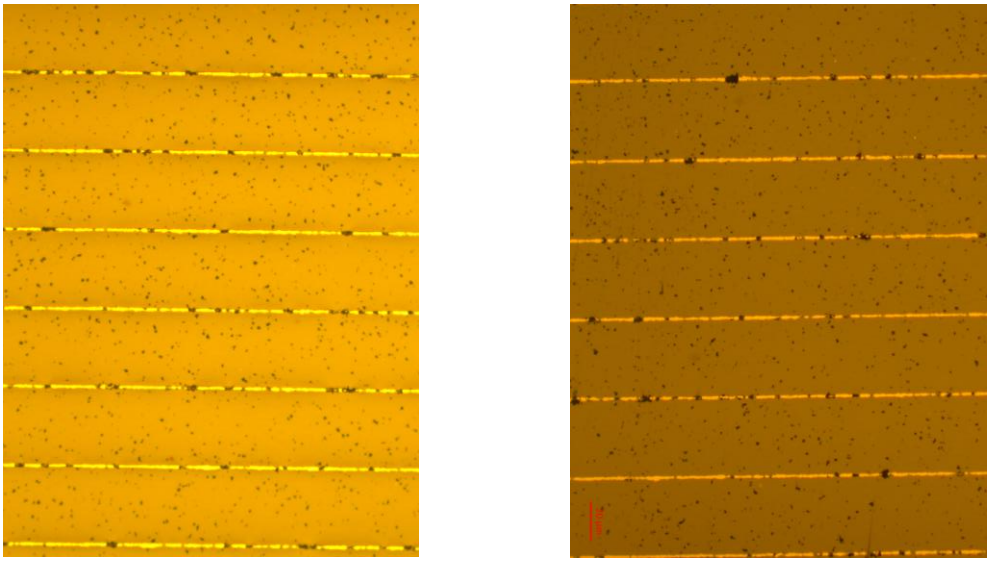

Figure 4.11 Images of the poled sample polished in 2 different ways: on the left is polished in direction parallel to the electrodes lenght; at the contrary on the right is polished perpendicular to the electrodes

lenght. Is possible to see that in the right image, the thickness of the surface is homogeneus everywhere, instead, on the left image, the area near the electrodes is higher than the zone in between them.

4.2 3D Reconstructions of the piezoresponse vector

In this section the three dimensional images obtained of the piezoresponse vector are shown. In these colored images, every pixel corresponds to a defined direction of the polarization vector calculated from the PFM data. The first image represent the X- signal of the Vertical, on its left there is the 3D image of the vector of polarization. Under these there is the meaning of the colors involved into the 3D image (legend) that is also explained in Figure 4.12 in which every color has a corresponding direction of the piezoresponse vector that it represents.

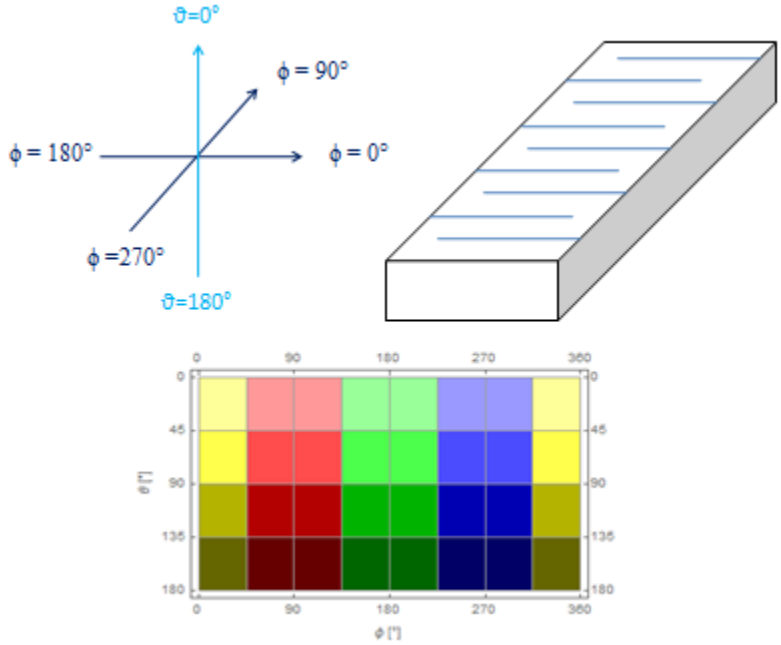

Figure 4.12 Schematic representation of the reference system used in the 3D reconstructions. The colors correspond to the direction with respect to the ϕ angle orientation (on the sample surface plane), and the brightness or darkness or the color is linked with the orientation with respect to the ϑ angle (orthogonal to the surface of the sample plane).

4.2.1 Initial Unpoled sample results

At the beginning of the measurements, two 3D reconstructions (10X10μm) have been done with a resolution of 256X256 pixels with the HA-HR-DCP tips. The results are shown in Figure 4.13 and 4.14.

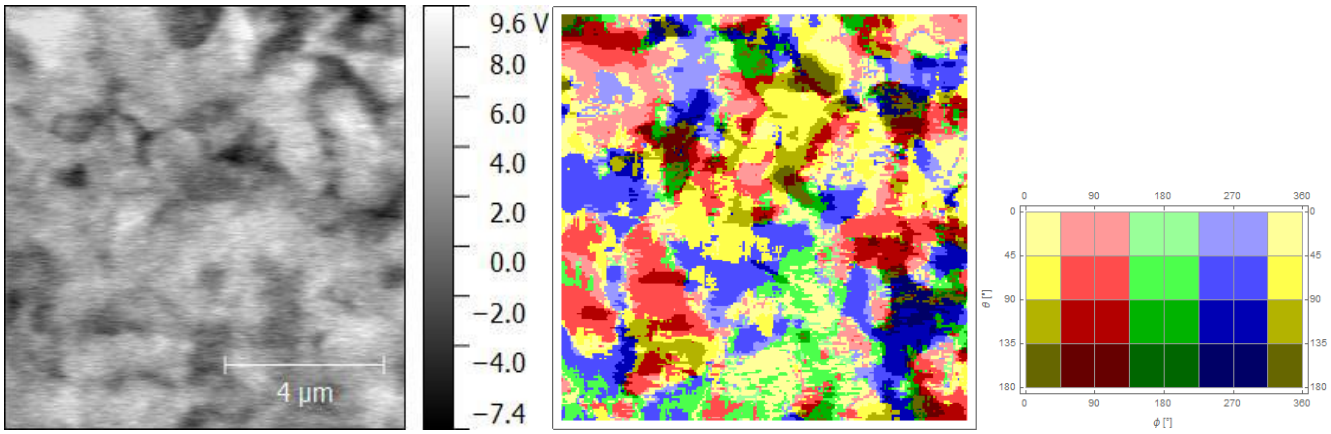

Figure 4.13 3D reconstruction of the piezoresponse vector of an area located in between of two electrodes (256X256 pixels, with HA-HR-DCP).

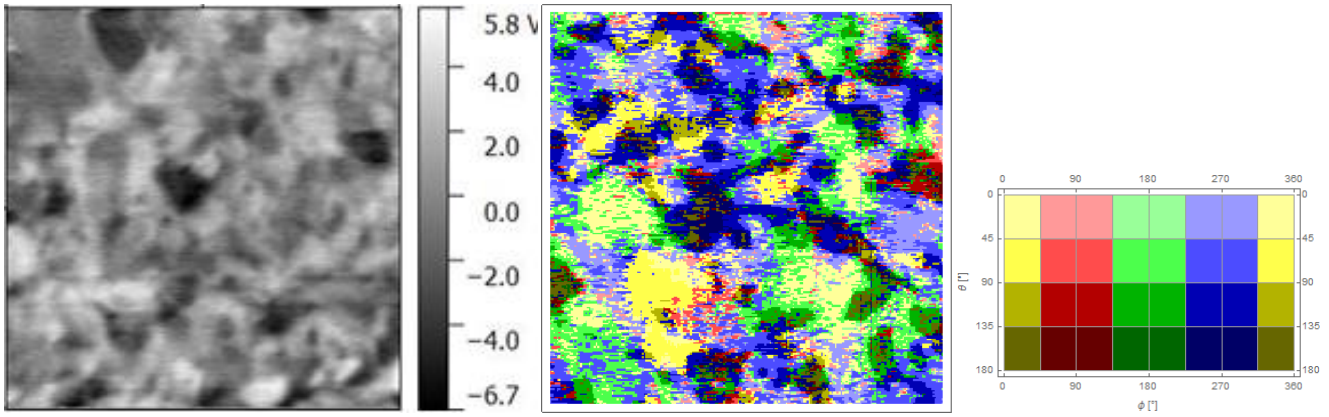

Figure 4.14 3D Reconstruction of the piezoresponse vector of an area located on the top of one electrode (256X256 pixels, with HA-HR-DCP.).

From the verticals and the final 3D reconstruction is possible to see that the contrast and the definition are really low. In fact, this images have been shown in this work only to make a comparison, and to understand the steps that have been done to arrive to the final results. To increase the quality of the contrast and the definition of the images, the other 3D representations have been done with a resolution of 512 X 512 pixels. The 512X512 pixels images have an higher definition, but need a lower scan rate to collect the higher number of pixels, and this increase considerably the measurement time.

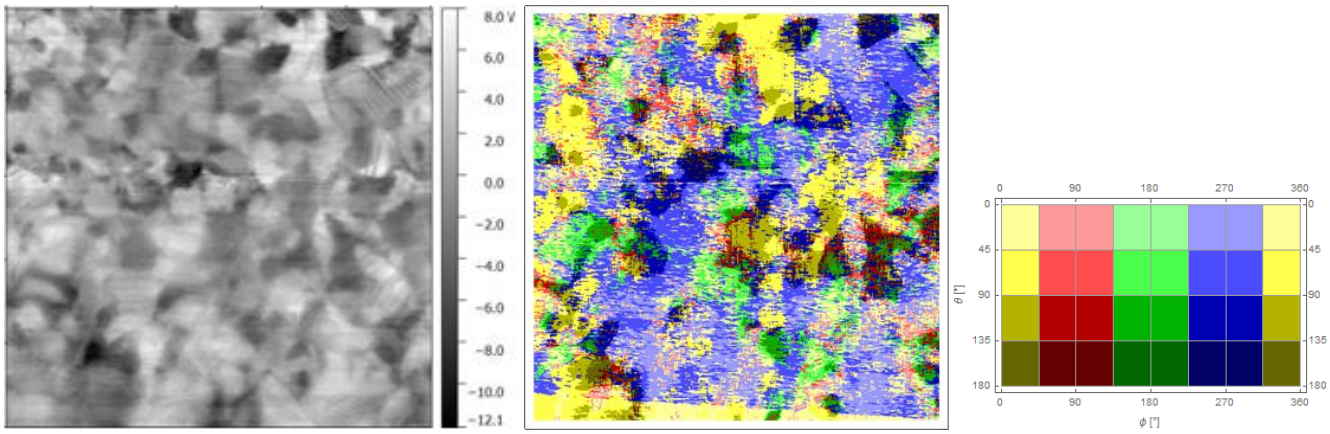

Figure 4.15 3D reconstruction of the piezoresponse vector of an area in between 2 electrodes (512X512 pixels, with HA-HR-DCP tip).

The yellow part in the bottom of the 3D Reconstruction is due to a little mismatch in the rotated image. It is possible to see in the Vertical response image, some stripe-like domains, but the contrast is not perfect because of line defects and small changes in contrast intensity. The HA-HR-DCP tips have stiff cantilevers that are really sensible to the surface variations and cleanliness; this means that the results are very often affected by contrast changing (due to the picking up of little particles by the tip, which leads to a lower contrast) and by lines (due to a quick change of the surface height or to the same mechanism of the contrast changing). The problem of this surface dependent tips is the fact that is impossible to find a 10X10 μm area without defects or metals inclusions (from the pressing sintering with electrodes), therefore is impossible to reach a good map of the polarization orientation. As a consequence of this behavior the tips has been changed to the DCP11 with lower stiffness. These tips are less surface dependent and give a better contrast.

4.2.2 Unpoled Sample Results

Here are shown the best obtained images and their interpretations. These images have been obtained using the DCP11 tips with a resolution of 512X512 pixels. The measurements have been done in 3 positions:

1) In between the electrodes: 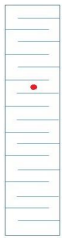 ;

2) On the top of one electrode (on its left): 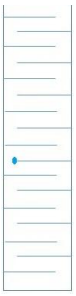 ;

3) In the inactive zone (60/80 µm far from the electrode top, on its left): .

The 3D images that will be presented are oriented in the same direction of these schemes and the results are shown with respect to the scheme in Figure 4.12.

-3D image of an area located in between of two electrodes:

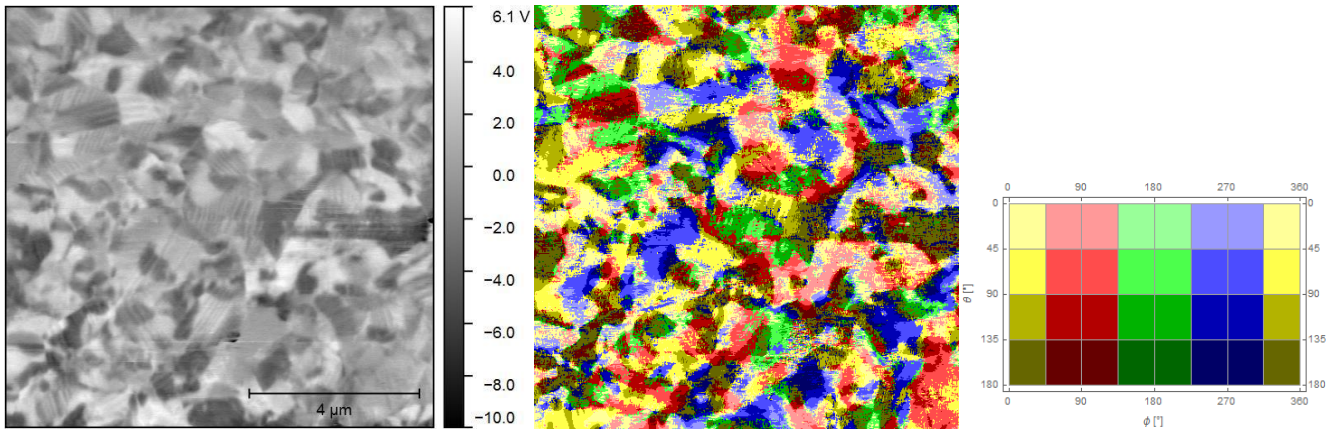

Figure 4.16 3D reconstruction of the piezoresponse vector of an area in between 2 electrodes made by DCP11 tip.

It’s possible to see that the colors of the domains in the 3D images are randomly distributed because the sample is unpoled and there is no preferential direction of polarization for the domains. The contrast is really good and is possible to see stripe-like domains also in the 3D image, this indicates the presence of tetragonal crystal domains.

-3D image of an area located on the top of one electrode:

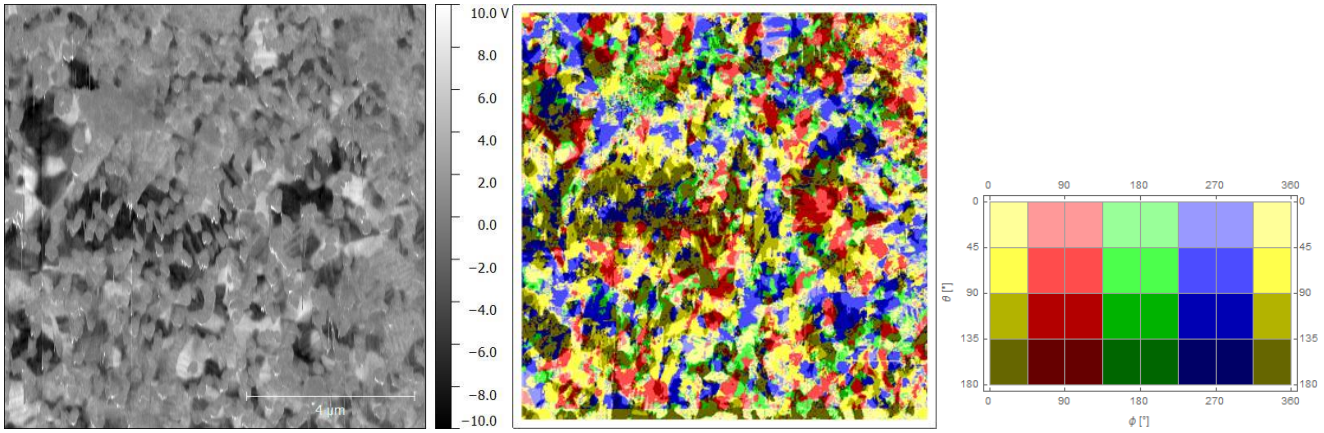

Figure 4.17 3D reconstruction of the piezoresponse vector of an area on the top of one electrode made by DCP11 tip.

As seen before for the area found in between of two electrodes, the ODF is similar in all the direction and there are not preferential direction of polarization. The area on the top of the electrode on the unpoled multilayer is characterized by the presence of metals inclusions and a different dimension of the grains and, as a consequence, of the domains. However, is possible to see some stripe-like domains also in this image, that corresponds to a tethragonal domain. The black spots and areas visible in Figure 4.17 are due to metal inclusions in the vicinity of the electrode

-3D image of an area located in the inactive zone:

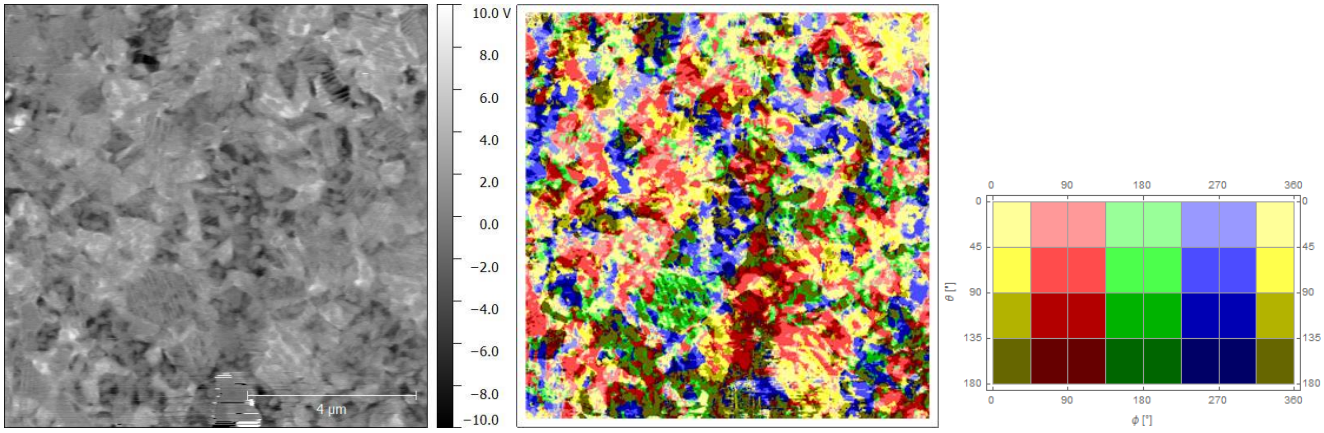

Figure 4.18 3D reconstruction of the piezoresponse vector of an area in the inactive zone made by DCP11 tip.

Again, there are not preferential direction of polarization for the domains, but some grains have a coherent orientation. Also here, from the lamellar domains feature is possible to see some areas with a tetragonal crystal structure. However, is important to note the decreasing of the domains dimension on the top of the electrode and in the inactive zone, this possibly due to a reduction of the grain size.

4.2.3 Mechanically Compressed sample results

The difficulty to find some reference points in the topography of this sample (and for the poled sample as well), induce the necessity to use some defects of the surface as reference points into the image. These defects in some cases could give a decrease of the overall quality of the reconstruction image. Also the lower and worse lateral contrast (in comparison with the unpoled sample) gave different 3D images, because in this case the colors are determined mostly by the vertical signal. The next results have been found using DCP11 tips and a resolution of 512X512 pixels.

-3D image of an area located in between of two electrodes:

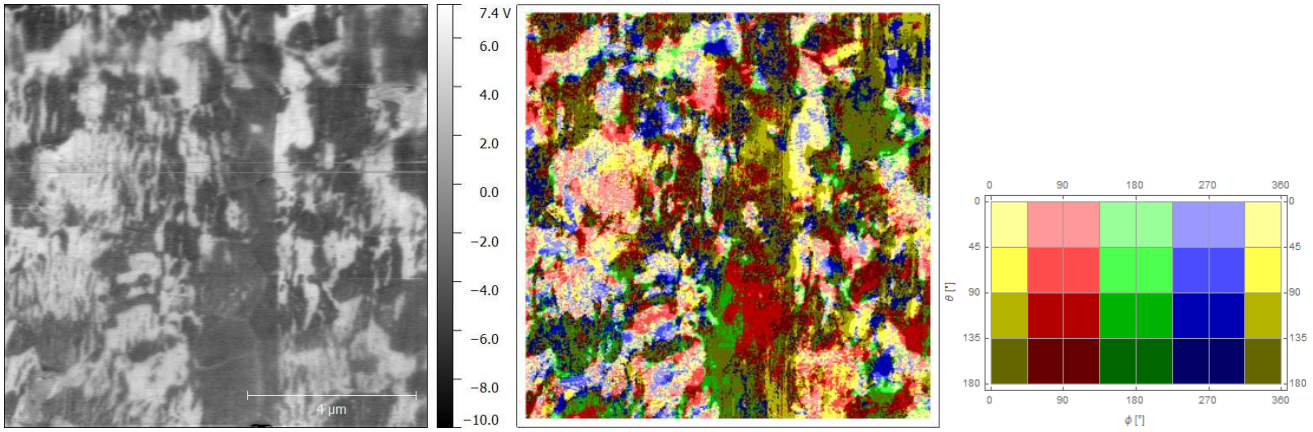

Figure 4.19 3D reconstruction of the piezoresponse vector of an area in between 2 electrodes made by DCP11 tip.

A representative area of 5X5µm has been selected for another evaluation to avoid the presence of artefacts in the 10X10 µm image and the presence of a dark area in the middle of the image. This was done because the artefact can affect the entire image, so all the 10X10 images have been cut and evaluated again with the Mathematica program. However, from the entire image is possible to see the size and orientation of the domains that is completely different with respect to the unpoled sample.

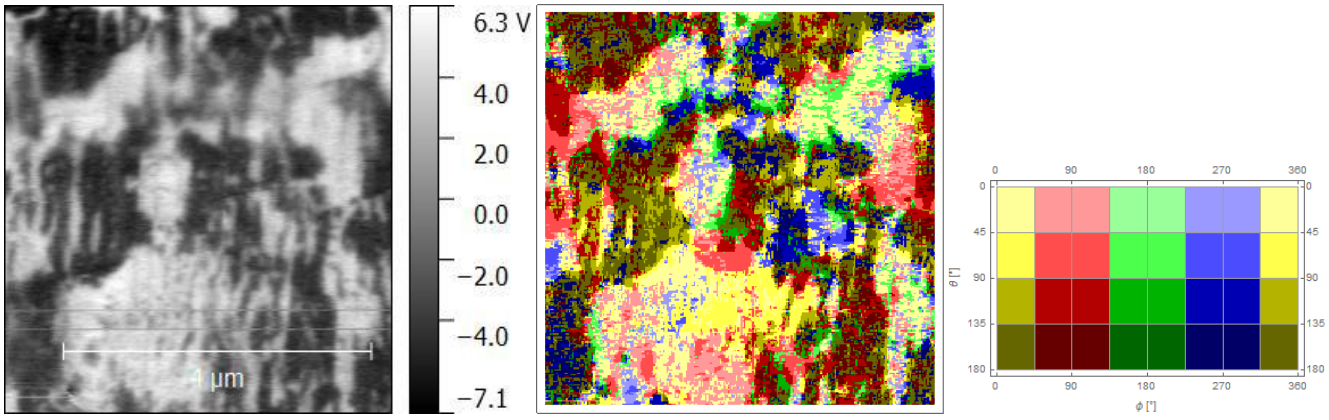

Figure 4.20 Evaluation of a representative area (5X5µm) from the last 3D reconstruction.

In this case the dominant color is the yellow that corresponds to a direction from 0° to 45°, so the domains are highly oriented parallel to the electrodes length. This is because of the applied compression, that align the domains perpendicular to it, so perpendicular to the sample length.

-3D image of an area located on the top of one electrode:

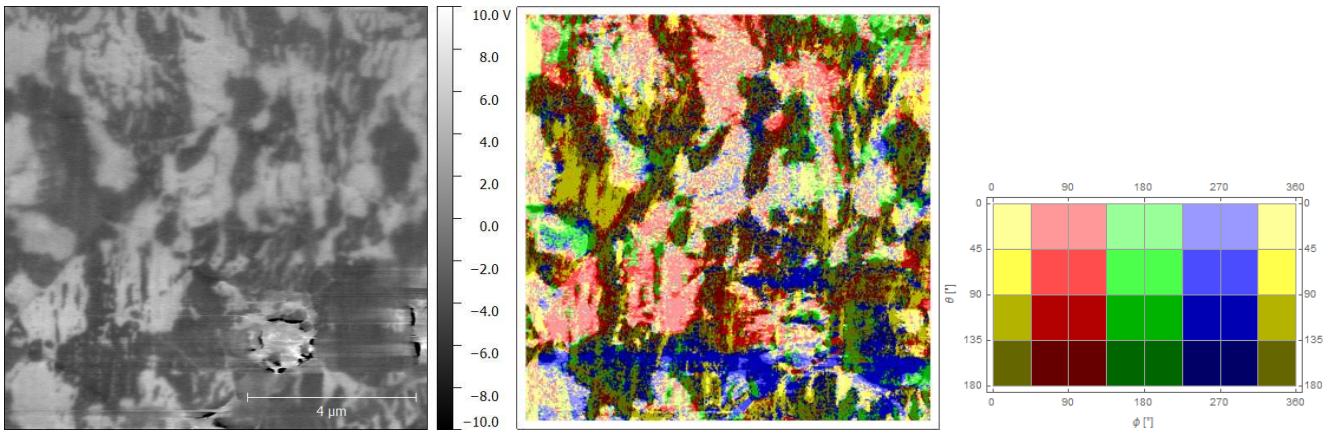

Figure 4.21 3D reconstruction of the piezoresponse vector of an area on the top of one electrode made by DCP11 tip.

Also in this case, was selected an area from the total 3D evaluation, because of the presence of a metal inclusion (on the bottom right) from the electrode's top that affect the evaluation.

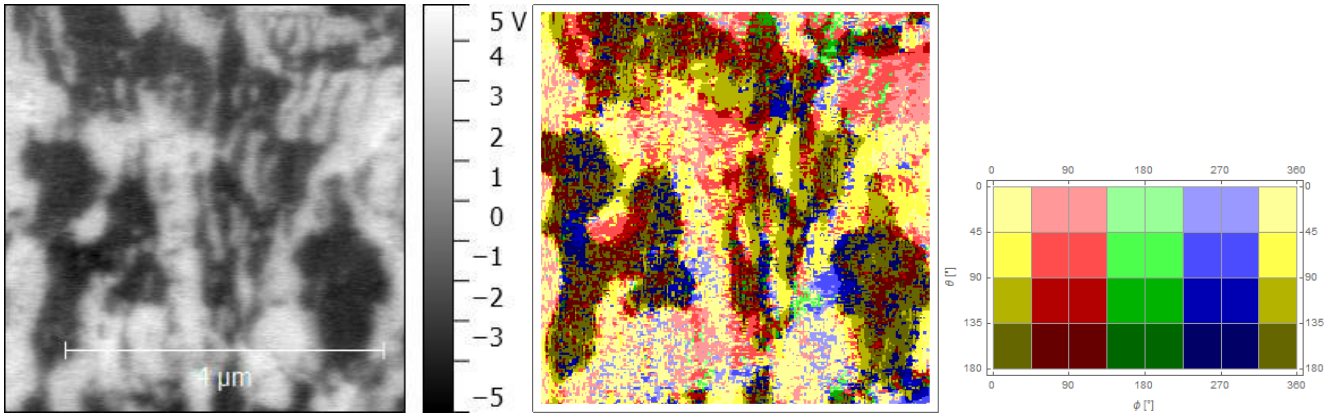

Figure 4.22 Evaluation of a representative area (5X5µm) from the last 3D reconstruction.

The selected area is again 5X5 and the main color is yellow, as seen before in the area in between the two electrodes. This corresponds to an high orientation of the domains in direction parallel to the electrodes and means that the compression influences also the zone near the electrodes top.

-3D image of an area located in the inactive zone:

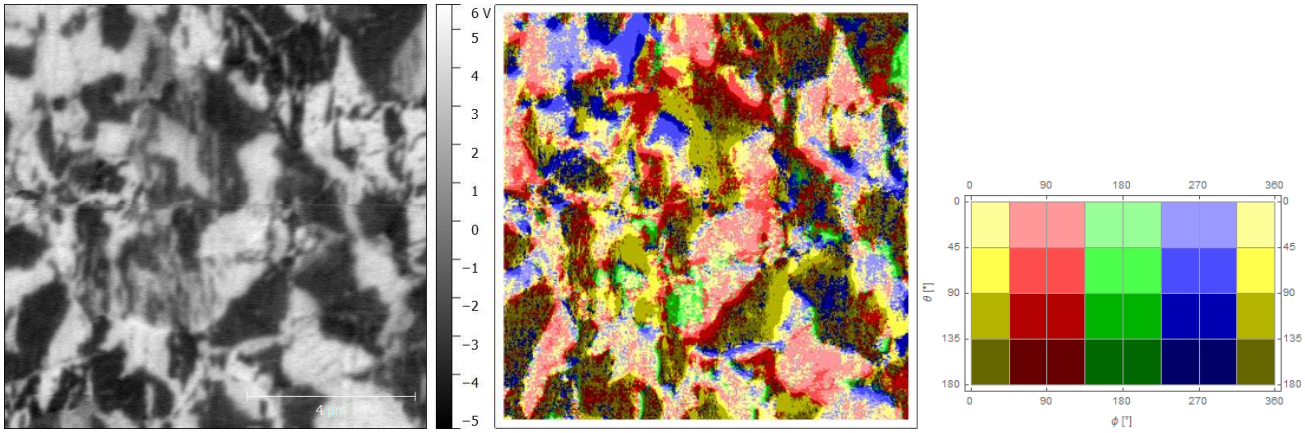

Figure 4.23 3D reconstruction of the piezoresponse vector of an area in the inactive zone made by DCP11 tip.

In the inactive zone the domains are more randomly distributed, which suggest that the compression didn't influence the domains orientation as strong as near the electrodes. This is probably due to the applied compressive stress being more homogeneous towards the center of the sample. Nevertheless, the dominant color is yellow, which confirms the preferential orientation parallel to the electrodes. This is also likely the reason why the domains in the inactive zone appear bigger than in the unpoled case.

4.2.4 Electrically poled sample results

The next results have been obtained using DCP11 tips and a resolution of 512X512 pixels. The electrically poled sample gave the worst results in terms of lateral signal, so as in the compressed samples, the resulted 3D images are mostly determined by the vertical signal.

-3D image of an area located in between of two electrodes:

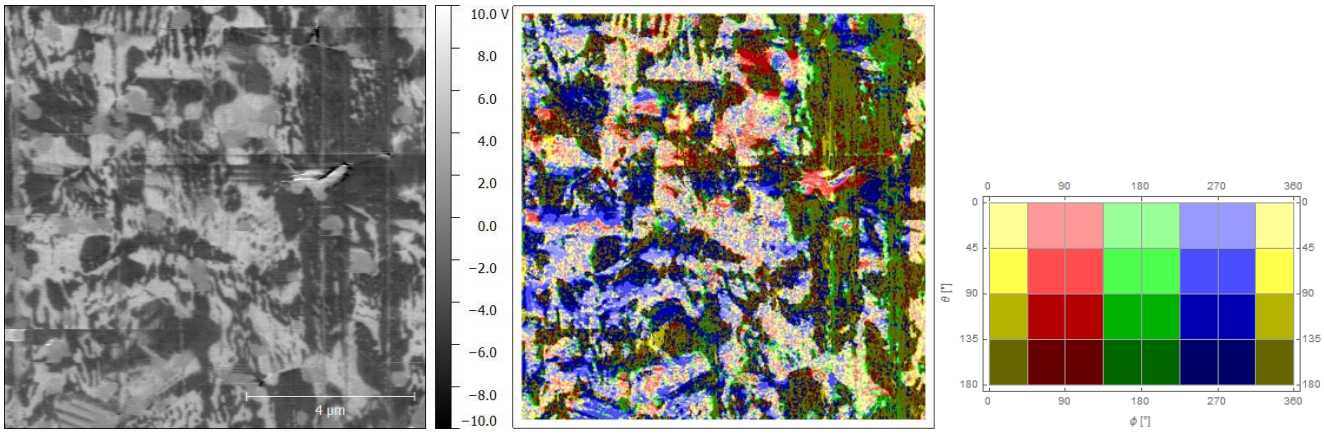

Figure 4.24 3D reconstruction of the piezoresponse vector of an area in between 2 electrodes made by DCP11 tip.

This area is affected from some line-shape artifacts, a metal inclusion, and a dark area on the right side. Therefore a representative area of 5X5 pixels was selected to avoid the presence of the line defects that can be seen in figure 4.24. However, from the complete image is possible to see that the domains shape is changed and is possible to speculate that the main phase in the poled multilayer is the rhombohedral one. This is in accord with recent XRD investigations on similar multilayer samples [13] There are also the presence of stripe-like domains as seen before in the vertical signal and in the orientation of polarization map, that show the presence of little areas in which the phase is tetragonal.

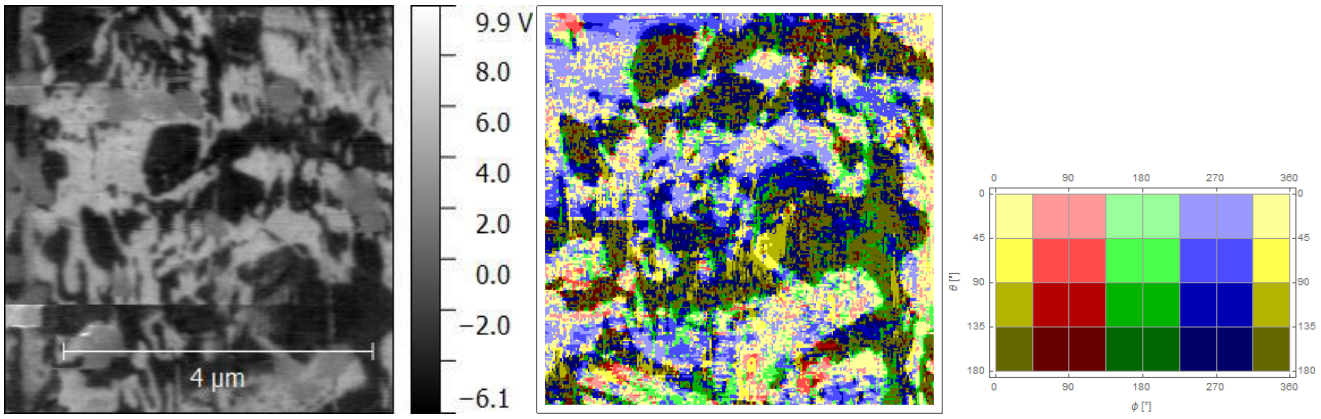

Figure 4.25 Evaluation of a representative area (5X5µm with 256X256 pixels) from the last 3D reconstruction.

From the selected area is possible to see that the most present color in the image is the blue, this means that the domains are mainly oriented in direction of 270° that is in direction perpendicular to the electrodes. This is due to the electric field (induced by the current flow in the electrodes) that was applied perpendicular to the electrodes.

-3D image of an area located on the top of one electrode:

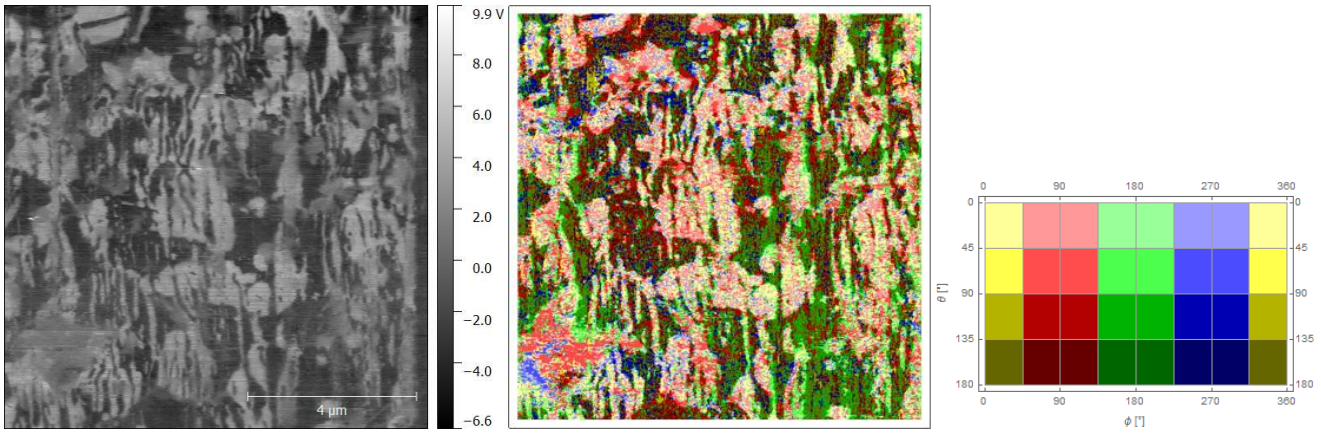

Figure 4.26 3D reconstruction of the piezoresponse vector of an area on the top of one electrode made by DCP11 tip.

On the top of one electrode the lines of the electric field start from the top of the electrode and move away from the electrode tip [14]. And this is what is possible to see from the 3D image, the position of the electrode top is on the left with respect of the area of the image and the response vector is oriented at 180°, that means parallel to electrode's length, and in direction away from the electrode. Watching away from the electrode tip, the colors change and become more red and blue, that means that at a certain point, the electric field's lines flow circularly in direction perpendicular to the previous direction. There is a preferential direction of the domains areas in the vertical response, that are elongated orthogonally with respect to the electrodes length.

-3D image of an area located in the inactive zone:

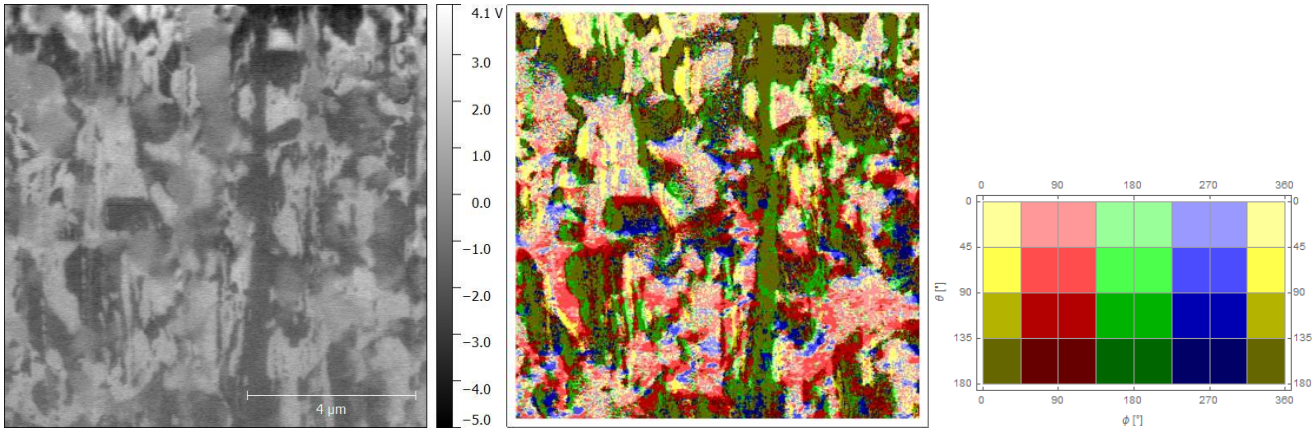

Figure 4.27 3D reconstruction of the piezoresponse vector of an area in the inactive zone made by DCP11 tip.

A representative area of 5X5 pixels was selected from the lower part of the 3D, because the upper part of the image was compromised by the fact that the lateral signal of the rotated sample was only background noise. In the complete image is possible to see that there is a little orientation of the domains areas in the vertical response but is not accentuated as on the top of the electrode. The domains dimension is larger for the inactive zone with respect to the other positions in the poled sample. This is due to the less influence of electric field that doesn't affect the dimension and the orientation of the domains in the inactive zone.

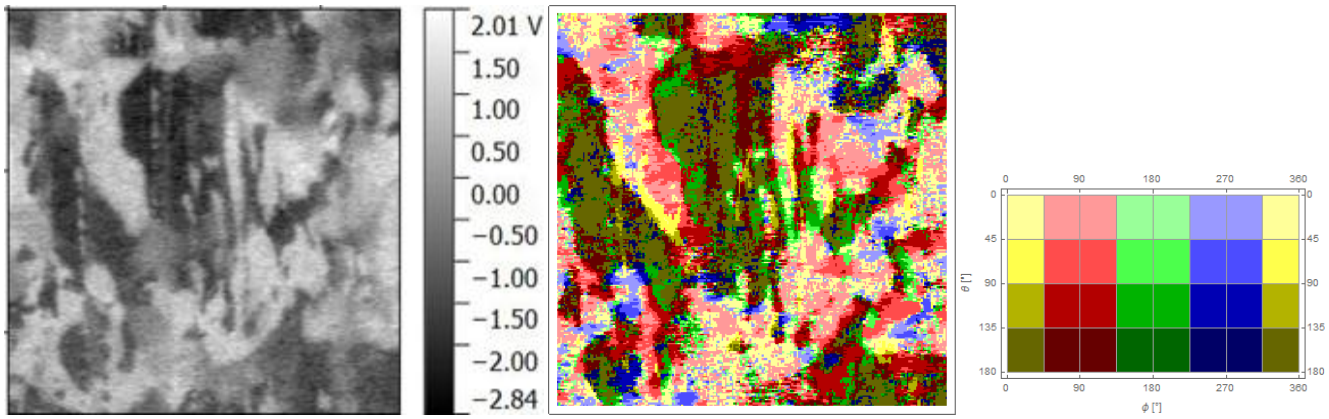

Figure 4.28 Evaluation of a representative area (5X5μm with 256X256 pixels) from the last 3D reconstruction.

As it is shown in the representative area, the domains are well distributed in almost all the direction, but in particular in the 90°/180° range. This is due to a small influence of the electrodes, that in the inactive zone are more distant each other, so the domains are in part oriented with respect of the electric field (90°, red areas), and in part remains unpoled (0°,yellow areas and 180°, green areas).

4.3 Domain orientation nearby cracks

In this work of thesis, some cracks have been produced on the unpoled sample to see the change of the domains orientation nearby the crack. The next images are shown as only preliminary results: As evident from below, more work and more time would be needed to perfect PFM measurements nearby cracks, and this was beyond the scope of the present work. The reference system is the same as before, as seen in Figure 4.12. To evaluate the orientation of polarization on the top of the crack, the indentation has been placed in two positions: between of two electrodes and on the top of one electrode. There will be two images for every shown area:

- topography,

- piezoresponse vector image with the highlighted crack.

4.3.1 Polarization direction in presence of cracks on the electrically unpoled sample

The position of the crack area analyzed with reference to the electrodes is shown in Figure 4.29.

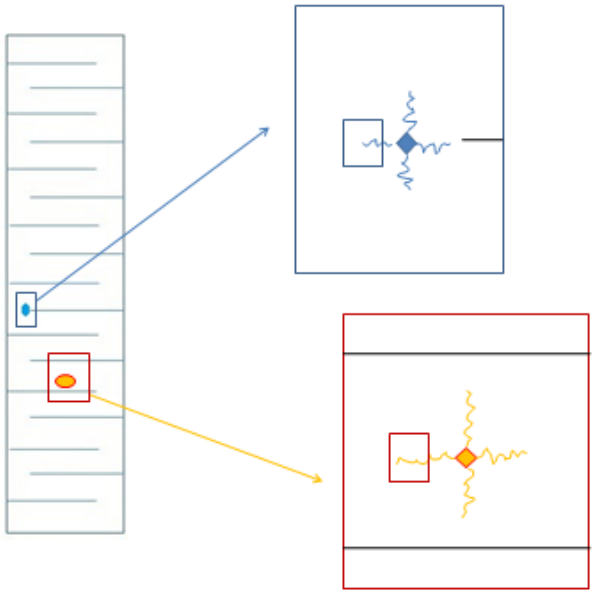

Figure 4.29 Scheme of the position of the cracks and the related analyzed area in the electrically unpoled sample.

-3D image of an area located in between of two electrodes:

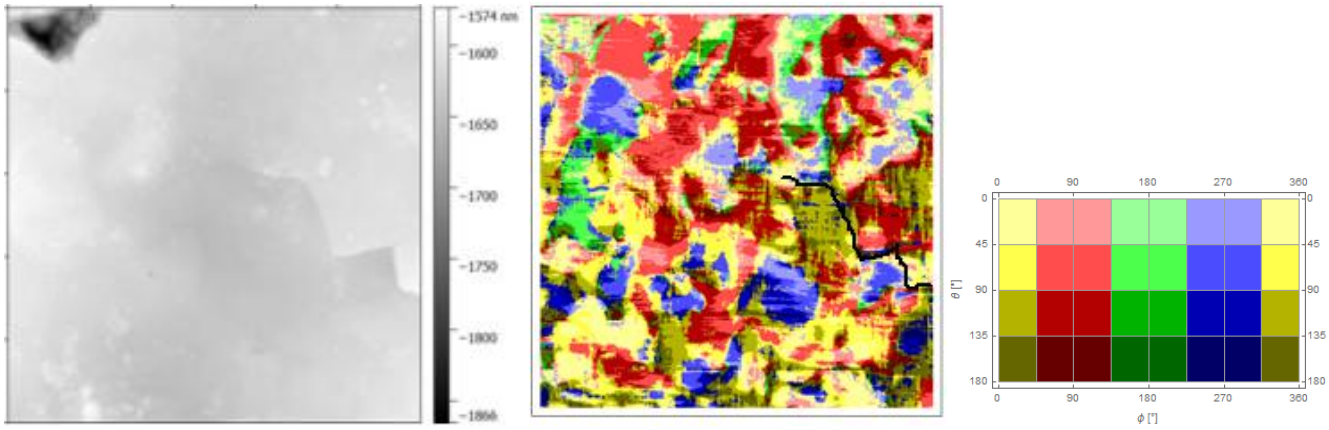

Figure 4.30 Images related to a crack area (10x10µm, 512x512 pixels with DCP 11) in the electrically unpoled sample between electrodes. In the piezoresponse vector representation the crack is highlighted.

The crack is intergranular, and in this specific case, it is possible to speculate that the crack propagation is stopped by the presence of a grain. However, there was not enough resolution to see the grain boundaries to confirm this, because the crack presence affected the quality of the tip contact with the surface. As a matter of fact the part on the left in the image, less affected by the crack presence, gives a little bit more information about the grain boundaries. The black spot on the left side of the topography was probably a metal inclusion that was used as a reference to find again the area after the sample rotation. Is important to see that there is not a strong influence of the crack on the domains, that have remained randomly distributed.

-3D image of an area located on the top of one electrode:

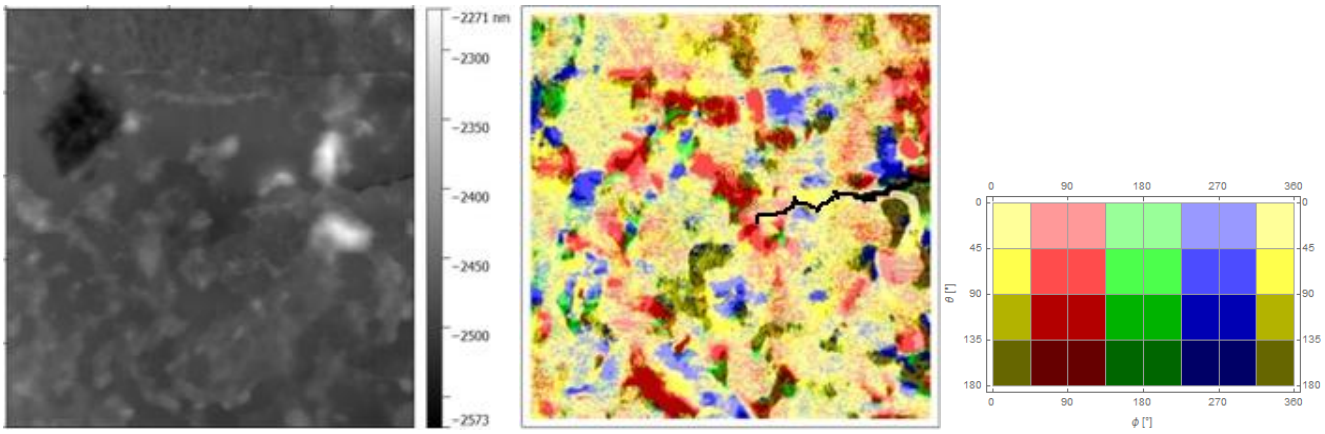

Figure 4.31 Images related to a crack area (10x10µm, 512x512 pixels with DCP 11) in the electrically unpoled sample on the top of one electrode. In the vector representation the crack is highlighted.

On the top of the electrode there is an high presence of imperfections and metal inclusions, and this evaluation of the piezoresponse map is highly affected by an horizontal artifact that could have been given by another crack coming from the indentation. This makes the final 3D vector representation not indicative of the real orientation of all the domains in the area. However it is possible to say that the domains are not affected by the crack presence.

4.3.2 Polarization direction in presence of cracks on the mechanically compressed sample

The position of the crack area analyzed with reference to the electrodes is shown in Figure 4.32.

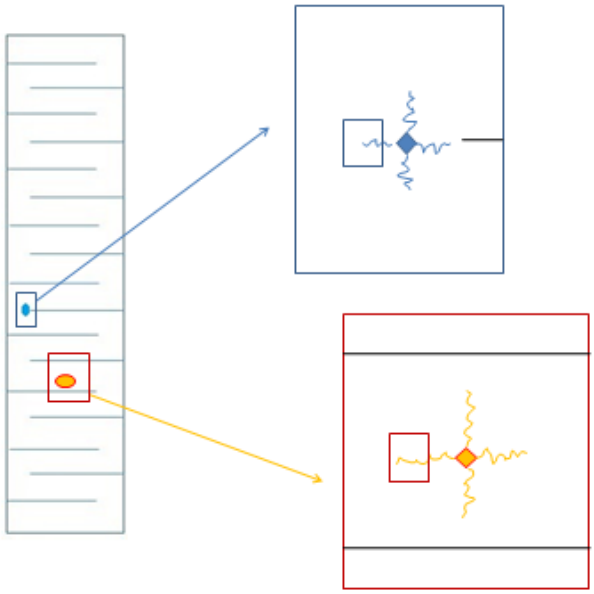

Figure 4.32 Scheme of the position of the cracks and the related analyzed area in the mechanically compressed sample.

-3D image of an area located in between of two electrodes:

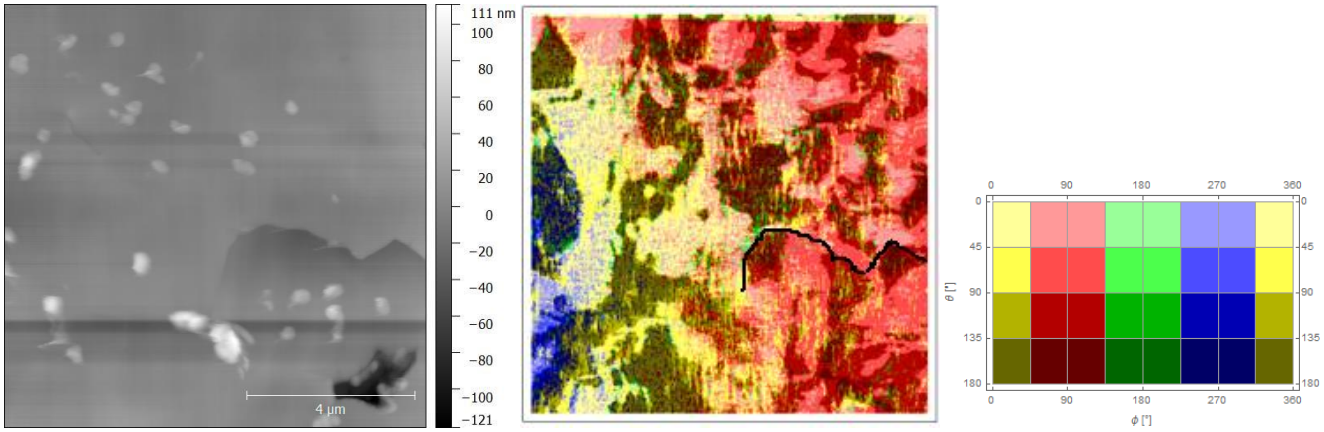

Figure 4.33 Images related to a crack area (10x10µm, 512x512 pixels with DCP11) between two electrodes in the mechanically compressed sample. In the vector representation the crack is highlighted.

The area near the crack has more visible stripe-like domains (from the 3D representation), than away from the crack top; this is because of the stress release given by the crack presence. Moreover, the most dominant orientation of the domains is perpendicular to the crack length (Red=90°), and after the crack curvature the main color is yellow, that means that the domains are oriented on 0°, parallel to the crack length.

-3D image of an area located on the top of one electrode:

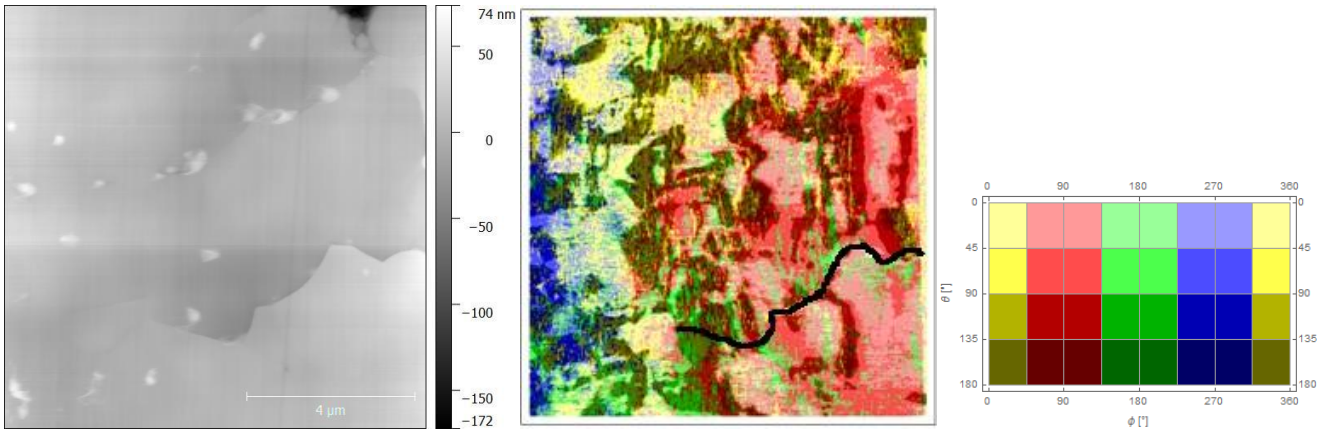

Figure 4.34 Images related to a crack area (10x10µm, 512x512 pixels with DCP11) on the top of the electrode in the mechanically compressed sample. In the vector representation the crack is highlighted.

Also in this case, the domains are oriented perpendicular to the crack length (90°). Going near the top of the crack, the color changes to green and then yellow, which corresponds to an orientation of the domains away from the crack top. It seems like the crack top greatly influences the domains directions. Is possible

also here to speculate that the crack movement was blocked by the presence of a grain that can be seen in the images.

4.3.3 Polarization direction in presence of cracks on the electrically poled sample

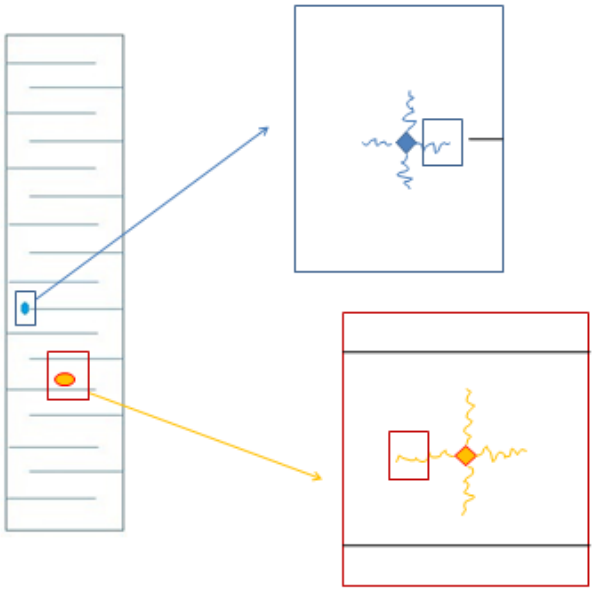

Figure 4.35 Scheme of the position of the cracks and the related analyzed area in the electrically poled sample.

-3D image of an area located in between of two electrodes:

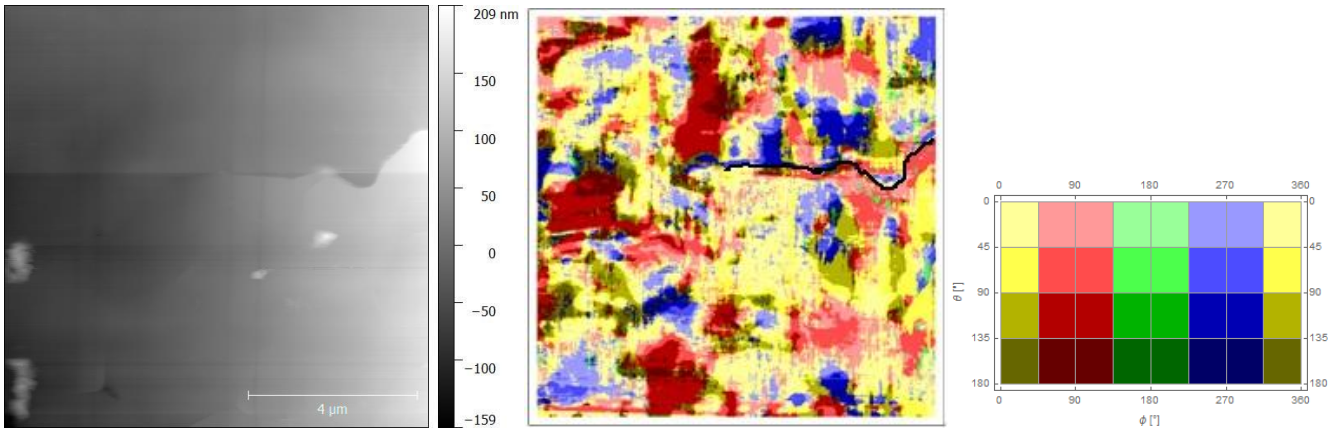

Figure 4.36 Images related to a crack area (10x10µm, 512x512 pixels with DCP11) between 2 electrodes in the electrically poled sample. In the vector representation the crack is highlighted.

Not all the domains are oriented with respect to the crack movement as seen before in the mechanically compressed sample, here some domains are oriented like the blue and the red ones perpendicular to the crack length. As a matter of fact near the top of the crack, above there is a large red domain oriented

perpendicular to the crack length, and below the main orientation is yellow, so parallel to the crack length. On the crack tip, the main orientation is 0° (yellow) so oriented away from the crack tip. The blue line on the crack is an artifact, and it was possible to see it in the vertical signal image. On the border below of the image is possible to see a little mismatch given by the not perfect correspondence of the area scanned before and after rotation.

-3D image of an area located on the top of one electrode:

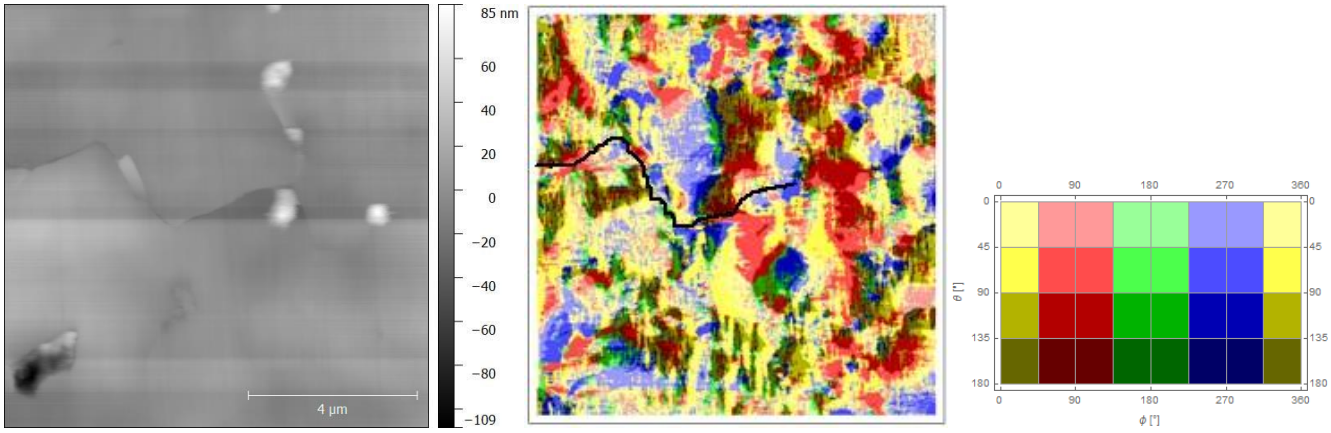

Figure 4.37 Images related to a crack area (10x10µm, 512x512 pixels with DCP11) on the top of the electrode in the electrically poled sample. In the vector representation the crack is highlighted.

Here the main orientation of the domains disposed along the crack is perpendicular to the crack length (blue and red areas), that is coherent with the theoretical tensional distribution along the crack. From this point of view this image is the most representative of all the cracks analyzed in this work. A peculiarity of this image is the presence of a large grain on the tip of the crack that blocks it and maintains the previous orientation (90°). There are some little roughness on the surface, other than the crack, that affect the quality of the topography image.

4.4 Schematic representation of the results

From the previous paragraph results, some schematic representations have been produced to better understand the domains direction of polarization. This schemes have been done also for the samples in presence of cracks. The unpoled sample results haven't been schematically represented because there is not a specific direction of the domains, on the contrary they remain randomly oriented also in presence of cracks.

4.4.1 Domains orientation in the mechanically compressed sample

- Domains orientation without cracks

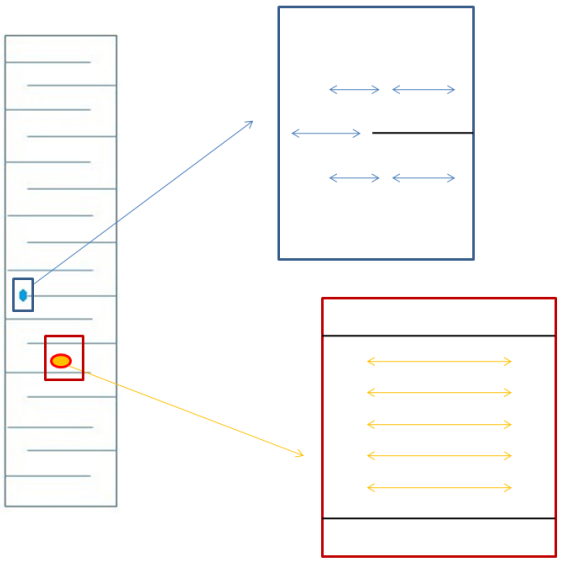

Figure 4.38 Domains orientation in 2 positions: on the top of the electrodes and in between the electrodes.

The domains, as seen in the last chapter, are oriented parallel to the electrodes length because of the mechanical stress of compression that orients the domains perpendicular to it. Also on the top of the electrodes there is this behavior of the domains. On the contrary, in the inactive zone the effect become less visible, because of the vicinity to sample edge, where the applied compressive stress is less homogeneus.

- *Domains orientation in presence of cracks*

The shown domains orientation in presence of cracks are representative only of the specific areas measured in this work.

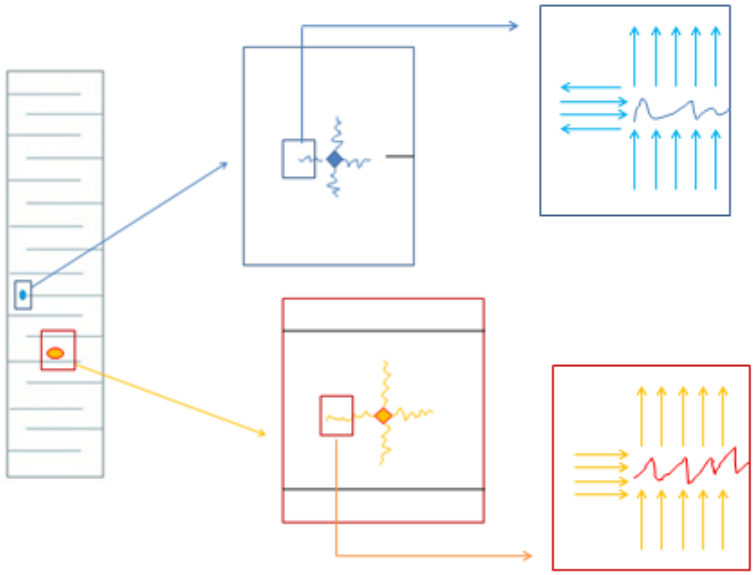

Figure 4.39 Scheme of the domains distribution in the areas near the crack and relative position of the crack examined.

As seen in Figure 4.33 and Figure 4.34, the main orientation alongside the crack was 90°, and so the crack presence affects heavily the domain orientation by turning them perpendicular to it. The behavior is equal in the top and in between the electrodes, the only difference is the presence on the top of the crack of domains oriented on 0 and 180°, for the area located on the top of one electrode, and in the area in between two electrodes, the domains are oriented only on zero degrees. This behavior is consistent with the ferroelastic effect at crack tip and along the crack wake, according to the theoretical distribution of residual stresses nearby Vickers indentations [15].

4.4.2 Domains orientation in the poled sample

- *Domains orientation without cracks*

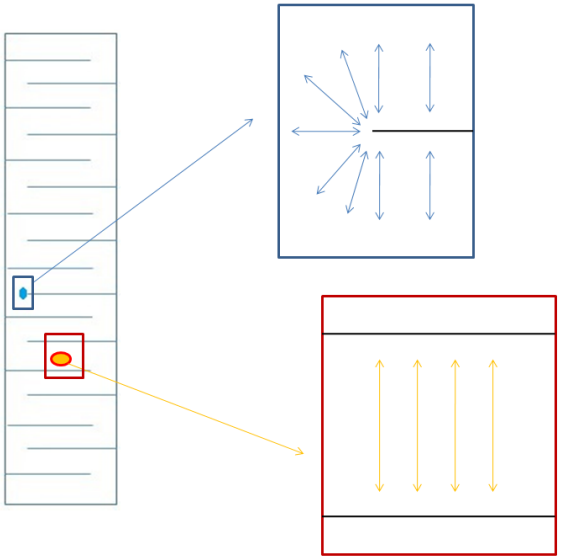

Figure 4.40 Scheme of domain orientation in 2 positions: in between the electrodes and on the top of the electrodes.

The domains are disposed perpendicular to the electrodes in the zone in between the electrodes, and also in the zone on the top of the electrodes, the domains are disposed circularly around the tip of the electrode, which is in accord with the lines of field present in this case [14].

- *Domains orientation in presence of cracks*

The shown domains orientation in presence of cracks are representative only of the specific areas measured in this work.

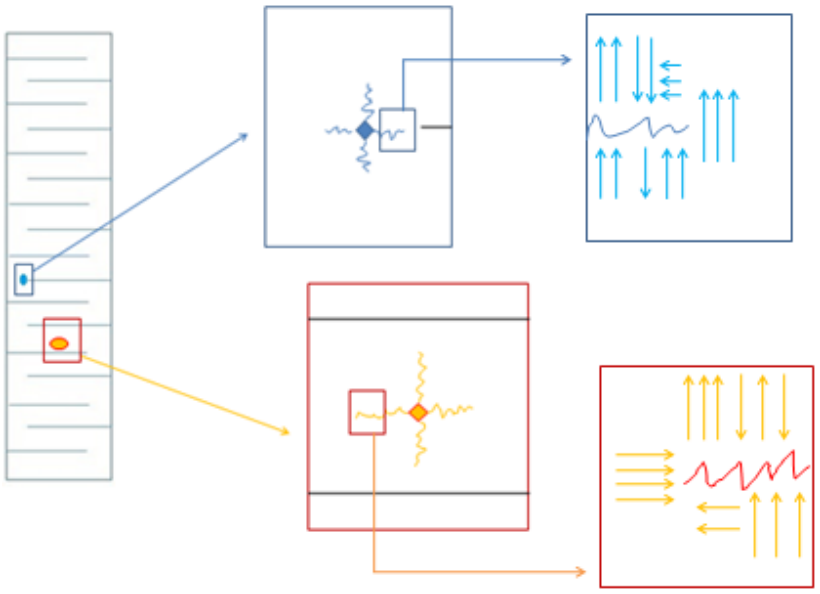

Figure 4.41 Scheme of the domains distribution in the area near the crack and relative position of the crack examined.

As it is possible to see from Figure 4.41 the domains could take an orientation given by the presence of the crack, or could remain unchanged. As a consequence, the greater part of the domains alongside the crack length are oriented perpendicular to it, and the other part of them remains oriented as before the indentation. On the top of the crack the situation changes in function of the position of the area analyzed:

-on the top of the electrode the domains are oriented at 90°, perpendicular to the crack length;

-in between the electrode the orientation of the domains is 0°, parallel to the crack length.

The difference is probably due to the inhomogeneous grain structure at the electrode tip.

Conclusions

During this thesis work 3 samples have been analyzed with a PFM system, one electrically unpoled, one mechanically compressed and one electrically poled. These samples were piezoelectric multilayer actuators, and one of the difficulty of the project was to adapt these devices to be scanned by a PFM. So the samples have been polished in different ways and some electric connection configurations has been used to find the better solution in terms of contrast and quality of the images obtained. A Mathematica code has been used to evaluate the direction of the piezoresponse vector in areas with several dimensions in different positions on the surface of the sample: in between of 2 electrodes, on the top of one electrode and in the inactive zone. The main results of this work are given by the main polarization directions of the domains in the 3 samples:

-Unpoled sample: the domains are randomly distributed in all the 3 different positions. The presence of stripe-like domains have been detected, and ensures the presence of tetragonal crystals. On the top of the electrodes the density of metal inclusions was higher than in the other areas, this was thought to be caused by the production process.

-Mechanically compressed sample: because of the presence of some artifacts, the images were cut to avoid possible influences. In between of 2 electrodes the domains are elongated in direction parallel to the electrode because of the compression. Also the zone on the top of the electrode is affected by the compression stress that align the domains parallel to the electrodes length. At the contrary, in the inactive zone the domains are randomly distributed, so this area is not affected by the compression stress, moreover the domains are bigger with respect to the inactive zone of the unpoled sample. These effects are probably associated with inhomogeneous compressive loading near the edge of the sample.

-Electrically poled sample: in between of 2 electrodes it's possible to speculate that the main phase present is the rhombohedral one, with little areas of tetragonal phase given by the stripe-like domains. The domains are mainly oriented in direction perpendicular to the electrodes as expected from electric field applications.
In position on the top of one electrode is possible to see that the domains are influenced by the lines of the electric field that starts from the top of the electrode and then move away from there with a circularly. Indeed, the domains are oriented in direction away from the electrode tip. It was possible to see that the domains areas are elongated perpendicular with respect to the electrodes length.
In the inactive zone the domains are in part oriented with the electric field of the electrodes that means perpendicular with respect to their length, and in part are not oriented, because of the greater distance between them.

To improve and refine the obtained results, it would be possible to use an automatic rotation system, in order to not rely on defects as reference points to find again the same area. This would allow to have better images, without big defects(that could compromise the entire 3D vector reconstruction), in less time. Without the rotation time and the time used to find again the previous area it would be possible to

do more scans and with an higher resolution, with lower scan speed, that could increase significantly the quality of the piezoresponse vector maps.
Some crack areas have been analyzed with the same procedure seen before, but the results shown are only preliminary and other PFM scans have to be done to achieve more valid data. Moreover, the crack presence affects not only the topography quality, but also the verticals and lateral images, because gives a discontinuity of the cantilever's tip contact, making it difficult to obtain reliable results. The way to achieve better results is by decreasing the scan speed and trying different kinds of cantilevers, and also testing different surface polishing to find the best configuration, exactly as has been done for the other measurements in this thesis work.

Nomenclature

A= Measurable piezoresponse amplitude

a = Calibration constant, function of the Lock-in settings and the sensitivity parameter

A_{el}= Electrostatic interactions between tip and surface

A_{nl}= Non linear contribution due to capacitive cantilever-surface interaction

A_{piezo}= Electromechanical contribution

A_{ik}= Rotation matrix

a,b,c= Proportional Coefficients

c^-= Ferroelectric domain in which the surface oscillation is in phase with the V_{tip} (φ=0°)

c^+= Ferroelectric domain in which the surface oscillation is out of phase with respect to the V_{tip} (φ=180°)

c= half of the length of the crack

d_{33}= Piezoelectric constant

D_2^{∞}= Remote electric displacement

d_{ij}^0= Piezoelectric constant tensor with the coordinate system related to the crystallographic coordinate system

E_i= Electric field vector

E_{Γ^-}= Remote electric displacement on a crack electrically conductive

f_{cont}= Contact resonance frequency

f_{free}= Resonance frequency

f_s= Sampling frequency

g= Direction of domains orientation

H= Tip height

k= Spring constant

K_{IV}= Stress intensity factor mode IV

K_E= Stress intensity factor mode E

K_F= Crack grow resistance

LPFM = Lateral Piezoresponce Force Microscopy

MRD= Multiple of random distribution

n= Cantilever orientation

N_{lj}= Rotation matrix

ODF= Orientation Distribution Function

P= Local polarization vector or P= indentation load

P_i= Polarization in an ideal piezoelectric crystal

Pr= Amplitude = X- output of the LIA

PR_l= Longitudinal piezoresponse (Buckling contribution)

PR_p= Perpendicular piezoresponse (Lateral contribution)

PR_v= Vertical piezoresponse

r= Small distance from the crack tip

R= Magnitude of the amplitude

(R, G, B)= Red, Green, Blue colors

$R_z(\theta_r)$= Rotation matrix

$R_z(\phi_r)$= Rotation matrix

T_C= Curie temperature

u= Displacement vector

V= Applied voltage

v= Scanning speed

VPFM = Vertical Piezoresponce Force Microscopy

vpr= Vertical piezoresponse normalized $\in (-1,1)$

V_{tip}= Periodic bias applied to the tip

w= Vector of the surface displacement

w_t= Displacement of the tip

X_1= Direction parallel to the crack length

X_2= Direction perpendicular to the crack length

X_j= Strain tensor

xpr= X- direction piezoresponse normalized $\in(-1,1)$

Y- = Output of the LIA free of any informations

ypr= Y-direction piezoresponse normalized $\in(-1,1)$

Greek Letters

ΔL= Length variation

ΔP_i= Change in spontaneous polarization

ΔK_B= Toughening grain size dependent

ΔK_F= Toughening magnetic field dependent

$\Delta K_{W,max}$= Max toughening in which the crack can move

$\Delta\varepsilon_{ij}$= Change in spontaneous strain (inelastic strain)

ϑ= φ= Phase

ϑ= Bragg angle

ϑ_d= Banding of cantilever angle= angle between the long axis of cantilever, and the X- axis of the lab coordinate system

(θ_r,ϕ_r)= Euler Angles

σ_{ij}= Mechanical stress matrix

τ= Time constant

(ϕ,θ,ψ)= Euler angles

χ= Shape parameter of the crack

Appendix: Mathematica program code

The following pages present the Mathematica program code with automatic evaluated functions and initialization cells appearing like this:
function[id]:=Max[id] !Min[id]

Readme: File IDs & PFM signal

Images :

-1 : Scan line: Trace (1), Retrace (2)

-2 : Channel : Topography (1), Deflection (2), Amplitude / R-Output (3), Phase / \[CapitalTheta]-Output (4), X-Output (5), Y-Output (6)

-3 : Signal: Vertical (0), Lateral (1)

-4 : Scan - Angle : 0 \[Degree] (0), 90 \[Degree] (1)

-5 : Sample - Rotation : 0 \[Degree] (1), 90 \[Degree] (2), 180 \[Degree] (3), 270 \[Degree] (4)

Example :

ID: name_of_file_21061.txt --> 90\[Degree] sample rotation, 90\[Degree] scan angle, vertical signal, Y-output, trace scan line

parameter .txt file:

This .txt file has to end with "_parameter.txt"

1st line: deflectionInvOLS vertical

2nd line: sensitivity vertical

3rd line: sensitivity lateral

4th line: phase offset

5th line: sensitivity vertical of background measurements

6th line: sensitivity lateral of background measurements

7th line: phase offset of background measurements

Example:

150.1 =150.1 nm/V deflectionInvOLS

1000 =1000\[Micro]V vertical sensitivity

200 =200\[Micro]V lateral sensitivity

0 =0\[Degree] phase offset

100 =100\[Micro]V vertical sensitivity of background measurements

20, =20\[Micro]V lateral sensitivity of background measurements,

0 =0\[Degree] phase offset of background measurements

PFM signal :

X-direction = 11;

Y-direction = 21;

Z-direction = 31;

0. Complete calculation

```
NotebookDirectory[];

SetDirectory[NotebookDirectory[]];

listAllFileNames = FileNames["*.txt"];

nFiles = Length[listAllFileNames];

Grid[Transpose[{Range[nFiles] // N, listAllFileNames}], Alignment -> Left];

dataToImport =
Table[{i,ToExpression[StringTake[listAllFileNames[[i]],{StringPosition[listAllFileNames[[i]],
"_"][[-1, 1]] + 1,

StringPosition[listAllFileNames[[i]], "."][[-1, 1]] - 1}]]}, {i, nFiles}];

listToOrder = SortBy[dataToImport, Last];

For[i = 1, i < Length[dataToImport] - 4, i++, listToOrder[[i]] =
ToExpression[StringReplacePart[ToString[listToOrder[[i]]], ToString[1], {-2, -2}]]];

dataToImport = SortBy[listToOrder, First];

listOfIDs = Sort[Transpose[dataToImport][[2]]];

MapThread[import[#1, #2] &, Transpose[dataToImport]];
```

```
imageID := 11051;

imageID90 := 21051;

imageID180 := 31051;

imageID270 := 41051;

imageIDLat := 10151;

imageID90Lat := 20151;

imageRefID := 11011;

imageRefID90 := 21011;

imageRefID180 := 31011;

imageRefID270 := 41011;

imageRefIDLat := 10111;

imageRefID90Lat := 20111;

imageRefIDBGXvert := 81058;

imageRefIDBGXlat := 80158;

imageRefIDBGYvert := 81068;

imageRefIDBGYlat := 80168;

npts = 4;

pts[1] = pts[2] = Table[{i, i}*10, {i, Range[npts]}];

marker = Evaluate[MapThread[Style[StringJoin["\[CenterDot]"], 40, #2] &, {Range[npts],
Take[ColorData[63, "ColorList"], npts]}]];

Grid[{{LocatorPane[Dynamic[pts[1]], Show[image[imageRefID], ImageSize -> 500], {{0, 0},
Dimensions[data[imageRefID]], {1, 1}}, Appearance -> marker],

    LocatorPane[Dynamic[pts[2]],

     Show[image[imageRefID90], ImageSize -> 500], {{0, 0}, Dimensions[data[imageRefID90]], {1,
1}}, Appearance -> marker]}, {Dynamic[pts[1]], Dynamic[pts[2]]}}, ItemSize -> 60, Frame -> All]

Dynamic[pts[1]]

Dynamic[pts[2]]
```

```
listToDo = listOfIDs[[1 ;; -6]];

phaseOffset = data[parameter][[4]][[1]];   (* \[Degree] *)

phaseOffsetBackground = data[parameter][[7]][[1]];   (* \[Degree] *)

deflectionInvOLSVertical = data[parameter][[1]][[1]]; (* nm/V *)

sensitivityVertical = N[data[parameter][[2]][[1]]*10^-6];(* V *)

sensitivityLateral = N[data[parameter][[3]][[1]]*10^-6] ; (* V *)

sensitivityVerticalBackground = N[data[parameter][[5]][[1]]*10^-6]; (* V *)

sensitivityLateralBackground = N[data[parameter][[6]][[1]]*10^-6]; (* V *)

backgroundVertX = Mean[Flatten[data[81058]]]*sensitivityVerticalBackground/10;

backgroundVertY = Mean[Flatten[data[81068]]]*sensitivityVerticalBackground/10;

backgroundLatX = Mean[Flatten[data[80158]]]*sensitivityLateralBackground/10;

backgroundLatY = Mean[Flatten[data[80168]]]*sensitivityLateralBackground/10;

listToCrop = Take[{imageRefID, imageRefID90, imageRefID180, imageRefID270},

    ToExpression[StringTake[ToString[Max[listToDo]], {-5}]]];

listRotateAngle = Flatten[Mod[{ArcCos[transFuncRot[#][[1, 1]]]/Degree, ArcSin[transFuncRot[#][[1,
2]]]/Degree, ArcSin[-transFuncRot[#][[2, 1]]]/Degree, ArcCos[transFuncRot[#][[2, 2]]]/Degree} & /@
listToCrop, 90]];

For[i = 1, i <= Length[listRotateAngle], i++, If[listRotateAngle[[i]] > 45, listRotateAngle[[i]],
listRotateAngle[[i]] = 90 - listRotateAngle[[i]]]]

angleMin = Min[listRotateAngle];

pixeladd = Ceiling[N[Cos[angleMin Degree]*512]] + 3

"pixeladd"

cropRangex[imageRefID] = {0, imageDim[imageRefID]};

cropRangey[imageRefID] = {0, imageDim[imageRefID]};

cropRangeAllx = {Max[Transpose[Map[cropRangex[#] &, listToCrop]][[1]]],

   Min[Transpose[Map[cropRangex[#] &, listToCrop]][[2]]]}

"cropRangeAllx"
```

```
cropRangeAlly = {Max[Transpose[Map[cropRangey[#] &, listToCrop]][[1]]],
Min[Transpose[Map[cropRangey[#] &, listToCrop]][[2]]]}

"cropRangeAlly"

Do[dataTrans[id] = ImageData[imageCropped[id]]*Max[data[id]], {id, listToDo}]

dataTrans[imageID] // Dimensions

"dimension of evaluated image"

id = imageID;

comp[31] = dataCorrX[id]

"z-direction: comp[31]"

id = imageIDLat;

comp[11] = dataCorrX[id]

"x-direction: comp[11]"

id = imageID90Lat;

comp[21] = dataCorrX[id]

"y-direction: comp[21]"

listAngleOct = MapThread[({Mod[\[Phi], 2 \[Pi]], \[Theta]} /. FindMinimum[funcOctant[#1, #2,
#3][\[Theta], \[Phi]], {{\[Theta], \[Pi]/2}, {\[Phi], 0}}][[2]]) &, {Sign[comp[11]], Sign[comp[21]],
Sign[comp[31]]}, 2]

"listAngleOct"

listAngleMin = MapThread[({Mod[\[Phi], 2 \[Pi]], \[Theta]} /. FindMinimum[funcOctant[#1, #2,
#3][\[Theta], \[Phi]], {{\[Theta], \[Pi]/2}, {\[Phi], 0}}, MaxIterations -> 1000][[2]])
&,{compAbsNorm[11], compAbsNorm[21], compAbsNorm[31]}, 2]

"listAngleMin"

nVectorOct = Dimensions[listAngleOct][[1]]*Dimensions[listAngleOct][[2]];

thstep = 90(*\[Degree]*);

psistep = 90(*\[Degree]*);

bc2mc = BinCounts[Flatten[listAngleOct, 1]/Degree, {0, 360, psistep}, {0, 180, thstep}];

bc2mcNormQuantity = bc2mc/nVectorOct // N;
```

```
npsisteps = 360/psistep;

normc = (Table[Integrate[Sin[x], {x, theta, theta + thstep*Degree}], {theta, 0, (180 - thstep)*Degree, thstep*Degree}]*2 \[Pi]/npsisteps) // N;

octants = Transpose[Transpose[bc2mcNormQuantity]/normc];

colorScheme = ColorData["TemperatureMap"];

figOctants =Labeled[ArrayPlot[Transpose[(octants/(1/(4 Pi)))/Max[octants/(1/(4 Pi))]],

    DataRange -> {{90/2, 360 - 90/2}, {-180 + 90/2, -90/2}},

    ColorFunction -> colorScheme, ColorFunctionScaling -> False, Mesh -> True,

    FrameTicks -> {{Transpose[{Range[-180, 0, 45], Range[180, 0, -45]}], Transpose[{Range[-180, 0, 45], Range[180, 0, -45]}]}, {Range[0, 360, 90], Range[0, 360, 90]}},

Frame -> True,

    FrameLabel -> {"\[Theta] [\[Degree]]", "\[Phi] [\[Degree]]"},

    LabelStyle -> Directive[Black, Bold], AspectRatio -> 1/GoldenRatio], DensityPlot[y, {x, 0, 210}, {y, 0, Max[octants]/(1/(4 Pi))},

    ColorFunction -> Function[{y}, colorScheme[y]],

    ColorFunctionScaling -> True, PlotRangePadding -> None, Frame -> True,

    FrameLabel -> {"", "", Style["ODF", Black, Bold], Style["[MRD]", Black, Bold]},

    FrameTicks -> {{None, Range[0, Max[octants]/(1/(4 Pi)), Round[((Max[octants]/(1/(4 Pi))) - .05)/4, .01]]}, {None, None}}, FrameStyle -> Black, BaseStyle -> {FontFamily -> "Helvetica", 14}, AspectRatio -> 12, ImageSize -> All], Right]

CreateDirectory[NotebookDirectory[] <> "Export"] // Quiet;

SetDirectory[%]

Export["octants.txt", octants // Transpose, "TSV"]

Export["octants.pdf", figOctants];

Export["octants.eps", figOctants];

Export["octants.tiff", figOctants];

nAngle = Dimensions[listAngleMin][[1]]*Dimensions[listAngleMin][[2]]

"Quantity of data points"
```

```
thstep = 45(*\[Degree]*);

psistep = 45(*\[Degree]*);

bc2mc = BinCounts[Flatten[listAngleMin, 1]/Degree, {0, 360, psistep}, {0, 180, thstep}];

bc2mcNormQuantity = bc2mc/nAngle // N;

(* Korrektur die Kugeloberfläche berücksichtigt *)

(* Correction taking the surface of a sphere into account *)

npsisteps = 360/psistep;

normc = (Table[Integrate[Sin[x], {x, theta, theta + thstep*Degree}], {theta, 0, (180 - thstep)*Degree,
thstep*Degree}]*2 \[Pi]/npsisteps) // N;

(* Überprüfen ob Summe der korrgierten Daten genau 4 Pi entspricht *)

(* Verify that sum of corrected data equals 4 Pi *)

Total[normc]*npsisteps == 4 \[Pi]

"Verify that sum of corrected data equals 4 Pi"

(* MRD - Multiple Random Distribution *)

odf1 = Transpose[Transpose[bc2mcNormQuantity]/normc]/(1/(4 \[Pi])) ;

maxODF = 6;

figure1 =Labeled[ArrayPlot[Transpose[odf1/maxODF],

    DataRange -> {{psistep/2, 360 - psistep/2}, {-180 + thstep/2, -thstep/2}},

    ColorFunction -> colorScheme, ColorFunctionScaling -> False, Mesh -> True,

    FrameTicks -> {{Transpose[{Range[-180, 0, 45], Range[180, 0, -45]}],

        Transpose[{Range[-180, 0, 45], Range[180, 0, -45]}]}, {Range[0, 360, 90], Range[0, 360, 90]}},

Frame -> True,

    FrameLabel -> {"\[Theta] [\[Degree]]", "\[Phi] [\[Degree]]"},

    LabelStyle -> Directive[Black, Bold], AspectRatio -> 1/GoldenRatio],

   DensityPlot[y, {x, 0, 1}, {y, 0, maxODF}, ColorFunction -> Function[{y}, colorScheme[y]],

    ColorFunctionScaling -> True, PlotRangePadding -> 0, Frame -> True,
```

```
    FrameLabel -> {{"", Style["[MRD]", Black, Bold]}, {"", Style["ODF", Black, Bold]}},
    FrameTicks -> {{None, Range[0, maxODF]}, {None, None}},
    FrameStyle -> Black, BaseStyle -> {FontFamily -> "Helvetica", 14},
    AspectRatio -> 12, ImageSize -> 68], Right]
Export["ODF_45.txt", odf1 // Transpose, "TSV"]
Export["ODF_45.pdf", figure1];
Export["ODF_45.eps", figure1];
Export["ODF_45.tiff", figure1];
thstep = 22.5(*\[Degree]*);
psistep = 22.5(*\[Degree]*);
bc2mc = BinCounts[Flatten[listAngleMin, 1]/Degree, {0, 360, psistep}, {0, 180, thstep}];
bc2mcNormQuantity = bc2mc/nAngle // N;
(* Korrektur die Kugeloberfläche berücksichtigt *)
(* Correction taking the surface of a sphere into account *)
npsisteps = 360/psistep;
normc = (Table[Integrate[Sin[x], {x, theta, theta + thstep*Degree}], {theta, 0, (180 - thstep)*Degree,
thstep*Degree}]*2 \[Pi]/npsisteps) // N;
(* MRD - Multiple Random Distribution *)
odf2 = Transpose[Transpose[bc2mcNormQuantity]/normc]/(1/(4 \[Pi])) ;
figure2 =Labeled[ArrayPlot[Transpose[odf2/maxODF],
    DataRange -> {{psistep/2, 360 - psistep/2}, {-180 + thstep/2, -thstep/2}},
    ColorFunction -> colorScheme, ColorFunctionScaling -> False, Mesh -> True,
    FrameTicks -> {{Transpose[{Range[-180, 0, 45], Range[180, 0, -45]}],
        Transpose[{Range[-180, 0, 45], Range[180, 0, -45]}]}, {Range[0, 360, 90], Range[0, 360, 90]}},
Frame -> True,
    FrameLabel -> {"\[Theta] [\[Degree]]", "\[Phi] [\[Degree]]"},
```

```
    LabelStyle -> Directive[Black, Bold], AspectRatio -> 1/GoldenRatio],
   DensityPlot[y, {x, 0, 1}, {y, 0, maxODF}, ColorFunction -> Function[{y}, colorScheme[y]],
    ColorFunctionScaling -> True, PlotRangePadding -> 0, Frame -> True,
    FrameLabel -> {{"", Style["[MRD]", Black, Bold]}, {"", Style["ODF", Black, Bold]}},
    FrameTicks -> {{None, Range[0, maxODF]}, {None, None}},
    FrameStyle -> Black, BaseStyle -> {FontFamily -> "Helvetica", 14},
AspectRatio -> 12, ImageSize -> 68], Right]
Export["ODF_225.txt", odf2 // Transpose, "TSV"]
Export["ODF_225.pdf", figure2];
Export["ODF_225.eps", figure2];
Export["ODF_225.tiff", figure2];
thstep = 15(*\[Degree]*);
psistep = 15(*\[Degree]*);
bc2mc = BinCounts[Flatten[listAngleMin, 1]/Degree, {0, 360, psistep}, {0, 180, thstep}];
bc2mcNormQuantity = bc2mc/nAngle // N;
(* Korrektur die Kugeloberfläche berücksichtigt *)
(* Correction taking the surface of a sphere into account *)
npsisteps = 360/psistep;
normc = (Table[Integrate[Sin[x], {x, theta, theta + thstep*Degree}], {theta, 0, (180 - thstep)*Degree,
thstep*Degree}]*2 \[Pi]/npsisteps) // N;
(* MRD - Multiple Random Distribution *)
odf3 = Transpose[Transpose[bc2mcNormQuantity]/normc]/(1/(4 \[Pi])) ;
figure3 =Labeled[ArrayPlot[Transpose[odf3/maxODF],
    DataRange -> {{psistep/2, 360 - psistep/2}, {-180 + thstep/2, -thstep/2}},
    ColorFunction -> colorScheme, ColorFunctionScaling -> False, Mesh -> True,
    FrameTicks -> {{Transpose[{Range[-180, 0, 45], Range[180, 0, -45]}],
```

```
        Transpose[{Range[-180, 0, 45], Range[180, 0, -45]}]}, {Range[0, 360, 90], Range[0, 360, 90]}},
Frame -> True,
    FrameLabel -> {"\[Theta] [\[Degree]]", "\[Phi] [\[Degree]]"},
    LabelStyle -> Directive[Black, Bold], AspectRatio -> 1/GoldenRatio],
   DensityPlot[y, {x, 0, 1}, {y, 0, maxODF},
    ColorFunction -> Function[{y}, colorScheme[y]],
    ColorFunctionScaling -> True, PlotRangePadding -> 0, Frame -> True,
    FrameLabel -> {{"", Style["[MRD]", Black, Bold]}, {"", Style["ODF", Black, Bold]}},
    FrameTicks -> {{None, Range[0, maxODF]}, {None, None}},
    FrameStyle -> Black, BaseStyle -> {FontFamily -> "Helvetica", 14},
    AspectRatio -> 12, ImageSize -> 68], Right]
Export["ODF_15.txt", odf3 // Transpose, "TSV"]
Export["ODF_15.pdf", figure3];
Export["ODF_15.eps", figure3];
Export["ODF_15.tiff", figure3];
dataAngleColor = listAngleMin*0;
For[i = 1, i <= Dimensions[dataTrans[imageID]][[1]], i++,
 For[n = 1, n <= Dimensions[dataTrans[imageID]][[2]], n++,
  Module[{indexChannel}, indexChannel = listAngleMin[[i]][[n]][[1]]; Which[indexChannel < 0,
dataAngleColor[[i]][[n]] = 0,
0 <= indexChannel <= \[Pi]/4, dataAngleColor[[i]][[n]] = Yellow, \[Pi]/4 < indexChannel <= 3/4*\[Pi],
dataAngleColor[[i]][[n]] = Red, 3/4*\[Pi] < indexChannel <= 5/4*\[Pi], dataAngleColor[[i]][[n]] =
Green, 5/4*\[Pi] < indexChannel <= 7/4*\[Pi], dataAngleColor[[i]][[n]] = Blue, 7/4*\[Pi] <
indexChannel , dataAngleColor[[i]][[n]] = Yellow]]]]
dataAngleColorAll = listAngleMin*0;
For[i = 1, i <= Dimensions[dataTrans[imageID]][[1]], i++,
 For[n = 1, n <= Dimensions[dataTrans[imageID]][[2]], n++,
```

```
  Module[{indexChannel}, indexChannel = listAngleMin[[i]][[n]][[2]]; Which[indexChannel <=
\[Pi]/4,

    If[dataAngleColor[[i]][[n]] == 0, dataAngleColorAll[[i]][[n]] = LightGray,
dataAngleColorAll[[i]][[n]] = Lighter[dataAngleColor[[i]][[n]], 0.6], dataAngleColorAll[[i]][[n]] =
Lighter[dataAngleColor[[i]][[n]], 0.6]], \[Pi]/4 < indexChannel <= \[Pi]/2,

    If[dataAngleColor[[i]][[n]] == 0, dataAngleColorAll[[i]][[n]] = LightGray,
dataAngleColorAll[[i]][[n]] = Lighter[dataAngleColor[[i]][[n]], 0.3], dataAngleColorAll[[i]][[n]] =
Lighter[dataAngleColor[[i]][[n]], 0.3]], \[Pi]/2 < indexChannel <= 3/4*\[Pi],

    If[dataAngleColor[[i]][[n]] == 0, dataAngleColorAll[[i]][[n]] = LightGray,
dataAngleColorAll[[i]][[n]] = Darker[dataAngleColor[[i]][[n]], 0.3], dataAngleColorAll[[i]][[n]] =
Darker[dataAngleColor[[i]][[n]], 0.3]], 3/4*\[Pi] < indexChannel,

    If[dataAngleColor[[i]][[n]] == 0, dataAngleColorAll[[i]][[n]] = LightGray,
dataAngleColorAll[[i]][[n]] = Darker[dataAngleColor[[i]][[n]], 0.6], dataAngleColorAll[[i]][[n]] =
Darker[dataAngleColor[[i]][[n]], 0.6]]]]] dataAngleColorUpDown = listAngleMin*0;

For[i = 1, i <= Dimensions[dataTrans[imageID]][[1]], i++,

 For[n = 1, n <= Dimensions[dataTrans[imageID]][[2]], n++,

  Module[{indexChannel}, indexChannel = listAngleMin[[i]][[n]][[2]]; Which[indexChannel <=
\[Pi]/2,

    If[dataAngleColor[[i]][[n]] == 0, dataAngleColorUpDown[[i]][[n]] = LightGray,
dataAngleColorUpDown[[i]][[n]] = Lighter[dataAngleColor[[i]][[n]], 0.6],
dataAngleColorUpDown[[i]][[n]] = Lighter[dataAngleColor[[i]][[n]], 0.6]], \[Pi]/2 < indexChannel <=
\[Pi],

    If[dataAngleColor[[i]][[n]] == 0, dataAngleColorUpDown[[i]][[n]] = LightGray,
dataAngleColorUpDown[[i]][[n]] = Darker[dataAngleColor[[i]][[n]], 0.3],
dataAngleColorUpDown[[i]][[n]] = Darker[dataAngleColor[[i]][[n]], 0.3]]]]]

Export["ODF_color_simple.pdf", ArrayPlot[dataAngleColor]]

Export["ODF_color_simple.eps", ArrayPlot[dataAngleColor]];

Export["ODF_color_simple.tiff", ArrayPlot[dataAngleColor]];

Export["ODF_color_all.pdf", ArrayPlot[dataAngleColorAll]]

Export["ODF_color_all.eps", ArrayPlot[dataAngleColorAll]];

Export["ODF_color_all.tiff", ArrayPlot[dataAngleColorAll]];
```

```
Export["ODF_color_up_down.pdf", ArrayPlot[dataAngleColorUpDown]]

Export["ODF_color_up_down.eps", ArrayPlot[dataAngleColorUpDown]];

Export["ODF_color_up_down.tiff", ArrayPlot[dataAngleColorUpDown]];

Export["X_Y_data_11011.pdf", ListPlot[Flatten[dataDiagramm[11011], 1], PlotRange -> {{-10, 10},
{-10, 10}}, AspectRatio -> 1]]

Export["X_Y_data_11011.eps", ListPlot[Flatten[dataDiagramm[11011], 1], PlotRange -> {{-10, 10},
{-10, 10}}, AspectRatio -> 1]];

Export["X_Y_data_11011.tiff", ListPlot[Flatten[dataDiagramm[11011], 1], PlotRange -> {{-10, 10},
{-10, 10}}, AspectRatio -> 1]];

Export["X_Y_data_10111.pdf", ListPlot[Flatten[dataDiagramm[10111], 1], PlotRange -> {{-10, 10},
{-10, 10}}, AspectRatio -> 1]]

Export["X_Y_data_10111.eps", ListPlot[Flatten[dataDiagramm[10111], 1], PlotRange -> {{-10, 10},
{-10, 10}}, AspectRatio -> 1]];

Export["X_Y_data_10111.tiff", ListPlot[Flatten[dataDiagramm[10111], 1], PlotRange -> {{-10, 10},
{-10, 10}}, AspectRatio -> 1]];

Export["X_Y_data_21011.pdf", ListPlot[Flatten[dataDiagramm[21011], 1], PlotRange -> {{-10, 10},
{-10, 10}}, AspectRatio -> 1]]

Export["X_Y_data_21011.eps", ListPlot[Flatten[dataDiagramm[21011], 1], PlotRange -> {{-10, 10},
{-10, 10}}, AspectRatio -> 1]];

Export["X_Y_data_21011.tiff", ListPlot[Flatten[dataDiagramm[21011], 1], PlotRange -> {{-10, 10},
{-10, 10}}, AspectRatio -> 1]];

Export["X_Y_data_20111.pdf", ListPlot[Flatten[dataDiagramm[20111], 1], PlotRange -> {{-10, 10},
{-10, 10}}, AspectRatio -> 1]]

Export["X_Y_data_20111.eps", ListPlot[Flatten[dataDiagramm[20111], 1], PlotRange -> {{-10, 10},
{-10, 10}}, AspectRatio -> 1]];

Export["X_Y_data_20111.tiff", ListPlot[Flatten[dataDiagramm[20111], 1], PlotRange -> {{-10, 10},
{-10, 10}}, AspectRatio -> 1]];
```

1. Import & input of data and parameters

General automatic evaluated functions

```
MeanArray[array_]:=Mean[Flatten[array]]
```

```
findGeometricTransformRigid[ptsRef_, ptsTgt_] := Module[{ptsTgtTrans, ptsDiff, merit,result,x,y},
  transFuncUndef = RotationTransform[\[CapitalTheta]].TranslationTransform[{a, b}];
  funcTrans[{x_, y_}] = transFuncUndef[{x, y}];
  ptsTgtTrans = Map[funcTrans[#] &, ptsTgt];
  ptsDiff = ptsRef - ptsTgtTrans;
  merit = Total[Map[Norm[#]^2 &, ptsDiff]];
  sol = FindMinimum[merit, {{a, 0}, {b, 0}, {\[CapitalTheta], \[Pi]/2}}];
result = {sol[[1]], transFuncUndef /. sol[[2]]}]
(* Gibt die ID des Referenzbildes mit der korrespondierende Transformationsmatrix aus *)
(* Puts out ID of reference image with the corresponding transformation matrix *)
getCorrespTransFunc[id_]:=Module[{transFuncid,indexSampleRotate,indexScanDirection},
indexSampleRotate=StringTake[ToString[id],{-5}];
Which[indexSampleRotate=="1",transFuncid=imageRefID,indexSampleRotate=="2",transFuncid=imageRefID90,indexSampleRotate=="3",transFuncid=imageRefID180,indexSampleRotate=="4",transFuncid=imageRefID270,True,transFuncid=imageRefID]]
(* Gibt ID der Amplitudendaten aus *)
(* Puts out ID of amplitude data *)
getIDAmp[id_]:=ToExpression[StringReplacePart[ToString[id],"3",{-2,-2}]]
(* Gibt ID der Phasendaten aus*)
(* Puts out ID of phase data *)
getIDPhase[id_]:=ToExpression[StringReplacePart[ToString[id],"4",{-2,-2}]]
(* Gibt ID der X-Daten aus *)
(* Puts out ID of X data *)
getIDX[id_]:=ToExpression[StringReplacePart[ToString[id],"5",{-2,-2}]]
(* Gibt ID der Y-Daten aus*)
(* Puts out ID of Y data *)
```

```
getIDY[id_]:=ToExpression[StringReplacePart[ToString[id],"6",{-2,-2}]]

Import of images

NotebookDirectory[]

(* Zeigt alle .txt Dateien im Ordner an und nummeriert sie *)

(* Shows all .txt files in the folder and numbers them consecutively *)

SetDirectory[NotebookDirectory[]]

listAllFileNames = FileNames["*.txt"];

nFiles = Length[listAllFileNames];

Grid[Transpose[{Range[nFiles] // N, listAllFileNames}], Alignment -> Left]

import[fileid_,id_]:=(importData[id]=Import[listAllFileNames[[(**)fileid(**)]],"Table"];)

image[id_]:=If[StringTake[ToString[id],{-2}]=="1",

Image[Abs[data[id]-Max[data[id]]]/Max[Abs[data[id]-Max[data[id]]]]], (* Für Topographiebilder wegen des Vorzeichens *) (* For topography images due to the sign *)

Image[data[id]/Max[data[id]]]]

imageDim[id_]:=ImageDimensions[image[id]][[1]]

(* Crops the data matrix by 3 pixels on each side *)

drop[m_,parts__List]/;Length@{parts}<=ArrayDepth[m]:=m[[##]]&@@MapThread[Complement,{Range@Dimensions[m,Length@{parts}],{parts}}]

data[id_]:=\!\(\*TagBox[RowBox[{"If", "[", RowBox[{RowBox[{RowBox[{"ToString", "[", "id", "]"}], "==", "\"\<parameter\>\""}], ",", RowBox[{"importData", "[", "id", "]"}], ",", RowBox[{"drop","[", RowBox[{RowBox[{"importData", "[", "id", "]"}], ",", RowBox[{"{", {"1", ",", "2", ",", "3", ",", "510", ",", "511", ",", "512"}], "}"}], ",", RowBox[{"{", RowBox[{"1", ",", "2", ",", "3", ",", "510", ",", "511", ",", "512"}], "}"}]}]}], "]"}]}],Function[BoxForm`e$,MatrixForm[BoxForm`e$]]]\)

dataToImport = Table[{i, ToExpression[StringTake[listAllFileNames[[i]], {StringPosition[listAllFileNames[[i]], "_"][[-1, 1]] + 1, StringPosition[listAllFileNames[[i]], "."][[-1, 1]] - 1}]]}, {i, nFiles}]

listToOrder = SortBy[dataToImport, Last]

For[i = 1, i < Length[dataToImport] - 4, i++, listToOrder[[i]] = ToExpression[StringReplacePart[ToString[listToOrder[[i]]], ToString[1], {-2, -2}]]]
```

```
dataToImport = SortBy[listToOrder, First]

SortBy[dataToImport, Last]

(* Auflisten und sortieren aller FileIDs *)

(* Lists and sorts all file-IDs *)

listOfIDs = Sort[Transpose[dataToImport][[2]]]

(* nur / alle Domänenscans - Backgroundscans werden nicht ausgewählt *)

(* Selects only the measured data - background data excluded *)

listToDo = listOfIDs[[1 ;; -6]]

(* Importieren der Daten *)

(* Import of data *)

MapThread[import[#1, #2] &, Transpose[dataToImport]]

(* Anzeigen aller normierten DatenIDs *)

(* Shows all normalizeddata IDs *)

Map[Labeled[image[#], #, Top] &, listOfIDs]

Assignment of images to reference IDs

Assignment for general calculation

imageID := 11051;

imageID90 := 21051;

imageID180 := 31051;

imageID270 := 41051;

imageIDLat := 10151;

imageID90Lat := 20151;

Assignment for image correlation

imageRefID := 11011;

imageRefID90 := 21011;

imageRefID180 := 31011;
```

```
imageRefID270 := 41011;

imageRefIDLat := 10111;

imageRefID90Lat := 20111;

Assignment for background correction

imageRefIDBGXvert := 81058;

imageRefIDBGXlat := 80158;

imageRefIDBGYvert := 81068;

imageRefIDBGYlat := 80168;

Input of measurement parameters

phaseOffset = data[parameter][[4]][[1]]; (* \[Degree] *)(* Phasenoffset der Versuche / Messungen *) (* Phase \offset of measurements *)

phaseOffsetBackground = data[parameter][[7]][[1]];(* \[Degree] *)(* Phasenoffset der Background Versuche / Messungen *) (* \Phase offset of background measurements *)

(* Eingabe des InvOLS zur Berechnung der Längenänderung und der \

Empfindlichkeiten vom LIA der jeweiligen Messungen *)

(* Input of the InvOLS for calculation of the length variation and the \sensitivities from the LIA of the corresponding measurements *)

deflectionInvOLSVertical = data[parameter][[1]][[1]]; (* nm/V *)

sensitivityVertical = N[data[parameter][[2]][[1]]*10^-6];(* V *)

sensitivityLateral = N[data[parameter][[3]][[1]]*10^-6] ; (* V *)

sensitivityVerticalBackground = N[data[parameter][[5]][[1]]*10^-6]; (* V *)

sensitivityLateralBackground = N[data[parameter][[6]][[1]]*10^-6]; (* V *)

(* Berechnung des Backgrounds *)

(* Calculation of the background *)

backgroundVertX = Mean[Flatten[data[81058]]]*sensitivityVerticalBackground/10;

backgroundVertY = Mean[Flatten[data[81068]]]*sensitivityVerticalBackground/10;

backgroundLatX = Mean[Flatten[data[80158]]]*sensitivityLateralBackground/10;
```

backgroundLatY = Mean[Flatten[data[80168]]]*sensitivityLateralBackground/10;

2. Image correlation

Find corresponding points

CorrespondingPoints in Two Images

(* cpfuncAutomatic findet automatisch die korrespondierenden Punkte in 2 verschiedenen Bildern und gibt die Punktkoordinaten aus *)

(* cpfuncAutomatic finds automatically corresponding points in 2 different images and puts out the coordinates *)

cpfuncAutomatic[id_,id2_]:=ImageCorrespondingPoints[image[id],image[id2],TransformationClass->"Rigid"]

Manual image correlation

npts = 4;

pts[1] = pts[2] = Table[{i, i}*10, {i, Range[npts]}];

marker = Evaluate[MapThread[Style[StringJoin["\[CenterDot]"], 40, #2] &, {Range[npts], Take[ColorData[63, "ColorList"], npts]}]];

Grid[{{LocatorPane[Dynamic[pts[1]], Show[image[imageRefID], ImageSize -> 700], {{0, 0}, Dimensions[data[imageRefID]], {1, 1}}, Appearance -> marker], LocatorPane[Dynamic[pts[2]], Show[image[imageRefID90], ImageSize -> 700], {{0, 0}, Dimensions[data[imageRefID90]], {1, 1}}, Appearance -> marker]}, {Dynamic[pts[1]], Dynamic[pts[2]]}}, ItemSize -> 60, Frame -> All]

Dynamic[pts[1]]

Dynamic[pts[2]]

(* cpfunc puts out the coordinates of the corresponding points *)

cpfunc[id_,id2_]:=If[{pts[1],pts[2]}!={{{10,10},{20,20},{30,30},{40,40}},{{10,10},{20,20},{30,30},{40,40}}},{pts[1],pts[2]},cpfuncAutomatic[id,id2]]

Graphic output

id = imageRefID90;

cp = ImageCorrespondingPoints[image[imageRefID], image[id], TransformationClass -> "Rigid"]

GraphicsRow[MapThread[Show[HighlightImage[image[#1], cp[[#2]], "HighlightColor" -> Green],

```
Graphics[{Yellow, MapIndexed[Inset[#2[[1]], #1] &, cp[[#2]]]}]] &, {{imageRefID, id}, {1, 2}}], ImageSize -> 600]
```

Fit TransformationFunction

```
(* findGeometricTransformRigid berechnet die Transformationsmatrix mit Hilfe der Punkte der cpfunc Funktion *)

(* findGeometricTransformRigid calculates the transformation matrix using the points obtained from the cpfunc function. Definition: imageRefID will not be rotated *)

transFunc[id_]:=If[id==imageRefID,{0,RotationTransform[0]},findGeometricTransformRigid[cpfunc[imageRefID,id][[2]]/imageDim[imageRefID],cpfunc[imageRefID,id][[1]]/imageDim[imageRefID]]]

(* transFuncTransRot enthält die Einträge der Transformatonsmatrix *)

(* transFuncTransRot contains the entries of the transformation matrix *)

transFuncRot[id_]:=TransformationMatrix[transFunc[getCorrespTransFunc[id]][[2]]][[1;;2,1;;2]]

(* transFuncTranslat gibt die Verschiebungen aus der Transformationsmatrix in X und Y Richtung aus *)

(* transFuncTranslat put out the offset of the transformation matrix in X and Y direction *)

transFuncTranslat[id_]:=TransformationMatrix[transFunc[getCorrespTransFunc[id]][[2]]][[1;;2,-1]]
```

ApplyTransformationFunction

```
(* fimageTrans fragt ab, ob Bild zusätzlich um 90\[Degree] gedreht werden muss, um Scandirection 0\[Degree] bzw. 90\[Degree] zu berücksichtigen. *)

(* fimageTrans checks if the picture has to be rotated by another 90\[Degree] to consider the scan direction (0\[Degree] respectively 90\[Degree]) *)

fimageTrans[id_]:=If[StringTake[ToString[id],{-4}]=="0",

ImageTransformation[image[id], RotationTransform[-90 \[Degree], {1/2, 1/2}].transFunc[getCorrespTransFunc[id]][[2]]],

ImageTransformation[image[id], transFunc[getCorrespTransFunc[id]][[2]]]]
```

Image crop

```
(* Verschiebung in X-Richtung berechnen *)

(* Calculation of the offset in X direction *)
```

```
shiftx[id_]:=(#-Round[#])&[transFuncTranslat[id][[2]]*imageDim[id]];
cropRangex[id_]:=If[Positive[shiftx[id]],{pixeladd,imageDim[id]-(Ceiling[Abs[shiftx[id]]]+pixeladd)}
,{(Ceiling[Abs[shiftx[id]]]+pixeladd),imageDim[id]-pixeladd}]
```

(* Verschiebung in Y-Richtung berechnen *)

(* Calculation of the offset in Y direction *)

```
shifty[id_]:=(#-Round[#])&[transFuncTranslat[id][[1]]*imageDim[id]];
cropRangey[id_]:=If[Positive[shifty[id]],{pixeladd,imageDim[id]-(Ceiling[Abs[shifty[id]]]+pixeladd)}
,{(Ceiling[Abs[shifty[id]]]+pixeladd),imageDim[id]-pixeladd}]
```

(* imageCropped gibt fertig gecropptes, gedrehtes Bild aus *)

(* imageCropped puts out the cropped and rotated pictures *)

```
imageCropped[id_]:=ImageTake[fimageTrans[id],cropRangeAlly,cropRangeAllx]
```

Calculation of pixeladd and crop range

Pixeladd

(* Erstellen der Liste, die nur File-IDs enthält, die gecroppt werden sollen \und existieren *)

(* Create list that only contains file IDs that need to be cropped and exist *)\

```
listToCrop = Take[{imageRefID, imageRefID90, imageRefID180, imageRefID270},
ToExpression[StringTake[ToString[Max[listToDo]], {-5}]]]
```

(* Berechnen des Winkels mit der größten Abweichung von 90\[Degree] *)

(* Calculation of the angle with the largest deviation from 90\[Degree] *)

```
listRotateAngle = Flatten[Mod[{ArcCos[transFuncRot[#][[1, 1]]]/Degree, ArcSin[transFuncRot[#][[1,
2]]]/Degree, ArcSin[-transFuncRot[#][[2, 1]]]/Degree, ArcCos[transFuncRot[#][[2, 2]]]/Degree} & /@
listToCrop, 90]];

For[i = 1, i <= Length[listRotateAngle], i++,

  If[listRotateAngle[[i]] > 45, listRotateAngle[[i]], listRotateAngle[[i]] = 90 - listRotateAngle[[i]]]]

angleMin = Min[listRotateAngle];

pixeladd = Ceiling[N[Cos[angleMin Degree]*512]] + 3Crop Range
```

(* Definition: Für imageRefID wird gesamte Bildgröße verwendet *)

(* Definition: For imageRefID whole image size is used *)

```
cropRangex[imageRefID] = {0, imageDim[imageRefID]};

cropRangey[imageRefID] = {0, imageDim[imageRefID]};

(* Maximaler Bildausschnitt der in allen ReferenzIDs enthalten ist in X und Y \Richtung *)

(* Maximum image section that is covered by all reference-IDs in X and Y \direection *)

cropRangeAllx = {Max[Transpose[Map[cropRangex[#] &, listToCrop]][[1]]],

   Min[Transpose[Map[cropRangex[#] &, listToCrop]][[2]]]}

cropRangeAlly = {Max[Transpose[Map[cropRangey[#] &, listToCrop]][[1]]],

   Min[Transpose[Map[cropRangey[#] &, listToCrop]][[2]]]}

Image =>data

(* dataTrans wandelt die gecroppten, gedrehten Bilder in Daten zurück *)

(* dataTrans converts the cropped and rotated pictures into data *)

dataTrans[id_]:=ImageData[imageCropped[id]]*Max[data[id]];

(* Einmalig alle Bilder der listToDo drehen und croppen *)

(* All pictures from listToDO will be cropped and rotated *)

Do[dataTrans[id] = ImageData[imageCropped[id]]*Max[data[id]], {id, listToDo}]

 (* Abmessungen der neuen Bilder / Datenmatrizen *)

(* Dimensions of the new pictures / data martrices *)

dataTrans[imageID] // Dimensions
```

3. Lock-In-Amplifier (LIA) data correction

LIA correction: Phase offset (regarding: \[CapitalTheta])

```
(* Nur für \[CapitalTheta]-Kanal: Addiert den "Referenz"-PhasenOffset, der am LIA eingestellt war, zum Output => Ergebnis: Systeminhärente Phasenverschiebung bleibt übrig. *)

(* Regarding \[CapitalTheta]: Adds the phase offset of the LIA to the output => Result: Only system inherent phase offset left. *)

dataTransCorr\[CapitalTheta][id_]:=(Mod[(dataTrans[getIDPhase[id]]+(phaseOffset/180*10(*V*)))+10,20]-10)
```

LIA correction: Sensitivity (regarding: R)

(* Nur für R-Kanal: Korrigiert die Spannungen mit der am LIA eingestellten Sensitivity; unterscheidet zwischen vertikal und lateral. *)

(* Formel aus Handbuch: Output=(signal/sensitivity-offset) x Expand x 10V; hier: Expand=1; Offset=0 *)

(* Regarding R: Corrects the voltage with the adjusted sensitivity; distinguishes between vertical and lateral. *)

(* Formula from handbook: Output=(signal/sensitivity-offset) x Expand x 10V; here: Expand=1; Offset=0 *)

dataTransCorrR[id_] := Module[{indexChannel}, indexChannel = StringTake[ToString[id], {-3, -3}]; Which[indexChannel == "0", dataTrans[getIDAmp[id]]*sensitivityVertical/10(*V*), indexChannel == "1", dataTrans[getIDAmp[id]]*sensitivityLateral/10(*V*)]]

LIA correction: Sensitivity (regarding: X and Y)

(* Für X-Kanal und Y-Kanal : Korrigiert die Spannungen mit der am LIA eingestellten Sensitivity; unterscheidet zwischen vertikal und lateral. *)

(* Formel aus LIA Handbuch: Output=(signal/sensitivity-offset) x Expand x 10V; hier: Expand=1; Offset=0 *)

(* For X and Y: Corrects the voltage with the adjusted sensitivity; distinguishes between vertical and lateral. *)

(* Formula from LIA handbook: Output=(signal/sensitivity-offset) x Expand x 10V; here: Expand=1; Offset=0 *)

dataTransCorrXY[id_] := Module[{indexChannel}, indexChannel = StringTake[ToString[id], {-3, -3}]; Which[indexChannel == "0", dataTrans[id]*sensitivityVertical/10(*V*), indexChannel == "1", dataTrans[id]*sensitivityLateral/10(*V*)]]

Convert R and \[CapitalTheta] into X and Y

(* Hier werden das erste Mal das Amplituden- und Phasenbild gemeinsam\verwendet *)

(* The amplitude and phase images (R and \[CapitalTheta]) are used together\for the first time at this point *)

(* Berechnung des X-Outputs über X = R * cos(\[CapitalTheta] - Phasenoffset) ohne InvOLS und Kalibrationsfaktor Korrektur *)

(* Calculation of the X output using X = R * cos(\[CapitalTheta] - phase offset) without InvOLS and calibration factor correction *)

dataTransX[id_]:=dataTransCorrR[getIDAmp[id]]*Cos[dataTransCorr\[CapitalTheta][getIDPhase[id]]/10*\[Pi]]

(* Berechnung des Y-Outputs über Y = R * sin(\[CapitalTheta] - Phasenoffset) ohne InvOLS und Kalibrationsfaktor Korrektur *)

(* Calculation of the Y output using Y = R * sin(\[CapitalTheta] - phase offset) without InvOLS and calibration factor correction *)

dataTransY[id_]:=dataTransCorrR[getIDAmp[id]]*Sin[dataTransCorr\[CapitalTheta][getIDPhase[id]]/10*\[Pi]]

dataTransXY[id_]:=MapThread[{#1,#2}&,{dataTransX[id],dataTransY[id]},2]

Selection of X and Y data

(* Auswahl der X-Daten aus den umgerechnten R und \[CapitalTheta] oder den gemessenen X-Daten *)

(* Selection of X data from converted R and \[CapitalTheta] data or from measured X data *)

getX[id_]:=Module[{indexChannel}, indexChannel = StringTake[ToString[id], {-2, -2}];
Which[indexChannel == "3",dataTransX[id], indexChannel == "4",dataTransX[id], indexChannel == "5",dataTransCorrXY[getIDX[id]], indexChannel == "6",dataTransCorrXY[getIDX[id]]]]

(* Auswahl der Y-Daten aus den umgerechnten R und \[CapitalTheta] oder den gemessenen Y-Daten *)

(* Selection of Y data from converted R and \[CapitalTheta] data or from measured Y data *)

getY[id_]:=Module[{indexChannel}, indexChannel = StringTake[ToString[id], {-2, -2}];
Which[indexChannel == "3",dataTransY[id], indexChannel == "4",dataTransY[id], indexChannel == "5",dataTransCorrXY[getIDY[id]], indexChannel == "6",dataTransCorrXY[getIDY[id]]]]

Subtract background from X and Y data

(* Berechnung des X-Output aus R und \[CapitalTheta] über Xlockin=Xbackgr+Xdomain-->Xdomain=Xlockin-Xbackgr-->Xdomain=dataTransX*sensitivity/10V-Xbackgr*sensitivity/10V *)

(* Xbackgr: Mittelwert aus der Backgroundmessung auf dem Glasplättchen *)

(* Calculation of X output from R and \[CapitalTheta] using Xlockin=Xbackgr+Xdomain-->Xdomain=Xlockin-Xbackgr-->Xdomain=dataTransX*sensitivity/10V-Xbackgr*sensitivity/10V *)

(* Xbackgr: Mean value from background measurements on glass slide *)

```
dataTransXcorr[id_]:=Module[{indexChannel},indexChannel=StringTake[ToString[id],{-3,-3}];Which[indexChannel=="0",getX[id]-backgroundVertX, (* vertical *)
indexChannel=="1",getX[id]-backgroundLatX]] (* lateral *)

(* Berechnung des Y-Output aus R und \[CapitalTheta] über
Ylockin=Ybackgr+Ydomain-->Ydomain=dataTransY*sensitivity/10V-Ybackgr*sensitivity/10V *)

(* Xbackgr: Mittelwert aus der Backgroundmessung auf dem Glasplättchen *)

(* Calculation of Y output from R and \[CapitalTheta] using
Ylockin=Ybackgr+Ydomain-->Ydomain=dataTransY*sensitivity/10V-Ybackgr*sensitivity/10V *)

(* Xbackgr: Mean value from background measurements on glass slide *)

dataTransYcorr[id_]:=Module[{indexChannel},indexChannel=StringTake[ToString[id],{-3,-3}];Which[indexChannel=="0",getY[id]-backgroundVertY, (* vertical *)

indexChannel=="1",getY[id]-backgroundLatY]] (* lateral *)

dataTransXYcorr[id_] := MapThread[{#1, #2} &, {dataTransXcorr[id], dataTransYcorr[id]}, 2]

Turn corrected X and Y data parallel to x-axis

(* Creates a matrix with the uncorrected X and Y data *)

(* Erstellen einer Matrix mit unkorrigierten X, Y Daten für Darstellung in X, Y Diagramm *)

matrixXY[id_]:=Transpose@{#&@@@Flatten[getX[id]],#&@@@Flatten[getY[id]]}

(* Calculates a regression line for uncorrected X and Y data *)

regLin[id_] := Fit[matrixXY[getIDX[id]], {1,x},x]

(* Angle alpha - ArcTan(Y/X) -, which the data points have to be rotated by *)

(* Winkel Alpha - ArcTan(Y/X) -, um den die Gerade auf die Ebene verdreht ist *)

alpha[id_]:=ArcTan[(Coefficient[regLin[id],x,0]+Coefficient[regLin[id],x,1]*2)/(2)]/Degree(* R = sqrt(X^2 + Y^2) *)

dataR[id_]:=Sqrt[Power[dataTransXcorr[id],2]+Power[dataTransYcorr[id],2]]

(* \[CapitalTheta] = arctan([Y / X] - angle alpha *)

dataTheta[id_]:=(ArcTan[dataTransXcorr[id],dataTransYcorr[id]]/Degree)-alpha[id]

(* Berechnung des X-Outputs über X = R * cos(\[CapitalTheta]) *)

(* Calculation of the X output using X = R * cos(\[CapitalTheta]) *)
```

```
dataCorrX[id_]:=dataR[id]*Cos[dataTheta[id]Degree]

(* Berechnung des Y-Outputs über Y = R * sin(\[CapitalTheta]) *)

(* Calculation of the Y output using Y = R * sin(\[CapitalTheta]) *)

dataCorrY[id_]:=dataR[id]*Sin[dataTheta[id]Degree]

dataCorrXY[id_]:=MapThread[{#1,#2}&,{dataCorrX[id],dataCorrY[id]},2]

PFM signal = amplitude + direction

id = imageID; (*vertical*)

comp[31] = dataCorrX[id]

id = imageIDLat; (*lateral, 0\[Degree]*)

comp[11] = dataCorrX[id]

id = imageID90Lat; (*lateral, 90\[Degree]*)

comp[21] = dataCorrX[id]
```

4. Calculation

Piezoelectric coefficients: PZT, tetragonal

```
d15=287 (*pm/V*);

d31=-97 (*pm/V*);

d33=218(*pm/V*);

d22=0 (*pm/V*);
```

Qualitative calculation: Octants of a sphere

```
(* Normieren von fdzx, fdzy und fdzz *)

(* Normalization of fdzx, fdzy and fdzz *)

fdzxNorm[\[Theta]_,\[Phi]_]:=(-(d31-d33+(d15+d31-d33) Cos[2\[Theta]]) Cos[\[Phi]]
Sin[\[Theta]])/d15

fdzyNorm[\[Theta]_,\[Phi]_]:=(-(d31-d33+(d15+d31-d33) Cos[2\[Theta]]) Sin[\[Phi]]
Sin[\[Theta]])/d15

fdzzNorm[\[Theta]_]:=((d31+d15)Sin[\[Theta]]^2Cos[\[Theta]]+d33 Cos[\[Theta]]^3)/d33
```

```
(* Wertungsfaktor für vertikale Messung (Z-Richtung) *)

(* Weighing factor for vertical measurements (Z-direction) *)

valueZ=1;

(* Wertungs-Funktion für die FindMinimum-Funktion *)

(* Weighing function for the FindMinimum function *)

funcOctant[x_,y_,z_][\[Theta]_,\[Phi]_]:=(x-fdzxNorm[\[Theta],\[Phi]])^2+(y-fdzyNorm[\[Theta],\[Phi
]])^2+valueZ*(z-fdzzNorm[\[Theta]])^2

(* Diese Funktion findet den besten Fit der Daten, wobei nur die Vorzeichen \

der Messwerte und 1 als Wert verwendet werden *)

(* This function gives the best fit for the given data, whereby only the sign \

of the data (value: 1 or -1) is considered *)

listAngleOct = MapThread[({Mod[\[Phi], 2 \[Pi]], \[Theta]} /. FindMinimum[funcOctant[#1, #2,
#3][\[Theta], \[Phi]], {{\[Theta], \[Pi]/2}, {\[Phi], 0}}][[2]]) &, {Sign[comp[11]], Sign[comp[21]],
Sign[comp[31]]}, 2]

Calculation of \[Theta] and \[Phi] from FindMinimum calculation

(* Kleinster Messwert (2,5% der Messwerte sind kleiner) *)

(* Smallest measured value (2,5% of the measured values are smaller) *)

sigmaMin[id_]:=Sort[Flatten[comp[id]]][[Round[Length[Flatten[comp[id]]]*0.025]]]

(* Größter Messwert (2,5% der Messwerte sind größer) *)

(* Largest measured value (2,5% of the measured values are larger) *)

sigmaMax[id_]:=Sort[Flatten[comp[id]]][[Length[Flatten[comp[id]]]-Round[Length[Flatten[comp[id]]
]*0.025]]]

(* Gibt den absolut größten Messwert der größten bzw. kleinsten Messwerte aus: id \[Rule] Richtung
(11,21,31) *)

(* Puts out the absolute biggest measured value of the largest respectively smallest measured values: id
\[Rule] direction (11,21,31) *)

getAbsMax[id_]:=If[Abs[sigmaMin[id]]>Abs[sigmaMax[id]],Abs[sigmaMin[id]],Abs[sigmaMax[id]]]

 (* Messdaten durch maximalen Wert dividieren *)
```

```
(* Dividing the data by maximum value *)

compAbsNormMean[id_]:=comp[id]/getAbsMax[id]

(* Ersetzen aller zu großen / kleinen Werte *)

(* Replacing all too large / small values *)

compAbsNorm[id_]:=ReplacePart[compAbsNormMean[id],{Position[compAbsNormMean[id],x_/;x>
1]->1,Position[compAbsNormMean[id],x_/;x<-1]->-1}]

(* Berechnen einer Liste der \[Theta] und \[Phi] Winkel mit Hilfe der \FindMinimum Funktion und den
normierten PFM Beiträgen *)

(* Calculation of a list containing \[Theta] and \[Phi] angles using the \FindMinimum function and
normalized PFM signals *)

listAngleMin = MapThread[({Mod[\[Phi], 2 \[Pi]], \[Theta]} /. FindMinimum[funcOctant[#1, #2,
#3][\[Theta], \[Phi]], {{\[Theta], \[Pi]/2}, {\[Phi], 0}}, MaxIterations -> 1000][[2]]) &,
{compAbsNorm[11], compAbsNorm[21], compAbsNorm[31]}, 2]

5. Illustration of results

1. Illustration from the octants of a sphere calculation

nVectorOct = Dimensions[listAngleOct][[1]]*Dimensions[listAngleOct][[2]]

thstep = 90(*\[Degree]*);

psistep = 90(*\[Degree]*);

bc2mc = BinCounts[Flatten[listAngleOct, 1]/Degree, {0, 360, psistep}, {0, 180, thstep}]

bc2mcNormQuantity = bc2mc/nVectorOct // N

(* Korrektur, die Kugeloberfläche berücksichtigt *)

(* Correction taking the surface of a sphere into account *)

npsisteps = 360/psistep;

normc = (Table[Integrate[Sin[x], {x, theta, theta + thstep*Degree}], {theta, 0, (180 - thstep)*Degree,
thstep*Degree}]*2 \[Pi]/npsisteps) // N

octants = Transpose[Transpose[bc2mcNormQuantity]/normc]

colorScheme = ColorData["TemperatureMap"];

figOctants =Labeled[ArrayPlot[Transpose[(octants/(1/(4 Pi)))/Max[octants/(1/(4 Pi))]],
```

```
    DataRange -> {{90/2, 360 - 90/2}, {-180 + 90/2, -90/2}},
    ColorFunction -> colorScheme, ColorFunctionScaling -> False, Mesh -> True,
    FrameTicks -> {{Transpose[{Range[-180, 0, 45], Range[180, 0, -45]}],
       Transpose[{Range[-180, 0, 45], Range[180, 0, -45]}]}, {Range[0, 360, 90], Range[0, 360, 90]}},
Frame -> True,
    FrameLabel -> {"\[Theta] [\[Degree]]", "\[Phi] [\[Degree]]"},
    LabelStyle -> Directive[Black, Bold], AspectRatio -> 1/GoldenRatio],
  DensityPlot[y, {x, 0, 210}, {y, 0, Max[octants]/(1/(4 Pi))},
    ColorFunction -> Function[{y}, colorScheme[y]],
    ColorFunctionScaling -> True, PlotRangePadding -> None, Frame -> True,
    FrameLabel -> {"", "", Style["ODF", Black, Bold], Style["[MRD]", Black, Bold]},
    FrameTicks -> {{None, Range[0, Max[octants]/(1/(4 Pi)), Round[((Max[octants]/(1/(4 Pi))) - .05)/4,
.01]]}, {None, None}},
    FrameStyle -> Black, BaseStyle -> {FontFamily -> "Helvetica", 14},
    AspectRatio -> 12, ImageSize -> All], Right]
CreateDirectory[NotebookDirectory[] <> "Export"] // Quiet;
SetDirectory[%]
Export["octants.txt", octants // Transpose, "TSV"]
Export["octants.pdf", figOctants]
Export["octants.eps", figOctants]
Export["octants.tiff", figOctants]
```

2. Illustration from FindMinimum calculation

```
nAngle = Dimensions[listAngleMin][[1]]*Dimensions[listAngleMin][[2]]
thstep = 45(*\[Degree]*);
psistep = 45(*\[Degree]*);
bc2mc = BinCounts[Flatten[listAngleMin, 1]/Degree, {0, 360, psistep}, {0, 180, thstep}]
```

```
bc2mcNormQuantity = bc2mc/nAngle // N

(* Korrektur die Kugeloberfläche berücksichtigt *)

(* Correction taking the surface of a sphere into account *)

npsisteps = 360/psistep

normc = (Table[Integrate[Sin[x], {x, theta, theta + thstep*Degree}], {theta, 0, (180 - thstep)*Degree,
thstep*Degree}]*2 \[Pi]/npsisteps) // N

(* Überprüfen ob Summe der korrgierten Daten genau 4 Pi entspricht *)

(* Verify that sum of corrected data equals 4 Pi *)

Total[normc]*npsisteps == 4 \[Pi]

(* MRD - Multiple Random Distribution *)

odf = Transpose[Transpose[bc2mcNormQuantity]/normc]/(1/(4 \[Pi]))

colorScheme = ColorData["TemperatureMap"];

maxODF = 6;

figure =Labeled[ArrayPlot[Transpose[odf/maxODF],

    DataRange -> {{psistep/2, 360 - psistep/2}, {-180 + thstep/2, -thstep/2}},

    ColorFunction -> colorScheme, ColorFunctionScaling -> False, Mesh -> True,

    FrameTicks -> {{Transpose[{Range[-180, 0, 45], Range[180, 0, -45]}],

        Transpose[{Range[-180, 0, 45], Range[180, 0, -45]}]}, {Range[0, 360, 90], Range[0, 360, 90]}},
Frame -> True,

    FrameLabel -> {"\[Theta] [\[Degree]]", "\[Phi] [\[Degree]]"},

    LabelStyle -> Directive[Black, Bold], AspectRatio -> 1/GoldenRatio],

   DensityPlot[y, {x, 0, 1}, {y, 0, maxODF}, ColorFunction -> Function[{y}, colorScheme[y]],

    ColorFunctionScaling -> True, PlotRangePadding -> 0, Frame -> True,

    FrameLabel -> {{"", Style["[MRD]", Black, Bold]}, {"", Style["ODF", Black, Bold]}},

    FrameTicks -> {{None, Range[0, maxODF]}, {None, None}},

    FrameStyle -> Black, BaseStyle -> {FontFamily -> "Helvetica", 14},
```

```
    AspectRatio -> 12, ImageSize -> 68], Right]

CreateDirectory[NotebookDirectory[] <> "Export"] // Quiet;

SetDirectory[%]

Export["ODF.txt", odf // Transpose, "TSV"]

Export["ODF.pdf", figure]

Export["ODF.eps", figure]

Export["ODF.tiff", figure]
```

3. More detailed illustration

```
(* Kodierung: 315\[Degree]-45\[Degree] \[Rule] Gelb, 45\[Degree]-135\[Degree] \\[Rule] Rot,
135\[Degree]-225\[Degree] \[Rule] Grün, \225\[Degree]-315\[Degree] \[Rule] Blau *)

(* Color code: 315\[Degree]-45\[Degree] \[Rule] yellow, 45\[Degree]-135\\[Degree] \[Rule] red,
135\[Degree]-225\[Degree] \[Rule] green, \225\[Degree]-315\[Degree] \[Rule] blue *)

dataAngleColor = listAngleMin*0;

For[i = 1, i <= Dimensions[dataTrans[imageID]][[1]], i++,

  For[n = 1, n <= Dimensions[dataTrans[imageID]][[2]], n++,

   Module[{indexChannel}, indexChannel = listAngleMin[[i]][[n]][[1]]; Which[indexChannel < 0,
dataAngleColor[[i]][[n]] = 0,

      0 <= indexChannel <= \[Pi]/4, dataAngleColor[[i]][[n]] = Yellow,\[Pi]/4 < indexChannel <=
3/4*\[Pi], dataAngleColor[[i]][[n]] = Red, 3/4*\[Pi] < indexChannel <= 5/4*\[Pi],
dataAngleColor[[i]][[n]] = Green, 5/4*\[Pi] < indexChannel <= 7/4*\[Pi], dataAngleColor[[i]][[n]] =
Blue, 7/4*\[Pi] < indexChannel , dataAngleColor[[i]][[n]] = Yellow]]]]

(* Kodierung: 0\[Degree]-45\[Degree] \[Rule] Lighter um Faktor 0.6, 45\\[Degree]-90\[Degree] \[Rule]
Lighter um Faktor 0.3, 90\[Degree]-135\[Degree] \\[Rule] Darker um Faktor 0.3,
135\[Degree]-180\[Degree] \[Rule] Darker um \Faktor 0.6 *)

(* Color code: 0\[Degree]-45\[Degree] \[Rule] Lighter by fraction of 0.6, 45\\[Degree]-90\[Degree]
\[Rule] Lighter by fraction of 0.3, 90\[Degree]-135\\[Degree] \[Rule] Darker by fraction of 0.3,
135\[Degree]-180\[Degree] \\[Rule] Darker by fraction of 0.6 *)

dataAngleColorAll = listAngleMin*0;

For[i = 1, i <= Dimensions[dataTrans[imageID]][[1]], i++,

  For[n = 1, n <= Dimensions[dataTrans[imageID]][[2]], n++,
```

```
  Module[{indexChannel}, indexChannel = listAngleMin[[i]][[n]][[2]]; Which[indexChannel <=
\[Pi]/4,

    If[dataAngleColor[[i]][[n]] == 0, dataAngleColorAll[[i]][[n]] = LightGray,
dataAngleColorAll[[i]][[n]] = Lighter[dataAngleColor[[i]][[n]], 0.6], dataAngleColorAll[[i]][[n]] =
Lighter[dataAngleColor[[i]][[n]], 0.6]],\[Pi]/4 < indexChannel <= \[Pi]/2,

    If[dataAngleColor[[i]][[n]] == 0, dataAngleColorAll[[i]][[n]] = LightGray,
dataAngleColorAll[[i]][[n]] = Lighter[dataAngleColor[[i]][[n]], 0.3], dataAngleColorAll[[i]][[n]] =
Lighter[dataAngleColor[[i]][[n]], 0.3]] \[Pi]/2 < indexChannel <= 3/4*\[Pi],

    If[dataAngleColor[[i]][[n]] == 0, dataAngleColorAll[[i]][[n]] = LightGray,
dataAngleColorAll[[i]][[n]] = Darker[dataAngleColor[[i]][[n]], 0.3], dataAngleColorAll[[i]][[n]] =
Darker[dataAngleColor[[i]][[n]], 0.3]], 3/4*\[Pi] < indexChannel,

    If[dataAngleColor[[i]][[n]] == 0, dataAngleColorAll[[i]][[n]] = LightGray,
dataAngleColorAll[[i]][[n]] = Darker[dataAngleColor[[i]][[n]], 0.6], dataAngleColorAll[[i]][[n]] =
Darker[dataAngleColor[[i]][[n]], 0.6]]]]]

(* Kodierung: 0\[Degree]-90\[Degree] \[Rule] Lighter um Faktor 0.6, 90\\[Degree]-180\[Degree] \[Rule]
Darker um Faktor 0.3 *)

(* Color code: 0\[Degree]-90\[Degree] \[Rule] Lighter by fraction of 0.6, 90\\[Degree]-180\[Degree]
\[Rule] Darker by fraction of 0.3 *)

dataAngleColorUpDown = listAngleMin*0;

For[i = 1, i <= Dimensions[dataTrans[imageID]][[1]], i++,

 For[n = 1, n <= Dimensions[dataTrans[imageID]][[2]], n++, Module[{indexChannel}, indexChannel =
listAngleMin[[i]][[n]][[2]]; Which[indexChannel <= \[Pi]/2,

    If[dataAngleColor[[i]][[n]] == 0, dataAngleColorUpDown[[i]][[n]] = LightGray,
dataAngleColorUpDown[[i]][[n]] = Lighter[dataAngleColor[[i]][[n]], 0.6],
dataAngleColorUpDown[[i]][[n]] = Lighter[dataAngleColor[[i]][[n]], 0.6]] \[Pi]/2 < indexChannel <=
\[Pi],

    If[dataAngleColor[[i]][[n]] == 0, dataAngleColorUpDown[[i]][[n]] = LightGray,
dataAngleColorUpDown[[i]][[n]] = Darker[dataAngleColor[[i]][[n]], 0.3],
dataAngleColorUpDown[[i]][[n]] = Darker[dataAngleColor[[i]][[n]], 0.3]]]]]

CreateDirectory[NotebookDirectory[] <> "Export"] // Quiet;

SetDirectory[%]

Export["ODF_color_simple.pdf", ArrayPlot[dataAngleColor]]
```

```
Export["ODF_color_simple.eps", ArrayPlot[dataAngleColor]]

Export["ODF_color_simple.tiff", ArrayPlot[dataAngleColor]]

CreateDirectory[NotebookDirectory[] <> "Export"] // Quiet;

SetDirectory[%]

Export["ODF_color_all.pdf", ArrayPlot[dataAngleColorAll]]

Export["ODF_color_all.eps", ArrayPlot[dataAngleColorAll]]

Export["ODF_color_all.tiff", ArrayPlot[dataAngleColorAll]]

CreateDirectory[NotebookDirectory[] <> "Export"] // Quiet;

SetDirectory[%]

Export["ODF_color_up_down.pdf", ArrayPlot[dataAngleColorUpDown]]

Export["ODF_color_up_down.eps", ArrayPlot[dataAngleColorUpDown]]

Export["ODF_color_up_down.tiff", ArrayPlot[dataAngleColorUpDown]]
```

6. Addition

1. Convert X and Y into R and \[CapitalTheta]

```
(* R = sqrt(X^2 + Y^2) *)

dataTransR[id_]:=Sqrt[Power[dataTrans[getIDX[id]],2]+Power[dataTrans[getIDY[id]],2]]

(* \[CapitalTheta] = arctan([Y / X] + phaseOffset of LIA) *)

dataTransTheta[id_]:=Mod[(N[ArcTan[dataTrans[getIDX[id]],dataTrans[getIDY[id]]]/Degree]+phase
Offset)/18,20,-10]

Illustration

id = imageID;

dataDiagramm[id_] := MapThread[{#1, #2} &, {dataTrans[getIDX[id]], dataTrans[getIDY[id]]}, 2]   (*
Darstellung der Messdaten aus X und Y *)(* Illustraionfrom X and Y \data *)

ListPlot[Flatten[dataDiagramm[id], 1]]

Flatten[MapThread[{#1, #2} &, {dataTransTheta[id]/10*\[Pi], dataTransR[id]}, 2], 1] (* Darstellung
der Messdaten in R und \[CapitalTheta] aus X und Y *)(* \Illutration from R and \[CapitalTheta] data
calculated from X and Y *)
```

```
ListPolarPlot[%]

2. Calculation of templateAllCrit

fdzx[\[Theta]_,\[Phi]_]:=-(d31-d33+(d15+d31-d33) Cos[2\[Theta]]) Cos[\[Phi]] Sin[\[Theta]]

fdzy[\[Theta]_,\[Phi]_]:=-(d31-d33+(d15+d31-d33) Cos[2\[Theta]]) Sin[\[Phi]] Sin[\[Theta]]

fdzz[\[Theta]_]:=(d31+d15)Sin[\[Theta]]^2Cos[\[Theta]]+d33 Cos[\[Theta]]^3

(* Berechnung des absoluten Maximums *)

(* Calculation of absolute maximum *)

absMax[matrix_]:=If[Max[matrix]<Abs[Min[matrix]],Abs[Min[matrix]],Abs[Max[matrix]]]

(* Erstellt eine Matrix mit allen \[Theta] Werten *)

(* Creates a matrix with all \[Theta] angles *)

ThetaValue1 = listAngleMin[[All, All, 2]];

(* Erstellt eine Matrix mit allen \[Phi] Werten *)

(* Creates a matrix with all \[Phi] angles *)

PsiValue1 = listAngleMin[[All, All, 1]];

(* Berechnung der PFM Beiträge in pm aus berechneten Winkel *)

(* Calculation of the PFM signals in pm using the calculated \[Theta] and \\[Phi] angles *)

xValue1 = MapThread[fdzx[#1, #2] &, {ThetaValue1, PsiValue1}];

yValue1 = MapThread[fdzy[#1, #2] &, {ThetaValue1, PsiValue1}];

zValue1 = MapThread[fdzz[#1] &, {ThetaValue1}];

(* Normieren der berechneten PFM Beiträge *)

(* Normalization of the calculated PFM signals *)

xNormValue1 = xValue1/absMax[xValue1];

yNormValue1 = yValue1/absMax[yValue1];

zNormValue1 = zValue1/absMax[zValue1];

(* Berechnung der Differenz der normierten Werte *)

(* Calculation of the deviation between the normalized values *)
```

```
xDiffValue1 = compAbsNorm[11] - xNormValue1;
yDiffValue1 = compAbsNorm[21] - yNormValue1;
zDiffValue1 = compAbsNorm[31] - zNormValue1;
Abs[Flatten[xDiffValue1]] // Mean
Abs[Flatten[yDiffValue1]] // Mean
Abs[Flatten[zDiffValue1]] // Mean
(* Erstellen der Nullmatrizen *)
(* Createszeromatrices *)
templateX = Round[dataTrans[imageID]*0];
templateY = Round[dataTrans[imageID]*0];
templateZ = Round[dataTrans[imageID]*0];
templateAllCrit = Round[dataTrans[imageID]*0];
(* Grenzwerte der erlaubten Differenzen *)
(* Limit for the alloweddeviations *)
limitX = 0.3;
limitY = 0.3;
limitZ = 0.3;
(* Beschreiben der Nullmatrix mit den Punkten, die die Grenzwerte erfüllen *)\
(* Fills the zero matrices with all the points that pass the corresponding \limit *)
For[i = 1, i <= Dimensions[dataTrans[imageID]][[1]], i++,
 For[n = 1, n <= Dimensions[dataTrans[imageID]][[2]], n++,
  If[Abs[xDiffValue1[[i]][[n]]] <= limitX, templateX[[i]][[n]] = 1, templateX[[i]][[n]] = 0]]]
For[i = 1, i <= Dimensions[dataTrans[imageID]][[1]], i++,
 For[n = 1, n <= Dimensions[dataTrans[imageID]][[2]], n++,
  If[Abs[yDiffValue1[[i]][[n]]] <= limitY, templateY[[i]][[n]] = 1, templateY[[i]][[n]] = 0]]]
For[i = 1, i <= Dimensions[dataTrans[imageID]][[1]], i++,
```

```
 For[n = 1, n <= Dimensions[dataTrans[imageID]][[2]], n++,

  If[Abs[zDiffValue1[[i]][[n]]] <= limitZ, templateZ[[i]][[n]] = 1, templateZ[[i]][[n]] = 0]]

(* Erstellen der Schablone die alle Grenzwerte erfüllen *)

(* Creates the final template containing the points that pass all the limits *)\

templateAllCrit = templateX*templateY*templateZ

(* Anzahl der Punkte die alle Kriterien erfüllen *)

(* Count of points that pass all the limits *)

Count[Flatten[templateAllCrit], 1]

ArrayPlot[templateAllCrit]

ArrayPlot[dataAngleColorAll*templateAllCrit]
```

3. Color schemes for more detailed illustration

```
thstep = 45(*\[Degree]*);

psistep = 45(*\[Degree]*);

color = {{Yellow, Yellow, Yellow, Yellow}, {Red, Red, Red, Red}, {Red, Red, Red, Red}, {Green,
Green, Green, Green}, {Green, Green, Green, Green}, {Blue, Blue, Blue, Blue}, {Blue, Blue, Blue,
Blue}, {Yellow, Yellow, Yellow, Yellow}}

colorAll = {{Lighter[Yellow, 0.6], Lighter[Yellow, 0.3], Darker[Yellow, 0.3 ],

    Darker[Yellow, 0.6]}, {Lighter[Red, 0.6], Lighter[Red, 0.3],

   Darker[Red, 0.3 ], Darker[Red, 0.6]}, {Lighter[Red, 0.6],

   Lighter[Red, 0.3], Darker[Red, 0.3 ],

   Darker[Red, 0.6]}, {Lighter[Green, 0.6], Lighter[Green, 0.3],

   Darker[Green, 0.3 ], Darker[Green, 0.6]}, {Lighter[Green, 0.6],

   Lighter[Green, 0.3], Darker[Green, 0.3 ],

   Darker[Green, 0.6]}, {Lighter[Blue, 0.6], Lighter[Blue, 0.3],

   Darker[Blue, 0.3 ], Darker[Blue, 0.6]}, {Lighter[Blue, 0.6],

   Lighter[Blue, 0.3], Darker[Blue, 0.3 ],
```

```
    Darker[Blue, 0.6]}, {Lighter[Yellow, 0.6], Lighter[Yellow, 0.3],
    Darker[Yellow, 0.3 ], Darker[Yellow, 0.6]}}
colorUpDown = {{Lighter[Yellow, 0.6], Lighter[Yellow, 0.6],
    Darker[Yellow, 0.3 ], Darker[Yellow, 0.3 ]}, {Lighter[Red, 0.6],
    Lighter[Red, 0.6], Darker[Red, 0.3 ],
    Darker[Red, 0.3 ]}, {Lighter[Red, 0.6], Lighter[Red, 0.6],
    Darker[Red, 0.3 ], Darker[Red, 0.3 ]}, {Lighter[Green, 0.6],
    Lighter[Green, 0.6], Darker[Green, 0.3 ],
    Darker[Green, 0.3 ]}, {Lighter[Green, 0.6], Lighter[Green, 0.6],
    Darker[Green, 0.3 ], Darker[Green, 0.3 ]}, {Lighter[Blue, 0.6],
    Lighter[Blue, 0.6], Darker[Blue, 0.3 ],
    Darker[Blue, 0.3 ]}, {Lighter[Blue, 0.6], Lighter[Blue, 0.6],
    Darker[Blue, 0.3 ], Darker[Blue, 0.3 ]}, {Lighter[Yellow, 0.6],
    Lighter[Yellow, 0.6], Darker[Yellow, 0.3 ], Darker[Yellow, 0.3 ]}}
figureColor = ArrayPlot[color // Transpose,
  DataRange -> {{psistep/2, 360 - psistep/2}, {-180 + thstep/2, -thstep/2}},
  ColorFunction -> ColorData["TemperatureMap"], ColorFunctionScaling -> True,
  Mesh -> True,
  FrameTicks -> {{Transpose[{Range[-180, 0, 45], Range[180, 0, -45]}], Transpose[{Range[-180, 0,
45], Range[180, 0, -45]}]}, {Range[0, 360, 90], Range[0, 360, 90]}}, Frame -> True,
  FrameLabel -> {"\[Theta] [\[Degree]]", "\[Phi] [\[Degree]]"},
  AspectRatio -> 1/GoldenRatio]
figureColorAll = ArrayPlot[colorAll // Transpose,
  DataRange -> {{psistep/2, 360 - psistep/2}, {-180 + thstep/2, -thstep/2}},
  ColorFunction -> ColorData["TemperatureMap"], ColorFunctionScaling -> True,
  Mesh -> True,
```

```
   FrameTicks -> {{Transpose[{Range[-180, 0, 45], Range[180, 0, -45]}], Transpose[{Range[-180, 0, 45], Range[180, 0, -45]}]}, {Range[0, 360, 90], Range[0, 360, 90]}}, Frame -> True,

   FrameLabel -> {"\[Theta] [\[Degree]]", "\[Phi] [\[Degree]]"},

   AspectRatio -> 1/GoldenRatio]

figureColorUpDown = ArrayPlot[colorUpDown // Transpose,

   DataRange -> {{psistep/2, 360 - psistep/2}, {-180 + thstep/2, -thstep/2}},

   ColorFunction -> ColorData["TemperatureMap"], ColorFunctionScaling -> True,

   Mesh -> True,

   FrameTicks -> {{Transpose[{Range[-180, 0, 45], Range[180, 0, -45]}], Transpose[{Range[-180, 0, 45], Range[180, 0, -45]}]}, {Range[0, 360, 90], Range[0, 360, 90]}}, Frame -> True,

   FrameLabel -> {"\[Theta] [\[Degree]]", "\[Phi] [\[Degree]]"},

   AspectRatio -> 1/GoldenRatio]

Export["colorcode.eps", figureColor]

Export["colorcode.tiff", figureColor]

Export["colorcodeGes.eps", figureColorAll]

Export["colorcodeGes.tiff", figureColorAll]

Export["colorcodeUpDown.eps", figureColorUpDown]

Export["colorcodeUpDown.tiff", figureColorUpDown]
```

4. Illustration of the X and Y data in a polar plot

```
dataDiagramm[id_]:=MapThread[{#1,#2}&,{dataTrans[getIDX[id]],dataTrans[getIDY[id]]},2]
```

References

[1] A. J. Moulson and J. M. Herbert: "Electroceramics: Materials, Properties, Applications", 2nd Ed., Wiley, Southern Gate (2003).

[2] A. Gruverman: "Principles and Applications of Piezoresponse Force Microscopy" University of Nebraska-Lincoln, USA, 2013 Joint UFFC, EFTF and PFM Symposium Prague, Czech Republic, July 21-25, 2013

[3] J. F. Nye: "Physical Properties of Crystals", Clarendon Press, Oxford (1957).

[4] M. Deluca: "Raman spectroscopy of lead-free ferroelectric and relaxor ceramics", Habilitation Thesis, Montanuniversität Leoben, 2016.

[5] F. X. Li et all: "Analytical saturated domain orientation texture and electromechanical properties of ferroelectric ceramics due to electric/mechanical poling" Journal of Applied Physics 101, 054110 (2007)

[6] https://www.ceramtec.com images; december 2016.

[7] W. Wersing: "Applications of Piezoelectric Materials: An Introductory Review", Siemens AG, Corporate Technology, Munich, Germany.

[8] G.A.Schneider: "Fracture Mechanical and Mechanical Properties of Piezoelectric Ceramics and Piezoceramics/Electrode Inferfaces Under High Electric Fields", Technical University Hamburg-Harburg, Advanced Ceramics Group, Denickestr. 15 D-21073 Hamburg, Germany;.

[9] Sergei V. Kalinin, Brian J. Rodriguez et all: "Vector Piezoresponse Force Microscopy", Microsc. Microanal. 12, 1–15, 2006.

[10] Elisabeth Soergel J.: "Piezoresponse Force Microscopy (PFM)", Phys. D: Appl. Phys. 44 (2011) 464003.

[11] Michael Lasnik: "Determination of the Orientation Distribution Function of PZT Ceramics by Piezoresponse Force Microscopy", Master Thesis, Institute of Physics Montanuniversit¨at Leoben, Austria; 2016.

[12] MFP 3D manual; Asylum Research, 2008.

[13] G. Esteves, C. M. Fancher, S. Röhrig, G. A. Maier, J. L. Jones, and M. Deluca: „Electric-field-induced structural changes in multilayer piezoelectric actuators during electrical and mechanical loading", Acta Materialia 132, 96-105 (2017)

[14] H. Schwaab, M. Deluca, P. Supancic, and M. Kamlah: "Effect of the electric conductivity on the modeling of the poling process of ferroelectric components", Journal of the Mechanics and Physics of Solids 61, 504-516 (2013).

[15] T. Fett, D. Munz, and G. Thun: "Bending strength of a PZT ceramic under electric fields", Journal of the European Ceramic Society 23, 195-202 (2003)

[16] Marco Deluca: Advances in Applied Ceramics, 115, 112-122 (2016).

[17] N. Setter: "ABC of Piezoelectricity and Piezoelectric Materials; Ceramics Laboratory", Swiss Federal Insitute of Tecnology EPFL, 1015 Lausanne, Switzerland,.

[18] K. Lubitz et all: "Material Aspect for Reliability and Life Time on PZT Multilayer Actuators", Siemens AG, Corporate Technology, Munich, Germany;

[19] Tobias Jungk et All: "Contrast Mechanisms for the detection of ferroelectric domains with scanning force microscopy" New Journal of Physics, 11(2009) 033029.

[20] R.P.Fernandes et all: "Area fraction quantification of ferroelectric domain orientations in $BaTiO_3$ using piezoresponce force microscopy", Insititute of Advanced Ceramics, Journal of Applied Physics 108, 044103 (2010).

[21] B. J. Rodriguez, A. Gruverman: " Three-dimensional high-resolution reconstruction of polarization in ferroelectric capacitors by piezoresponse force microscopy" Journal of Applied Physics Volume 95, number 4.

Acknowledgments

First of all I wanted to say thanks to all the SPM Group Leoben for the help, the friendship and the special way in which they included me inside the group. A particular thanks to Markus Kratzer and Michael Lasnik for all the time spent to teach me how to use the machine properly, for the technical help during the measurements and for the data treatments; to the Professor Christian Teichert, Christian Ganser and Alexandar Matkovic for the endless good advices during the Group Meetings, that help me a lot to improve this work. A special thanks also to all the MCL group, that gave me the opportunity to live this experience and to improve a lot myself as from the professional point of view, as from the personal point of view. And finally I wanted to say the biggest thanks to the Professor Marco Deluca for all the help and the endless patience and time that he used to help me as for this work, as to make me live the best experience possible in Austria. Thanks.